Upconversion: Making the Invisible - Visible for Efficient Silicon Solar Cells

Sean Kye Wallace MacDougall, BSc (Hons.)

A dissertation submitted for the degree of Doctor of Philosophy

On completion of research conducted at the

INSTITUTE OF PHOTONICS AND QUANTUM SCIENCES
SCHOOL OF ENGINEERING AND PHYSICAL SCIENCES
HERIOT-WATT UNIVERSITY
EDINBURGH
EH14 4AS
SCOTLAND

May 2015

FOREWORD

It is said that "The Great Learning" is the gate of elementary learning. Whenever you go to a house, first you go in through the gate. Therefore the gate is a sign that you have reached the house. Going through this gate, you enter the house and meet the host.

Learning is the gate to attainment of the Way. Therefore learning is the gate, not the house. When you see the gate, do not think it is the house. You have to go through the gate to get to the house, which is inside, behind it.

Since learning is a gate, when you read books do not think this is the Way. This misconception has made many people ignorant of the Way no matter how much they study or how many words they know. Even if you can read as fluently as a commentary of an ancient, if you are unaware of the principals, you cannot make the Way your own.

- ***Yagyū Munrnori***

The book of Family Traditions on the Art of War: The Killing Sword

ABSTRACT

Upconversion (UC) for photovoltaics (PV) aims to mitigate the intrinsic losses associated with the transmission of sub-band gap photons. The potential enhancement of a PV device via a coupled UC layer has not been realised experimentally due to the weak absorption coefficient of ~6 cm^{-1} at 1523 nm across a narrow bandwidth (100 nm) and non-linear nature of the active UC erbium ion (Er^{3+}). These limiting properties have resulted in the characterisation of the UC layer conducted with high power monochromatic lasers at the strongest resonant wavelength which is dissimilar to that of the solar spectrum.

Herein, a novel method is developed to determine the photoluminescent quantum yield (*iPLQY*) of an UC layer under broadband excitation through the correct determination of the absorption spectrum unaffected by re-emission. This method is used to evaluate the *iPLQY* of the UC material under increasing bandwidths of excitation where saturation is seen for bandwidths greater than 60 nm, significantly shorter than the 100 nm absorption spectrum. Although an *iPLQY* of 16.2% was achieved, with the normalisation to the solar spectrum this equates to a solar concentration beyond what is attainable on Earth. Therefore, advanced photon management techniques are necessary to realise a working device. An in-depth investigation is conducted on the optimisation of an UC material across a wide range of solar concentrations and doping of the active UC ion which indicates β-$NaYF_4$: 25% $Er^{3+}$to be the most suitable for a coupled PV device.

ACKNOWLEDGEMENTS

This thesis represents my dedicated work and effort for the past four years, and a bit more. Although the work contained within it is mine, I would not have been able to reach this destination without the support of those close to me.

I would first of all like to express my love and gratitude to my Mother and Father for their endless encouragement and belief in me. They have supported me both emotionally and financially throughout my life which, I hope to repay them for their kindness someday, at least in part. I would also like to thank my Sister, Naomi, her husband, Niall and my beautiful niece, Megan. I have always enjoyed our time together for Friday dinner when I can pretend to play with Megan just to watch cartoons and draw with crayons.

To Eilidh, my gorgeous girl, you have always been there for me when I have found it difficult or hard and pushed me to keep going. You have forgiven me for missing your birthday when I was giving a talk at a conference and waited for me when I was working in China for three months. If it wasn't for your giving, kind and loving heart I would not have been able to reach this point.

I would also like to show my appreciation to all my family; to my grandparents, aunties, uncles and cousins thank you for encouraging me along the way. To my friends, thank you for never asking what I do and giving me a distraction when I needed it and sometimes when I didn't.

I would like to thank Bryce for giving me this opportunity and for his supervision.

Thank you to Aruna, Hari and Ajoy for supervising me through the final stages of my work when it was not your responsibility; I will always be grateful. Especially Ajoy, you have mentored me since my undergraduate degree and have always supported me beyond your duty to do so.

This work would not be possible without the contributions and guidance of others. I would like to thank Karl Kramer for his expert skills at synthesising phosphors and our

discussions. The work contained herein was funded mostly from the EU 7th Framework Programme “Nanospec” which I am especially grateful. I would also like to thank the EPSRC, The Royal Society of Edinburgh and Professor Wang from the Chinese Academy of Sciences for their partial funding. This made it possible for me to carry out research in Fujian, China, where I was supervised by Daqin Chen and met many great people.

I have worked with many people at Heriot-Watt University and although this was founded on our shared passion in the research of solar energy they have become treasured friends. I would therefore like to acknowledge; Tapas, Nabin, Sam, Serena, Dave, Jonny, Ale, Georgios, Rosario, Dan, Brian, Gavin, Brenda, Gudrun, Dorothy, Efthymios, Paolo, Mandy, Martina, Eliyas, Jose, Leo and again Aruna for their support and friendship.

CONTENTS

PUBLICATIONS BY THE AUTHOR

Peer reviewed journal articles by the author

1. Sean K. W. MacDougall, Aruna Ivaturi, Jose Marques-Hueso, Karl W. Krämer, Bryce S. Richards, "Broadband Photoluminescent Quantum Yield Optimisation of Er^{3+}-doped β-$NaYF_4$ for Upconversion in Silicon Solar Cells", Sol. Ener. Mat. Sol. Cells, Vol. 128, p18–26 (2014), http://dx.doi.org/10.1016/j.solmat.2014.05.004

2. Sean K. W. MacDougall, Aruna Ivaturi, Jose Marques-Hueso, and Bryce S. Richards, "Measurement Procedure for Absolute Broadband IR Up-Conversion Photoluminescent Quantum Yields: Correcting for Absorption/Re-Emission", Rev. Sci. Instrum., Vol. 85, 063109 (2014), http://dx.doi.org/10.1063/1.4881537

3. Sean K.W. MacDougall, Aruna Ivaturi, Jose Marques-Hueso, Karl W. Krämer, and Bryce S. Richards, "Ultra-high photoluminescent quantum yield of β-$NaYF_4$: 10% Er^{3+} via broadband excitation of upconversion for photovoltaic devices", Opt. Exp., Vol. 20, Issue S6, pp. A879-A887 (2012), http://dx.doi.org/10.1364/OE.20.00A879

4. Aruna Ivaturi, Sean K.W. MacDougall, Jose Marques-Hueso, Karl W. Krämer, and Bryce S. Richards, "Optimizing infrared to near infrared upconversion quantum yield of β-$NaYF_4$:Er^{3+} in fluoropolymer matrix for photovoltaic devices", J. Appl. Phys., Vol. 114, 013505 (2013); http://dx.doi.org/10.1063/1.4812578

Conference papers by the author

1. Jan Christoph Goldschmidt, Stefan Fischer, Barbara Herter, Benjamin Fröhlich, Karl W. Krämer, Bryce S. Richards, Aruna Ivaturi, Sean K.W. MacDougall, Jose Marques Hueso, Elena Favilla, Mauro Tonelli, "Record Efficient Upconversion Solar Cell Devices", 29th European PV Solar Energy Conference and Exhibition, New Materials and Concepts for Cells, Amsterdam (2014)

2. Sean K.W. MacDougall, Daqin Chen, Jose Marques-Hues, Feng Huang, Yuansheng Wang, and Bryce S. Richards "Making the Invisible, Visible: Upconversion via Capped Er-doped $NaGdF_4$ Nanoparticles for Harvesting Sub Bandgap Photons", OSA, Renewable Energy and the Environment Congress, Optics for Solar Energy (SOLAR),

Optical Nanostructures and Advanced Materials for Photovoltaics, Arizona 2013, http://dx.doi.org/10.1364/PV.2013.PT3C.3

3. Bryce S. Richards, J. Marques-Hueso, Sean K. MacDougall, Alessandro Boccolini, Jonathan Morton, E. D. Mammo, Georgios E. Arnaoutakis, and Aruna Ivaturi, "Progress Towards Enhancing the Performance of c-Si Photovoltaic Devices via Up- and Down-Conversion", OSA, Renewable Energy and the Environment Congress, Optics for Solar Energy (SOLAR), Optical Nanostructures and Advanced Materials for Photovoltaics, Arizona 2013, http://dx.doi.org/10.1364/PV.2013.PT3C.1

4. Jan Christoph Goldschmidt, Urs Aeberhard, Richard Capek, Michael G. Debije, Wiel Evers, Stefan Fischer, Benjamin Fröhlich, Martin Hermle, Barbara Herter, Aruna Ivaturi, Karl W. Krämer, Efrat Lifshitz, Rosa Martín-Rodríguez, Sean K. W. MacDougall, Andries Meijerink, Etienne A. Moulin, Thomas C. M. Müller, Ulrich Paetzold, Bryce S. Richards, Sebastian Wolf, Marek Warzecha, Claudia Wouters, Yiming Zhao, "Developing Efficient Upconverter Silicon Solar Cell Devices", OSA, Renewable Energy and the Environment Congress, Optics for Solar Energy (SOLAR), Optical Nanostructures and Advanced Materials for Photovoltaics, Arizona 2013, http://dx.doi.org/10.1364/PV.2013.PT3C.2

5. Sean K.W. MacDougall, Aruna Ivaturi, Jose Marques-Hueso, Bryce S. Richards, "Spectral Leverage: Enhancing the Photoluminescent Quantum Yield of Upconversion via Broadband Excitation", Proceedings of OSA Renewable Energy and the Environment, Optics for Solar Energy (SOLAR), Luminescence and Up/Down Conversion, Eindhoven (2012), http://dx.doi.org/10.1364/OSE.2012.ST4A.4

6. Abdelfateh Kerrouche, Dorothy A Hardy, Aruna Ivaturi, Sean K. W. MacDougall, S C Roaf and B S Richards, "Ray-trace Modelling of a Combined Up-converter: Luminescent Solar Concentrator", 27th European Photovoltaic Solar Energy Conference and Exhibition, Silicon Solar Cell Characterization and Modelling, p 1398-1400, Frankfurt (2012), doi: 10.4229/27thEUPVSEC2012-2BV.5.23

7. Sean K.W. MacDougall, Aruna Ivaturi, Jose Marques-Hueso, Daqin Chen, Yuansheng Wang, Bryce S. Richards, "Broadband excitation of upconversion in lanthanide doped fluorides for enhancement of Si solar cells", Proc. of SPIE 8438, Photonics for Solar Energy Systems IV, Belgium (2012), http://dx.doi.org/10.1117/12.922644

8. Bryce S Richards, Aruna Ivaturi, Sean K.W. MacDougall, Jose Marques-Hueso, "Up- and down-conversion materials for photovoltaic devices", Proc. SPIE 8438, Photonics for Solar Energy Systems IV, p 843802, Belgium (2012), http://dx.doi.org/10.1117/12.923298

9. Jose Marques-Hueso, Hans J. Schöpe, Thomas Palberg, Sean K.W. MacDougall and Bryce S. Richards, "3D Colloidal Photonic Crystal Fabrication Improved by AC Fields for Frequency Conversion Enhancement for Solar Cells", Proc. of IEEE 37th Photovoltaic Specialists Conference (PVSC), p 899-903, Seattle (2011)

10. Jose Marques-Hueso, Daqin Chen, Sean K. W. MacDougall, Yuansheng Wang, and Bryce S. Richards, "Advances in spectral conversion for photovoltaics: up-converting Er^{3+} doped YF_3 nano-crystals in transparent glass ceramic", Proc. SPIE 8111, Next Generation (Nano) Photonic and Cell Technologies for Solar Energy Conversion II, p 811102, San Diego (2011), http://dx.doi.org/10.1117/12.897526

11. Sean K.W. MacDougall, Jose Marques-Hueso, Gudrun Kocher, and Bryce S. Richards, "Enhancement of Upconversion Efficiency by Manipulation of Photonic Structures: A Review", Proc. of 7th Photovoltaic Science, Applications and Technology Conference (PV-SAT), Edinburgh (2011)

LIST OF FIGURES

CHAPTER 1

CHAPTER 2

CHAPTER 3

CHAPTER 4

CHAPTER 5

CHAPTER 6

LIST OF TABLES

GLOSSARY

Acronym/Abbreviation	*Definition*
A	Absorption
AM1.5G	Air Mass Global Spectrum
AM1.5d	Air Mass Direct Spectrum
AOTF-HP	High Power Acousto-optical Tuneable Filter
a-Si	Amorphous-silicon
a-Si:H	Amorphous-silicon: hydrogenated
BF	Bi-facial
CdTe	Cadmium Telluride
CIGS	Copper Indium Gallium (di)selenide
CO_2	Carbon Dioxide
cps	Counts per Second
CPV	Concentrating Photovoltaic
CR	Cross Relaxation
c-Si	Crystalline-silicon
DC	Downconversion
DS	Down-shifting
DSC	Dye-sensitised Solar Cell

EDX	Energy-dispersive X-ray Diffraction
e-h	Electron-hole pair
ePLQY	External Photoluminescent Quantum Yield, $ePLQY = \frac{No.\ of\ Photons\ Emitted}{No.\ of\ Photons\ Incident}$
EQE	External Quantum Efficiency, $EQE = \frac{No\ of\ electrons\ Generated}{No.\ of\ Photons\ Incident}$
ESA	Excited State Absorption
ETU	Energy Transfer Upconversion
EVA	Ethylene-vinyl acetate
FWHM	Full width half maximum
FZ	Fluorozirconate
IB	Intermediate band
IQE	Internal Quantum Efficiency, $IQE = \frac{No\ of\ electrons\ Generated}{No.\ of\ Photons\ Absorbed}$
IR	*Infra*-red
I-V	Current-Voltage
LDS	Luminescent Down Shifting
LED	Light Emitting Diode
Ln^{3+}	Lanthanides
LSP	Localised Surface Plasmons

MEG	Multiple Exciton Generation
MEOP	Metallated porphyrin macrocycles
MPR	Multi Phonon Relaxation
NIR	Near *infra*-red
NP	Nano-particle
PBG	Photonic Band-gap
PDMS	Poly (dimethylsiloxane)
PF	Polyfluorenes
PFCB	Perfluorocyclobutyl
PhC	Photonic crystal
PMMA	Poly (methylmethacrylate)
PU	Poly urethane
QD	Quantum dot
QTH	Quartz-Tungsten-Halogen
RE^{3+}	Rare Earths
SC	Supercontinuum
SEM	Scanning Electron Microscopy
SHG	Second Harmonic Generation
Si	Silicon

SPP	Surface Plasmon Polaritons
S-Q	Shockley-Queisser
TEM	Transmission Electron Microscopy
TGC	Transparent Glass Ceramic
TPA	Two-photon Absorption
TTA	Triplet-triplet Annihilation
UC	Upconversion
UCNP	Upconversion nano-particle
UC-PV	Upconversion-photovoltaic
UNSW	University of New South Wales
UV	*Ultra*-violet
Xe	Xenon
XRD	X-ray Diffraction

NOMENCLATURE

Symbol	*Definition*
α	Absorption Coefficient (cm^{-1})
β	Hexagonal phase
Δ	Average crystal domain size (nm)
f	The fraction of excitation photons which are incident on the sample directly
γ	Parameter dependent on the full-width half maximum of the diffraction peak
h	Planck's Constant (6.626×10^{-34} J s)
I	Current (A)
I_D	Diode dark current
I_o	Incident Intensity (Wm^2)
I_r	Reflected Intensity (Wm^2)
I_{sc}	Short-circuit current
I_s	Scattered Intensity (Wm^2)
k	Boltzmann's Constant (1.38×10^{-23} $m^2kg\ s^{-2}K^{-1}$)
κ	Shape factor parameter
λ	Wavelength (nm)

L_a	Excitation spectrum when the integrating sphere is empty (Photon Counts per Second (cps))
L_b	Excitation spectrum when the sample is directly illuminated (cps)
L_c	Excitation spectrum when the sphere is illuminated first (cps)
μ	The fraction of photons that are absorbed by the sample after reflection from the integrating sphere wall
η	Efficiency
P_b	The emission of the sample when, directly illuminated by the excitation source (cps)
P_c	The emission of the sample when, illuminated from all angles due to the reflection from the internal sphere walls (cps)
P_{in}	Incident power (W)
q	Unit charge (-1.6×10^{-19} C)
Q	Heat (J)
S	Entropy ($J\ kg^{-1}K^{-1}$)
T	Temperature (K)
θ	Angle (degrees)
v	Electromagnetic frequency (s^{-1})
V	Voltage ($kg\ m^2s^{-3}A^{-1}$)
V_{oc}	Open-circuit voltage

W	Work (J)

CHAPTER 1 - INTRODUCTION

1.1 Motivation and Overview

Research into the application of upconversion (UC), to tackle the fundamental loss mechanism associated with the spectral mismatch between the solar spectrum and the absorption of a photovoltaic (PV) device, has received increasing interest. The intrinsic losses in the conversion of solar energy, defined by the Shockley-Queisser (S-Q) limit, give a limiting efficiency of 31%. With the application of an UC layer behind the PV device this limit can be circumvented, with a corresponding potential efficiency of 47.6%. Although the electricity production from PV's is now achieving grid parity, such as in Germany, UC could significantly enhance current technology to supply cheaper and greener energy. UC can improve the *infra*-red (IR) response of a coupled cell by converting two lower energy photons which are transparent to the cell to a higher energy photon that can be absorbed. However, much research is needed to realise the potential benefits of this "third generation" photovoltaic technology. The materials that have demonstrated UC properties, which are currently being investigated, are lanthanides (Ln^{3+}). One of the most promising is erbium which has shown near *infra*-red (NIR), visible and even *ultra*-violet (UV) emission under IR excitation. However, the weak absorption coefficient (~6 cm^{-1} at 1523 nm) over a relatively narrow bandwidth (100 nm), due to the forbidden nature of the energy transitions limits its application potential. This is compounded by the non-linear response of the UC process where higher irradiances are required for larger efficiencies. Therefore, the evaluation and characterisation of these upconversion-photovoltaic (UC-PV) devices has been predominantly conducted with high power monochromatic lasers which are unlike the broad solar spectrum encountered from the sun. Hence, broadband characterisation is necessary to optimise these materials and to assess their true potential to enhance the energy harvesting of PV devices.

It is necessary to first explain the social, political and environmental drivers which have created a need for harvesting renewable energy to help tackle climate change which, will be covered in section 1.2. Due to the abundance of solar energy, PV's can contribute significantly to this aim. In section 1.3, the concepts important to understanding the current progress of PV technology will be discussed. This will include the intrinsic loss mechanisms and efficiency limits which restrict their potential benefits. In section 1.4 the three major generations of PV research are elucidated in

relation to progression towards those efficiency limits and reducing the cost of producing electrical power from the sun. One of the approaches to surpass the so called S-Q limit is spectral conversion of the solar spectrum. There are three main approaches to this optical technique which will be discussed in section 1.5 with an emphasis on UC, the focus of this thesis.

1.2 The Need for Sustainability

One of the most important issues for contemporary society is the demand for energy and the effect this has on the environment. With increasing world population [1] the demand for energy continues to follow suit. That demand has been historically supplied by fossil fuels such as coal, oil and gas [2], which also have geo-political implications due to an uneven distribution of resources. The use of these fossil fuels also shows a considerable correlation with the production of carbon dioxide (CO_2) which is associated with the rise in average global temperatures. This has been proven to be linked to climate change and severe weather events [3]. If the trend in rising temperatures continues, this could lead to catastrophic climate events at a significant cost to all. It is therefore an imperative for the world community to find more sustainable solutions to reduce the production of CO_2, with the associated affects this has on the environment. There have been several agreements with various political and national organisations to impose financial deterrents to encourage this change towards a sustainable future, such as the EU 2020 targets [4]. One of the major pathways to realising this is the use of at least 20% renewable energy to replace the use of carbon intensive sources such as fossil fuels by 2020.

Solar energy is a renewable resource which can be harnessed globally. This source of energy could be used to supply heat or electricity for a single home or even a city. The potential solar energy which can be harnessed from the sun in one hour is more than the global energy consumption for one year [5]. Although practical considerations makes this level of generation very unlikely the fact still remains that this renewable technology can supply a significant proportion of world energy demand. There may be a social and environmental need for renewable energy generation but there must also be an economic incentive for the investment and adoption of this alternative technology. This is in part motivated by the financial penalties on energy generators or nations which do not achieve the agreed goals in CO_2 mitigation such as the EU 2020 directive [4]. However, this has been described as a false economy due to the need for subsidies

that are highly volatile, which would not be necessary for a technology or industry that is economically viable in relation to current fossil fuelled based counterparts. The economic merit is evaluated by the cost per Watt (usually in $/W) of energy production of a given technology. The technologies based on fossil fuels have reached a mature stage and the cost of energy production is close to a minimum. Therefore, a less mature technology such as solar energy must find ways of being cost competitive either through increasing the efficiency of the conversion of solar energy or making this process cheaper. Research into the fundamental challenges which inhibit the wide utilisation of this technology is important to exploit the abundant natural resource and to achieve a sustainable future. The historical advancement in PV's and the important considerations in enhancing the efficiency of this technology will now be discussed.

1.3 Photovoltaic Technology

1.3.1 Background

Photovoltaic devices can convert "light" directly to electricity. The word "photovoltaic" comes from "photo", which means light and "voltaic" is the production of a voltage via a chemical reaction. This effect was first discovered by Becquerel in 1839 where electrodes placed in an electrolyte produced a voltage proportional to the incident illumination [6]. In 1905 Einstein published a paper on the photoelectric effect [7], using Planck's theory of the quantisation of light [8], for which he was awarded the Nobel Prize in 1921. This law describes the basic operating principal for a PV device, a key milestone in the understanding of this technology. It was not until 1954 that the first commercial silicon (Si) PV device was created at Bell Laboratories with an efficiency of around 6% [9]. The first applications were used to power satellites as early as 1958. This device was created using a *p*-*n* junction, which still forms the basic operation of the majority of today's solar cells.

PV devices are commonly made from the combination of two semiconductor materials oppositely doped. One of which is negatively doped, *n*-doped, usually phosphorous doping in the case of Si; the other is positively doped, *p*-doped, usually boron. Electron-hole (*e*-*h*) pairs are created when photons of energy greater than or equal to that of the band gap (E_g) of the semiconductor are absorbed, see Figure 1.1. This is defined by Equation 1.1:

$$h\nu \geq E_g$$ Equation 1.1

where h (6.626×10^{-34} Js) is Planck's constant and ν is the electromagnetic frequency of the incident photon. The electron in the valance band absorbs the energy of the incident photon followed by promotion to the conduction band. The flow of those *e*-*h* pairs establishes a current when connected to an external circuit, hence electrical power is generated. The current-voltage (*I*-*V*) characteristics of the solar cell can be defined by the ideal diode law, with the equation:

$$I = I_D \left(e^{\frac{qV}{kT}} - 1 \right)$$ Equation 1.2

where, I is the current flowing in the device, I_D is the diode dark current, V is the applied voltage, T is the absolute temperature, q (-1.6×10^{-19} C) and k (1.38×10^{-23} $m^2kgs^{-2}K^{-1}$) are the constants of electron charge and Boltzmann respectively. The efficiency (η) of the PV device can therefore be defined by the power generated by the solar cell, which is the product of V and I, divided by the incident power (P_{in}) of illumination.

$$\eta = \frac{IV}{P_{in}}$$ Equation 1.3

It would therefore be desirable to increase both the voltage and current for a greater efficiency. However, these interdependent properties are related to that of the semiconductor material which therefore must be optimised. These relationships and their corresponding loss mechanisms are discussed in the following section.

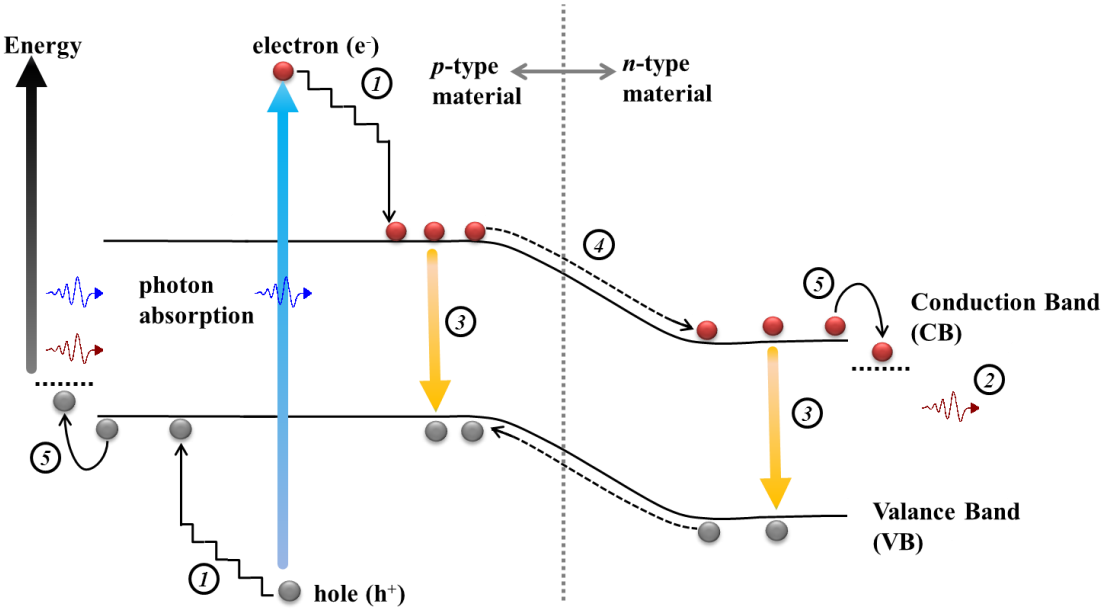

Figure 1.1 Schematic diagram of carrier generation with the associated intrinsic loss mechanisms for a PV device. This includes losses due to thermalisation ①, sub-band gap photons ②, recombination ③, junction voltage loss ④ and voltage drop at the contacts of the device ⑤.

1.3.2 Fundamental Losses of Photovoltaics

As mentioned, the energy of a photon must be greater than the band gap energy of the semiconductor for *e-h* pair generation (Equation 1.1). If the energy of the absorbed photon is not equal to the E_g of the semiconductor this leads to a reduction in efficiency. Thermalisation occurs when an incident quantum of light, photon, has energy greater than the band gap of the semiconductor. The excess energy is dissipated to the lattice structure of the semiconductor via phonons, ① in Figure 1.1. These phonons are vibrations of the lattice and generate heat which increases the short-circuit current (I_{sc}) marginally but causes an almost linear decrease in voltage [6]. This loss mechanism accounts for approximately 30% of the sun's energy for a Si device. The effect could be reduced by increasing the E_g (or equivalently the voltage) of the semiconductor material used for the PV device but would lead to a greater amount of sub-band gap photons (or loss of current). These sub-band gap photons with energy less than E_g appear transparent (② in Figure 1.1) to the device meaning that 20% of incident energy (for a Si device) is simply not used (see Figure 1.2). Both of these losses mentioned above are due to a mismatch between the choice of semiconductor material and the broad solar spectrum which result in a conversion limit of around 44% [10]. This value only takes in to consideration the effect of photon energy and neglects more

complicated losses associated with an operating device. However, this highlights the potential improvements that can be achieved by utilising more of the solar spectrum. In addition to these, there are also losses due to the device and its use. Other losses which are shown schematically in Figure 1.1 include recombination ③, voltage drop across the junction ④ as well as defects introduced via contacts to the cell ⑤. These intrinsic loss mechanisms must be addressed to improve conversion efficiency leading to a reduction in the cost of electricity produced.

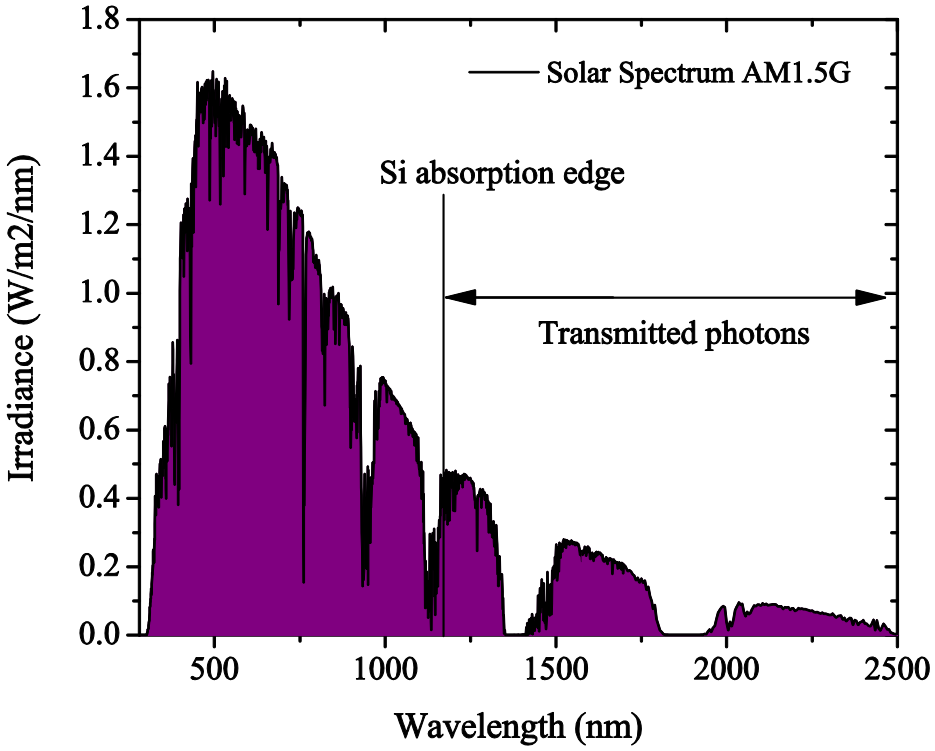

Figure 1.2 The AM1.5G solar spectrum is shown with the Si absorption band-edge where photons with a wavelength above this are not absorbed. This accounts for approximately 20% of the sun's energy.

1.3.3 Photovoltaic Limitations: The Shockley-Queisser Limit

Understanding the various loss mechanisms is important for determining the scope for improvements and hence the performance limits that can be achieved in a PV device. The theoretical efficiency on the conversion of solar energy has been modelled taking into account the 1st and 2nd laws of thermodynamics as 93% [11] (also known as the Lansberg limit). This limit is achieved when considering a given amount of radiation from the sun with an energy (E) and entropy (S) transformed by a solar converter to produce work (W) and heat (Q). However, these were for ideal solar energy converters and therefore a more realistic model was required to give an evaluation of efficiencies

of real devices. A more realistic method based on the principal of detailed balance, where the effect of carrier recombination as well as thermalisation and transmission losses were analysed (loss mechanism ①, ② and ③ in Figure 1.1, respectively) has been developed by Shockley and Queisser in 1961 [12]. This allowed a more realistic comparison to a single junction device in contrast to more simplistic thermodynamic models. Theoretical results were taken into account for various values of solar concentration and its relation to the angular selectivity of the converter [12]. Furthermore, optimum efficiencies were predicted with relation to band gap and solar concentration. This showed that an efficiency of approximately 30% could be achieved for a 1.1eV device such as crystalline silicon (c-Si) without solar concentration. Although there have been improvements on the model of detailed balance [13], the S-Q limit still stands as the key milestone in the evaluation of solar cell performance and the drive for the current third generation of PV technology.

1.4 Generations of Photovoltaic Devices

1.4.1 First Generation

The first generation of PV devices is often considered exclusive to high efficiency single junction solar cells such as c-Si. Although working PV devices have been demonstrated since the 1930's [14], the efficiencies were too low to achieve commercialisation. These devices aimed simply to achieve the highest possible efficiency and reliability due to their remote applications as a power source for satellites. The move to terrestrial applications has been associated with the oil embargos of the 70's, though their main use was still for remote applications during that time [15]. For first generation devices such as single junction c-Si, the maximum efficiency achieved so far is 25% by the University of New South Wales [16]. This is comparable to that of gallium arsenide (GaAs) devices (see Figure 1.2) which are approaching the S-Q limit of 30%. Hence, first generation devices are reaching the theoretical limits and novel techniques are required to advance this technology further. Historically, reduction in cost, which is dominated by the starting materials such as the Si wafer and the protective glass cover [17], was achieved by minimising the use of these materials. Although cost saving techniques was the next technological step – termed second generation PV, c-Si solar cells still hold the market share mainly due to a large increase in manufacturing experience which led to 20% reduction in cost when total production volume was doubled [18].

1.4.2 Second Generation

The second generation focus is in making PV as cheap as possible via thin film devices. The economic viability of thin film technologies is also improved by economy of scale, better manufacturing methods and throughput, which are less energy intensive [19]. Common thin film PV technologies and the maximum efficiencies achieved (taken from Figure 1.3) are; copper indium gallium diselenide (CIGS, 23.3%), hydrogenated amorphous-silicon (a-Si:H, 13.4%), cadmium telluride (CdTe, 20.4%), organic semiconductors (11.1%) [20] and dye-sensitized solar cells (DSC, 11.9%). A significant advantage of thin film devices is their flexibility, which has allowed the development of niche markets unsuitable for 1st generation devices. However, these devices have struggled to make a large impact in total PV production due to factors such as; low efficiency, higher costs than originally expected and toxicity of materials. More specifically a-Si based devices have poor conductivity and low efficiency which degrades further under sunlight [21]. Another possibility to reduce material costs is to use geometrical concentration of sunlight. Therefore, replacing expensive semiconductor material with a cheaper polymer or glass optical concentrator. Amonix, who specialise in Si devices, have been working with concentrating PV since the late 80's, achieved an efficiency of 27.6% for a single junction c-Si cell under 92 suns [22]. The use of concentrating photovoltaics (CPV) requires high solar irradiances and tracking technology to increase power generation and to cover the balance of systems cost. This highlights thefact that, not only the efficiency and capital investment but also the geographical location and the available resources determine the cost per unit power produced.

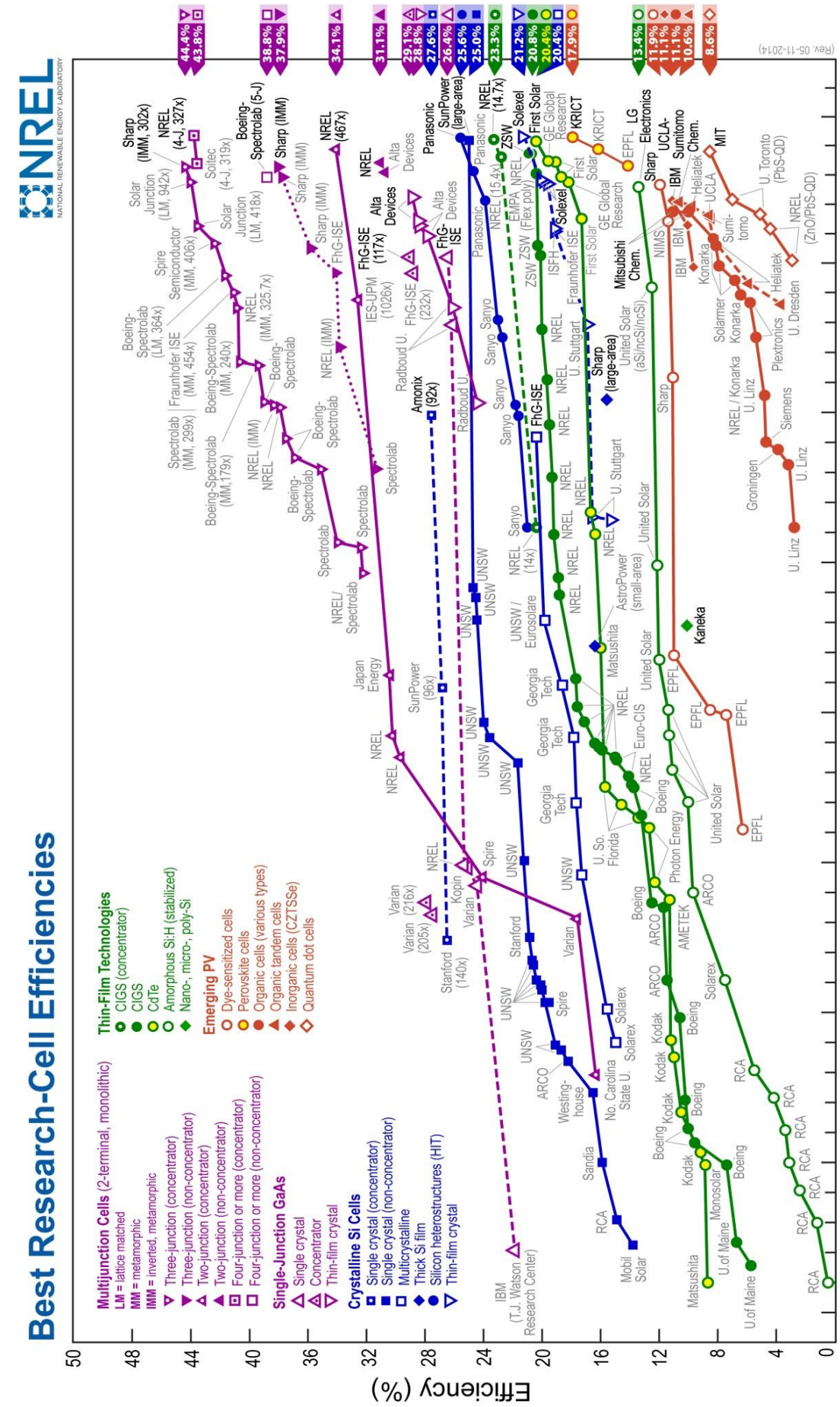

Figure 1.3 The trend in PV efficiencies for various solar cell technologies achieved in the last 35 years, from [23].

1.4.3 Third Generation

The PV community is now in its third generation, which aims to combine the efforts of the proceeding generations of increased efficiency and lower material costs. Hence, a requirement of third generation devices is to achieve a cost per unit power as low as 0.2 $/W (Figure 1.4). This in most part requires third generation PV to surpass the S-Q limit of single junction cells, which is 31% for a 1.3 eV device under 1 sun (or 40.8% for concentrated light and a 1.1 eV device) [12]. As discussed above, the main loss mechanisms are due to spectral mismatch which accounts for approximately 44% of the sun's energy. There are two pathways to tackle this loss mechanism; firstly, the semiconductor absorption can be modified to absorb a greater proportion of the solar spectrum; secondly, the solar spectrum can be modified to better suit the absorption of the semiconductor. Therefore, multi energy threshold devices have been the main focus to achieve the goal of third generation PV [24]. The research in the former area includes – for example – multi junction tandem devices [25], quantum dot solar cells [26], multiple exciton generation (MEG) [27], impurity photovoltaics (IPV; also known as intermediate band solar cells, IB) [28] and hot carrier cells [29]. The highest efficiencies achieved in the last few years have been for CPV made from multi junction cells of III-V semiconductors. The main contenders have been Fraunhofer ISE, NREL and Boeing-Spectrolab who have recently achieved a 41.6% efficient device which is now on the commercial market (see Figure 1.3 above). However, this is for III-V semiconductors which are expensive to produce and require multiple axes tracking to maintain performance.

Less of a focus has been on Si multi junction devices as a third generation approach due to their low efficiency compared to other tandem devices. However, Si has been the dominant choice of material for the PV market to date due to its abundance, non-toxicity and an E_g which is close to the optimum (although indirect). However, Si devices are approaching the S-Q efficiency limit; therefore applying third generation techniques would allow a significant advancement of this already well-established technology. The next section will focus on "spectral conversion" which is a third generation technology that can be applied to any semiconductor to overcome the S-Q limit through the modification of the solar spectrum.

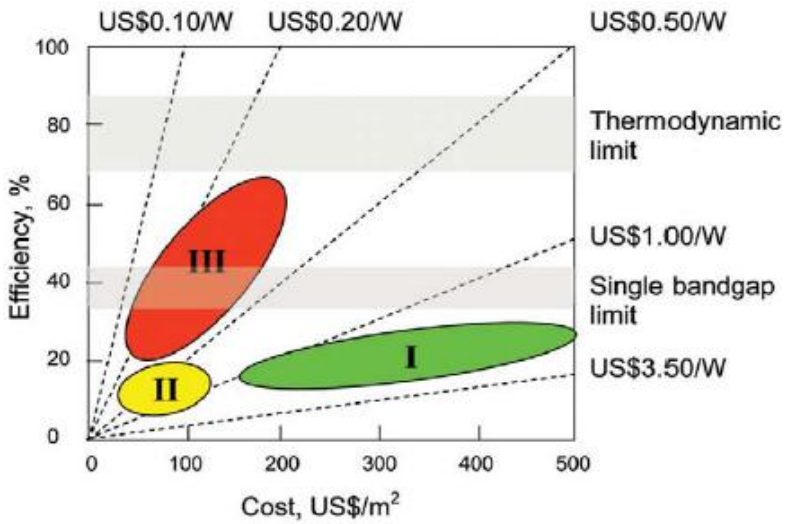

Figure 1.4 The diagram depicts the three generations of PV technology including the respective aims in regards to both efficiency and cost (adapted from Conibeer [24]).

1.5 Spectral Conversion: Transforming the Solar Spectrum

Spectral conversion, as is used in PV research, involves the absorption and subsequent emission of a photon at a different wavelength by a luminescent material. The intrinsic losses due to the spectral mismatch between the absorption of a PV device and the solar spectrum can thus be reduced through the modification of the latter via spectral conversion.

1.5.1 Down Shifting

Down shifting (DS), also known as luminescent down shifting (LDS), is an optical process where a high energy photon absorbed by a luminescent species is emitted at a lower energy. Figure 1.5 shows the absorption and the red-shifted emission spectra for an organic dye which could be used for such a purpose. This type of photon conversion has a limiting quantum efficiency of $\leq 100\%$ as no more than one photon can be emitted for each absorption process. DS materials can be used in conjunction with PV devices to convert short wavelength photons around 300-500 nm (UV or blue light), which would normally cause thermalisation (see process ① in Figure 1.1), to longer wavelengths where the device performs better. The red-shift in wavelength, of the absorbed to emitted photon, is known as Stokes' principle demonstrated in Figure 1.5. High energy photons are absorbed near the front surface of the semiconductor material hence, the DS layer is placed on front of the PV device to make better use of photons which cause thermalisation. The DS material can therefore be doped within the encapsulation material such as ethylene-vinyl acetate (EVA) which is already a

component of the module design [30]. This technology is therefore nonintrusive and can be implemented on the module scale. Although there are many benefits to this technique there are also some limitations due to the introduction of an additional layer at the front of the solar cell. 1) the luminescent material emits isotropically and a fraction of the emitted light escapes back through the front and side surfaces due to the incident angle being less than the angle of total internal reflection (escape cone losses). 2) the quantum efficiency of the luminescent species can be less than unity which reduces the conversion of the incident photons. 3) in combination with the previous point, there is often an overlap in the absorption and emission spectrum of the luminescent species which causes re-absorption and is a compounding factor for non-unity efficiencies. Working devices and modules have already been demonstrated for various semiconductor materials [31, 32] which show real potential for DS efficiency enhancement for PV devices. An extensive review on DS can be found in the work of Klampaftis *et al.* [33].

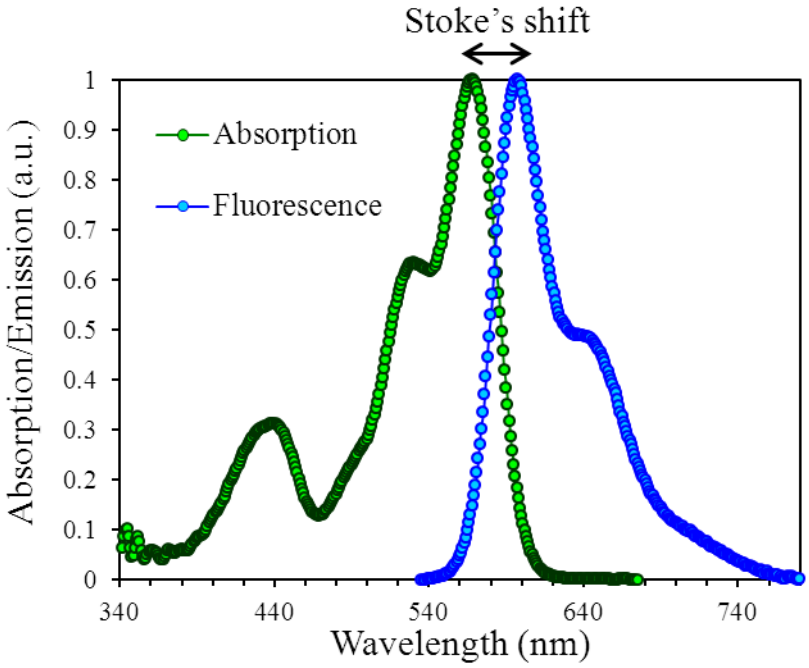

Figure 1.5 An example of a typical Stokes' emission where the fluorescence is red-shifted in comparison to absorption.

1.5.2 Downconversion

Downconversion (DC; also known as quantum splitting) is similar to DS, whereby high energy photons are absorbed however; in this case it is possible for multiple lower energy photons to be emitted. This means that quantum efficiencies over 100% are possible and values as high as 190% have been calculated [34]. This was first proposed

by Dexter as far back as 1957 in his paper "Possibility of Luminescent Quantum Yields Greater than Unity" [35] and found initial applications in light emitting devices. This technique is also utilised to reduce the thermalisation losses and resulting lower spectral response in the UV similar to DS, but involves the use of different absorbing materials. Some limitations such as the almost isotropic emission of the materials leads to photons escaping through the front and side edges of the thin films deposited on the PV device lowering the efficiency. Other challenges to overcome are the interaction of the DC layer with the incident spectrum before the cell leading to scattering or absorption of photons in the range, of the device, with higher spectral response. A more detailed discussion on this process and its practicalities as a method to enhance PV performance can be found in Richards' [36] paper and the references therein.

1.5.3 Upconversion: Introduction

UC is a process in which multiple lower energy photons, or even phonons, interact with an electron, which leads to the emission of a photon with an energy higher than the individual photons absorbed. This process is the opposite of DC and has the capacity to absorb photons that are transparent to the cell which would otherwise be unutilised. Furthermore, it is described as an anti-Stokes process, due to the convention of the Stokes' principle. The majority of research in this area before the 1960's was based on the excitation of trapped electrons via phonons with energy on the order of a few kT [37]. When UC was first conceptualised by Bloembergen [38] in 1959, it was suggested that rare earths (RE^{3+}) or transition ions could be doped into a host lattice to achieve UC with potential applications as *infra*-red (IR) quantum counters. UC is now used in many areas of optical based research such as 3D displays [39], lasers [40] and biological imaging [41].

More specifically, in relation to the application of a PV device, an UC layer can be coupled to the rear of a PV device to absorb light transparent to the cell and emit the upconverted photons back to the device generating charge carriers, see Figure 1.6. The simple three-level energy UC system in Figure 1.6 shows how the energy of two IR photons is converted to a higher energy photon. UC is shown to be more effective with an advantage over DS and DC systems as it does not interfere with the incident spectrum for which, the device has been optimised. The quantum efficiency is however limited to 50%, as at least two photons are absorbed for the emission of one higher energy photon. Since the device and the UC layer are not electrically connected, the

configuration does not limit the performance of the overlying device with all improvements absolute. Furthermore, escape cone losses can be reduced by using a reflector on all sides UC layer which is not possible with DS or DC.

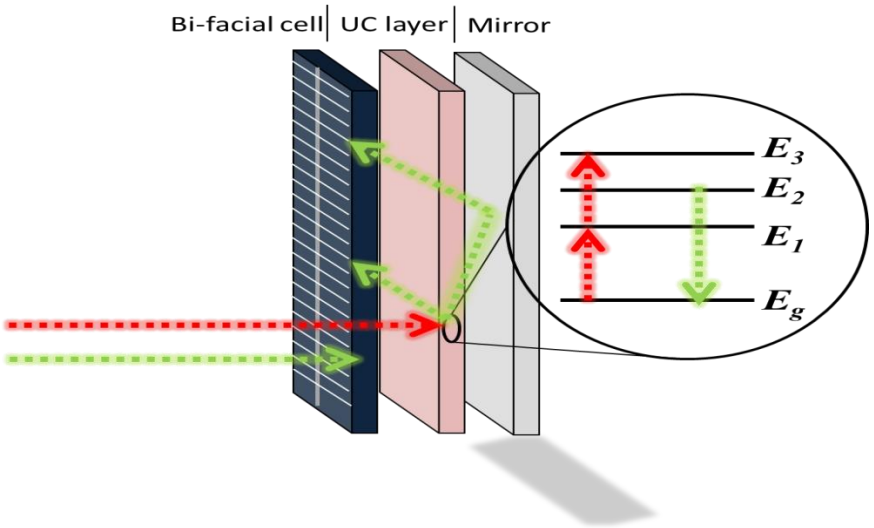

Figure 1.6 Schematic diagram of an upconversion photovoltaic device with rear reflector. A basic two-photon UC process in a 3-level system which shows the IR radiation (red arrows) transmitted by the cell can be converted (green arrows) and re-directed to the cell.

UC has predominantly been shown via the use of (RE^{3+}) ions. More recently, the use of actinides and transition metals [37] as well as organic compounds such as metallated porphyrin macrocycles (MOEP) [42] have also been explored. RE^{3+} doped UC materials have been the preferred choice for integration with c-Si PV devices due to the desired range of absorption and emission. Lanthanides (Ln^{3+}), part of the RE^{3+} group, are now receiving more interest in the field of PV for their DS [43], DC [44] and UC [45] properties. Furthermore, the Ln^{3+} erbium (Er^{3+}), has been used in many applications such as lasers [46, 47], optical amplifiers [46, 48-51], sensors [52] and solar energy harvesting [53-59]. This is due to a convenient energy ladder with resonant transition steps of 1540 nm allowing IR excitation into the visible or UV wavelengths. Er^{3+} is suitable for solar energy harvesting as the AM1.5G spectrum has ~25 Wm^{-2} in the lower absorption range of the phosphor (1480-1580 nm) [54]. Ln^{3+}'s are often found in the trivalent state hence, have the donation 3+. Optical properties of these ions are due to their $4f^n$ valance band transitions, where *n* represents the number of valance electrons (Ce^{3+}=1 to Yb^{3+}=13), and are only weakly affected by doping into a host lattice. This is because of the shielding effect of the *5s* and *5p* outer electron shells.

The work conducted by Dieke [60], which is now commonly known as the Dieke diagram, is often referenced to display the manifolds associated with the plethoric energy transitions observed for these free ions.

With regard to Ln^{3+} ions, transitions within the inner *4f* electron shell are parity forbidden, Laporte rule, which are only accessible due to odd components of the crystal field at the local site of the active ion or phonons [37]. The free ion energy levels undergo Stark splitting due to interactions with the crystal field of the host lattice. Because these transitions are forbidden this leads to weak absorption of sub-band gap photons, approximately 6 cm^{-1} at the peak resonant wavelength of Er^{3+} doped within the efficient host crystal lattice, hexagonal phase sodium yttrium fluoride (β-$NaYF_4$:Er^{3+}) [61]. Therefore, to achieve high efficiencies in UC-PV devices high values of irradiances are needed to overcome low absorption coefficients and the non-linear UC process. This has led to characterisation of both materials and UC-PV devices with high power monochromatic sources to attain higher efficiencies. However, UC can be achieved with bandwidths of 100 nm which would indicate that similar efficiencies could be achieved at lower powers of excitation if a broader spectrum of illumination is used. New methods are therefore required to investigate these materials under broadband excitation to truly understand their performance and the potential impact this technology will have on enhancing the IR response of Si solar cells. Hence, the work conducted herein will focus on the development of a new method to evaluate the efficiency of the UC process under broadband excitation similar to that encountered in their application. Hitherto, this method will then be applied to optimise and evaluate UC materials applied for the enhancement of c-Si PV devices.

1.6 Summary

There is a clear need for renewable technologies to harness clean energy to supply the increasing energy demand of human activities. This can be met by the vast potential for harvesting the radiant energy of the sun through PV devices. However, there are still limitations on the conversion of solar energy into electricity due to mismatch in the absorption of the semiconductor materials used and the incident solar spectrum. These losses have been explored and discussed as well as the generations of research in PV technology which aim to increase efficiency. PV research is now in its third generation which looks to surpass the S-Q limit to achieve a cost of generation below 0.2 $/W. The motivation for the research into upconversion is to mitigate the spectral losses from

photons, which are transparent to the cell and account for 20% of the sun's energy to overcome the S-Q limit of 30%.

Upconversion is however, limited by its non-linear nature which is further compounded by the absorption properties of the most commonly used luminescent species Er^{3+}. Due to these limitations, characterisation of their optical performance has been conducted with high power lasers at the peak absorption wavelength of 1523 nm to achieve improved efficiencies. These methods are unlike the illumination conditions expected for the application of UC-PV devices. Thus, there is a need to characterise these UC materials under broadband excitation, more similar to the sun, to understand their potential for enhancing Si solar cells response.

1.7 Aims

The main aims of this thesis are as follows;

- Develop a method for measuring the *iPLQY* of UC phosphors to better understand their performance under an excitation spectrum more similar to that of the solar spectrum.

- To quantify any differences that an increase in the bandwidth of excitation spectrum has on the performance of an UC phosphor with respect to the solar concentration required to achieve this.

- Optimisation of the Er^{3+} concentration in the efficient host lattice β-$NaYF_4$ as a function of incident solar concentration and under broadband excitation.

1.8 Thesis Outline

The following chapter in this thesis will look at the historic research in the use of UC for PV devices and how this has progressed to current efforts. Firstly, the RE^{3+}'s, which are the most commonly used luminescent species for UC with Si solar cells, will be introduced including the photophysical mechanisms which dictate this process. As for PV devices, an analogous model to that of the S-Q limit will show the theoretical limitations of an ideal UC-PV system. A detailed description will be given on the method for characterising the optical efficiency of the UC process which is necessary

for evaluating the potential enhancement for PV. There are still many challenges in the realisation of an UC-PV device; hence, some of the advanced system designs will be alluded to for understanding the trajectory of future research.

In Chapter 3, the synthesis techniques of the UC materials such as β-$NaYF_4$:Er^{3+} characterised in the later chapters will be described as well as the respective host matrices that are used to bind the phosphor. This chapter will also refer to the equipment used for determining their physical and optical properties as well as the standard methods used in the measurement of these materials.

In Chapter 4, a method has been developed to measure the optical efficiency of luminescent materials under broadband excitation, more similar to that of the solar spectrum. The method has been analysed with regards to the effect of re-emission on the determination of absorptance. Due to the non-linear nature of the UC process with the efficiency, which is further dependent on the doping of the active material, this method is evaluated for a range of irradiances and concentrations.

Chapter 5 will show the first determination of quantitative measurements under broadband excitation. The photoluminescent properties are determined with regards to increasing bandwidths of excitation. The performance of the UC material is evaluated in regards to its application within a working device. These measurements are also analysed in regards to the equivalent solar concentration. This is necessary for a more tangible understanding of the practical conditions to achieve a desired performance and why this method is important for investigating UC materials for PV applications.

Chapter 6 focusses on the characterisation and optimisation of an efficient UC material using the newly developed method for broadband excitation. The optimum doping of the UC material is determined in regards to a wide range of powers of excitation and a different optimum is found in comparison to the literature. The relevance to previous methods of characterisation is discussed and what advances in this technology are required to realise a working UC-PV device.

In the last Chapter the overall conclusion will be given in regards to the research which has been undertaken as well as the impact this has had on the field of UC-PV. A

discussion on possible future work which can be developed from this thesis will also be given. Finally, some projections will be made on where research in UC-PV will likely be heading through the use of integrated advanced light management techniques.

CHAPTER 2 - PROGRESS IN UPCONVERSION-PHOTOVOLTAICS

2.1 Introduction

In this review chapter, the progression to current research in the field of UC-PV devices will be discussed in detail. This will aid in contextualising the investigation conducted within this thesis and its contribution to advancing the understanding of UC-PV technology. The dominant mechanisms, which dictate the non-linear photoluminescent properties of these materials, will first be explored to comprehend later discussions on their performance. Section 2.3 will include the theoretical model, comparable to the S-Q limit, which determines the efficiency limit of an ideal UC-PV device. The remainder of this section will give a detailed review of UC-PV devices from conception to the contemporary. This will include the important advances and techniques which have enhanced their performance. Section 2.4 will focus on material optimisation through the controlled doping of the UC phosphor. In section 2.5 a review of the optical characterisation methods that are developed further in this thesis is presented. Additionally, an indication of how these techniques are advancing to better represent the illumination conditions of a working device will be explained. The necessity of photon management and advanced systems which combine geometric, optical, and photonic phenomena as a solution to the limitations so far encountered for UC-PV will be described in Section 2.6.

2.2 Upconversion Mechanisms

There are several mechanisms that dictate the UC process and hence, its effectiveness in enhancing the performance of the coupled PV device. These mechanisms are dependent on; 1) the irradiance of excitation, 2) the *4f* energy transitions of the Er^{3+} ion, and 3) the effect of the host lattice on the properties of the doped Er^{3+}. Hexagonal phase sodium yttrium fluoride (β-$NaYF_4$) is one of the most efficient host lattices for Er^{3+} reported in the literature and is the predominant material used for investigation within this thesis. Therefore, the UC mechanisms discussed below will be described with regards to this host and its properties which make it so efficient.

The absorption of sub-band gap photons is the primary prerequisite for an UC process, shown in Figure 2.1 as ground state absorption (GSA). Figure 2.1 shows the energy levels and the possible transitions within the Er^{3+} ion, which randomly substitutes for

Y^{3+} in the host lattice of β-$NaYF_4$ matrix. As mentioned previously, the optical properties of these ions are due to their $4f^n$ valance band transitions, which are parity forbidden, leading to weak absorption (6 cm^{-1} at 1523 nm in β-$NaYF_4$: 20% Er^{3+} [61]). However, the crystal field and phonon energies of the host can influence these transitions within the Er^{3+} ion. Specifically, in the efficient UC phosphor β-$NaLnF_4$ (Ln =Y, La-Lu) there are two lanthanide sites with microscopic disorder which cause an extraordinary inhomogeneous broadening of the energy transitions [62]. This leads to a wider absorption spectrum (~100 nm) and improved energy transfer from an increased overlap of interacting energy levels, beneficial for harvesting a greater fraction of the sub-band gap photons. Phonon broadening also contributes to increase the photon energies that can be absorbed within a given host lattice. However, if the phonon energy of the host is too high this can also lead to a reduction in emission. Due to the almost evenly spaced energy levels in Er^{3+}, NIR, visible and UV UC emission is possible with monochromatic excitation with the highest absorption cross section at 1523 nm [63]. This has resulted in the characterisation of β-$NaYF_4$: Er^{3+} conducted predominantly with monochromatic lasers [54, 55, 57], rather dissimilar to the broadband illumination, such as the sun, encountered by a working UC-PV device.

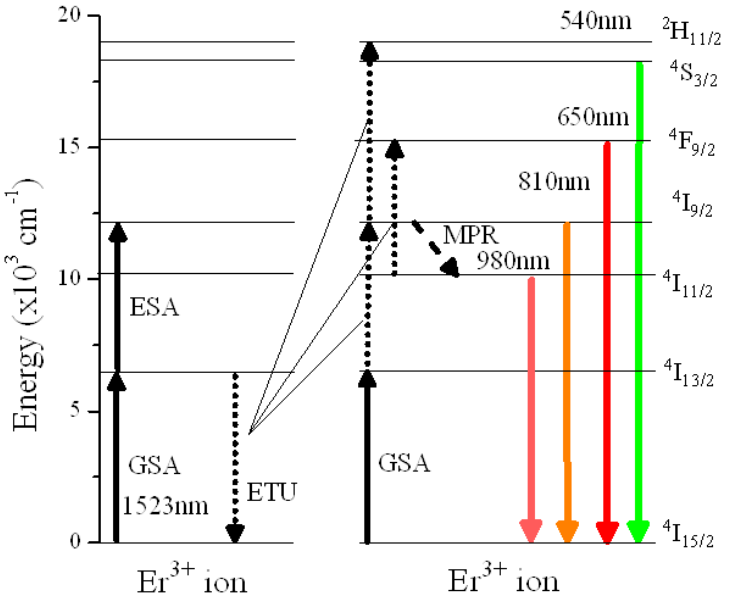

Figure 2.1 Energy level diagram that describes the possible UC processes such as ground state absorption (GSA), excited state absorption (ESA), cross relaxation (CR), multi phonon relaxation (MPR) and energy transfer upconversion (ETU) for Er^{3+} ions. Possible two- and three-photon emission processes are also displayed under resonant 1523 nm excitation.

UC is a non-linear process due to the necessity for the absorption of at least two lower energy photons for the subsequent emission of each higher energy photon. This can occur through sequential ground state absorption (GSA, $^4I_{15/2} \rightarrow {}^4I_{13/2}$) followed either by excited state absorption (ESA, $^4I_{13/2} \rightarrow {}^4I_{11/2}$ or $^4I_{13/2} \rightarrow {}^4I_{9/2}$) or energy transfer upconversion (ETU; $^4I_{13/2} \rightarrow {}^4I_{9/2,}$ $^4I_{11/2} \rightarrow {}^4F_{9/2}$ and $^4I_{9/2} \rightarrow {}^2H_{11/2}$) as depicted in Figure 2.1 for Er^{3+} ions. The small energy difference of about 2000 cm^{-1} between the $^4I_{9/2}$ and $^4I_{11/2}$ levels leads to non-radiative (NR) decay through multi phonon relaxation (MPR) and the dominant emission at 980 nm. The MPR is considerable for small energy level transitions which are up to six times the phonon energy of the host lattice. The maximum phonon energy in the β-$NaYF_4$ host is approximately 355 cm^{-1} which helps reduce NR decay compared to oxide hosts with maximum phonon energy typically around 600 cm^{-1} [55]. Although emission from higher levels is possible ($^4F_{9/2}$, $^4S_{3/2}$ and $^2H_{11/2}$, for example) these involve a greater number of photon interactions and are inherently less efficient. The emission at 980 nm, from IR excited UC in β-$NaYF_4$:Er^{3+}, contributes to 97% of total emission [64] and hence the charge generation in an overlying Si PV device.

The first UC mechanism, GSA followed by ESA, occurs within a single ion. This requires the absorption of the second photon within the lifetime of the intermediate excited state, which is typically in the milliseconds range for β-$NaYF_4$:Er^{3+} [65]. This process has been shown to be inherently less efficient than ETU [37]. ETU in the Er^{3+} system occurs between different ions, a sensitiser (or donor) and activator (or acceptor), which are both originally in the first excited state (usually populated through GSA). The relaxation of the sensitiser results in the transfer of energy to the activator non-radiatively. The probability of the ETU process, the dominant mechanism for β-$NaYF_4$:Er^{3+} [54, 66], is dependent on the ion-ion separation as well as the population density of the intermediate energy level. It is therefore governed by the Er^{3+} concentration within the host lattice and the irradiance, which makes these parameters critical for UC-PV optimisation. Although the coefficient of ETU is independent of the irradiance, the ETU rate is dependent; hence, UC emission and efficiency are power dependent. Furthermore, energy transfer mechanisms (such as ETU), absorption and the internal photoluminescent quantum yield, *iPLQY*, which is defined as the number of photons emitted to those absorbed, are all concentration dependent. Therefore, it is important to evaluate the optimum concentration under a range of irradiances to determine the most effective material for UC-PV application within a working device.

The reverse of the ETU process can also be responsible for the depletion of the UC emission due to cross relaxation (CR). In this process an ion in the higher excited state relaxes to the intermediate level with NR energy transfer to a neighbouring ion in the ground state, see Figure 2.2. Energy migration from one ion to another through the material can also increase the probability of NR decay at a defect site [67]. All of these mechanisms depend on lifetimes of the excited states, the irradiance and the concentration of ions. This is because ETU and co-operative effects depend on Coulomb, dipole-dipole, dipole-quadrapole and quadrapole-quadrapole interactions and the characteristic distances that these occur for each. Therefore for high concentrations absorption is increased but this can also lead to luminescent quenching due to NR relaxation.

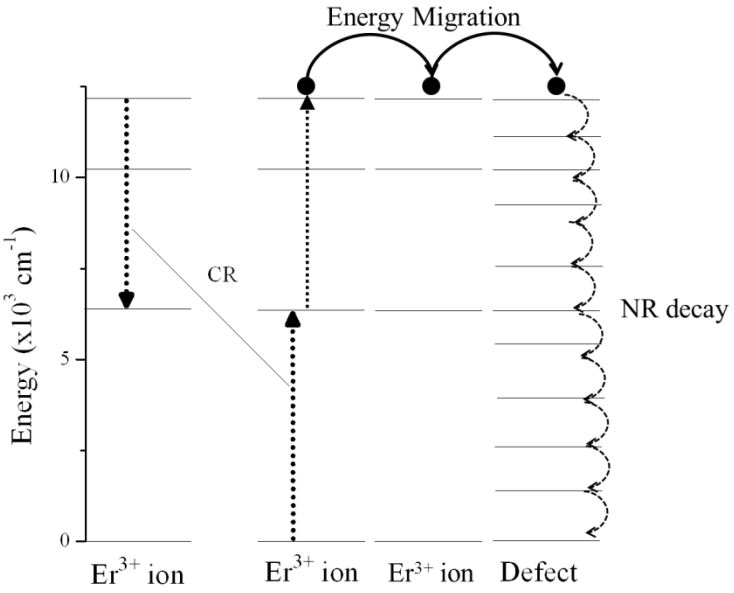

Figure 2.2 Cross-relaxation due to high concentrations of Er^{3+} ions in an upper excited state leading to luminescent quenching. Energy migration to a defect site followed by non-radiative decay is also shown.

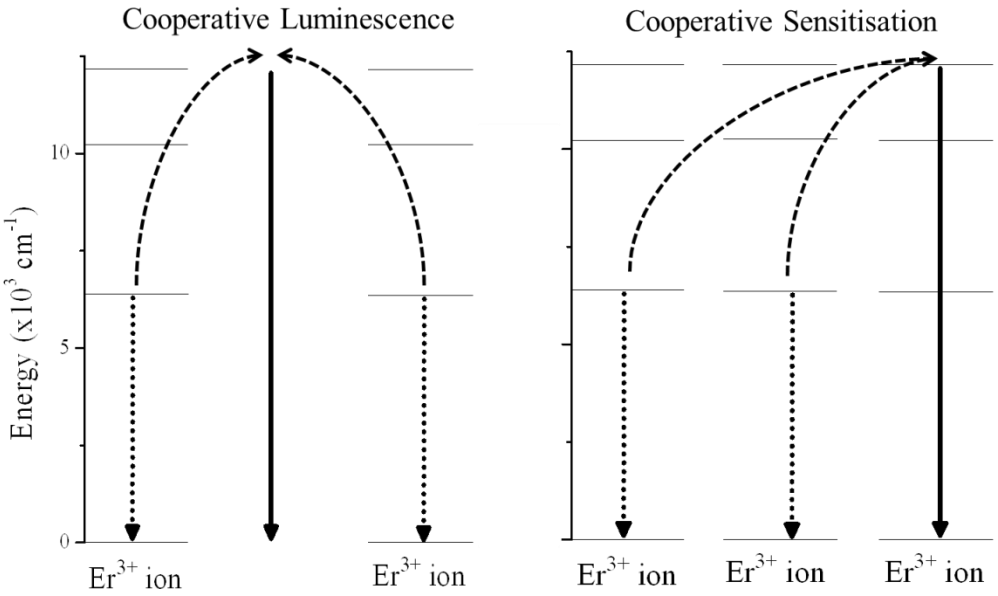

Figure 2.3 Schematic diagram displays the difference between co-operative sensitisation and luminescence UC mechanisms [55]. The main difference is that co-operative luminescence involves an imaginary energy level rather than a real one.

There are also other UC mechanisms such as; co-operative sensitisation, co-operative luminescence, second harmonic generation (SHG) and two-photon absorption (TPA), of which the former two are shown in Figure 2.3. Co-operative sensitisation occurs when two sensitizer ions transfer their energy to a third ion. This is different to co-operative luminescence whereby two excited ions combine their energies for emission of UC radiation. These UC mechanisms are less efficient than ETU and ESA. Therefore, the materials that are dominated by less efficient mechanisms are not chosen for their application within UC-PV systems.

An understanding of the non-linear processes which govern the emission of upconverted light has been given above. This is important for understanding the material properties which affect the efficiency of this UC process, thus impacts the development of an optimum UC-PV device. In the next section, the theoretical limit for an UC-PV device will be described including an overview of applied research which aims to meet these targets.

2.3 Upconversion-Photovoltaic Devices

2.3.1 Upconversion Modelling: Detailed Balance Limit

It is important to know how an UC layer interacts with a PV device so as to determine the limiting efficiency associated with UC as a process. The aim to reduce sub-band gap losses to surpass the S-Q limit, important for third generation technologies, can therefore be evaluated. Work carried out in 2002 by Trupke *et al.* [68] analysed the limiting efficiency of a 3-level UC system placed at the rear of a PV device, similar to that shown in Figure 1.6. This was inspired by previous work conducted by Wolf [69] on impurity photovoltaics and the demonstration of a working UC-PV device by Gibart *et al.* [70]. The model was based on a detailed balance analysis of a bi-facial cell optically coupled to an UC layer with an ideal mirror at the rear. This model can be compared directly to the S-Q limit as it is based on the same principal laws of physics through the analysis of detailed balance. The model was designed to be representative of the GSA/ESA UC mechanism. It is convenient to describe the analogy equivalent circuit of the system to better understand the modelled process, which is shown in Figure 2.4.

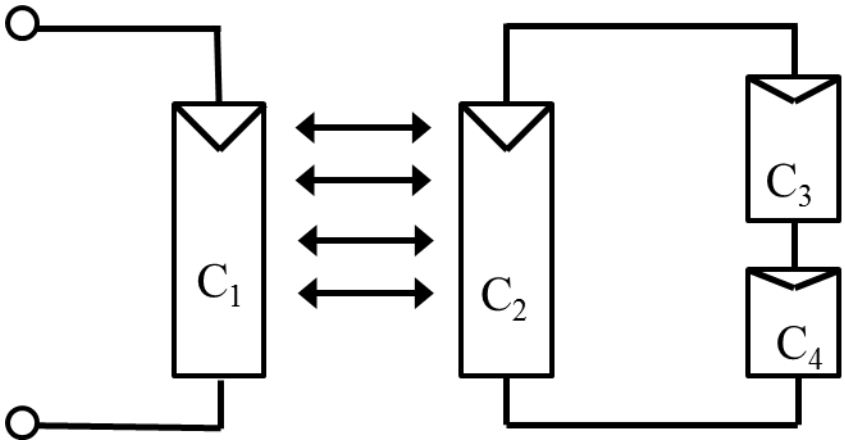

Figure 2.4 Adapted from Trupke et al. [68] showing the equivalent circuit of the proposed UC-PV system. C_1 can be thought of as the solar cell at the front and C_2 a diode or the source of UC radiation that illuminates C_1. C_2 is powered via currents generated in C_3 and C_4 which represent the intermediate transitions of the UC process.

This model can be thought of as a solar cell C_1 receiving light from a large band gap light emitting diode (LED) C_2. C_2 emits upconverted photons that generate carriers in C_1. C_2 is controlled by two PV cells, C_3 and C_4, which have energy less than C_1 hence, absorb the transmitted photons. Results assumed a highly idealised system with an

optimised energy level configuration and without non-radiative decay. These assumptions are not relative to a practical device but serve a purpose in establishing the limits that cannot be overcome regardless of best performance. The limiting efficiency was calculated to be 61.4% for the highest possible solar concentration of 46 x10^3 Suns. Again, the maximum level of solar concentration modelled is impractical. The best performing PV devices measured (see Figure 1.3) have only achieved concentrations of 924 suns, with 100's of suns more common place. As expected, due to the non-linear UC response, higher efficiencies were predicted for higher concentrations with only marginal increases expected for non-concentrated sunlight. Significant improvements under non-concentrated sunlight were calculated if thermalisation to a non-radiative state was to occur; therefore leading to an efficiency of 47.6%. Although these efficiencies are cited in the literature they are purely theoretical. In regards to a practical device, such as the record cell from Amonix with an efficiency of 27.6% for a c-Si cell under a concentration of 92 Suns [22]; an UC-PV efficiency limit of 38% is achievable under a concentration of 100 Suns for a material with an E_g of 1.1eV [68]. Therefore, significant enhancements are possible under achievable solar concentrations and operating conditions.

The model was later evaluated in further detail by Badescu and Badescu in 2009 [71]. Here, consideration on the effect of different refractive index (*n*) of the PV device and the UC layer was analysed. Analysis was also conducted on the effect of placing the UC layer at the front or at the rear of the device. It was shown that a difference in the refractive index of the UC layer and PV device had significant effect on the photon flux exchanged between the two. A higher refractive index of the PV device was beneficial and no improvement was seen for UC layer in front of the cell. Other advances such as the consideration of non-ideal devices and UC systems have been incorporated in to this model but conclusions still remain that an UC can only increase the efficiency of a coupled PV device [72]. Johnson and Conibeer [73] developed this method explicitly for c-Si devices and incorporated more realistic material parameters such as free carrier absorption. They estimated that, similarly to Trupke *et al.* [68], an ideal UC layer could enhance a Si solar cell from 33% to 40% efficiency.

The theoretical limits derived by Trupke *et al.* [68] show a significant potential to raise the efficiency of single junction cells well beyond the S-Q limit. The model and its derivatives also give some of the important considerations for achieving such a

performance for an ideal UC system however, so far the practical devices have not achieved this potential. The applied research will now be discussed to explain some of the practical limits which are necessary to overcome to meet these targets.

2.3.2 Erbium-Based Upconversion-Photovoltaics

The first paper published on an UC-PV device was by Gibart *et al.* in 1996 [70]. Although two-photon UC had been known for around 30 years this is the first account of combining this effect with a GaAs substrate-free solar cell (or any other solar cell). The benefit of using GaAs as the PV device is that it has a large band gap of 1.45 eV, compared to Si of 1.1 eV, and therefore suffers from greater transmission losses; hence, a greater fraction of the solar spectrum is available to upconvert. The UC-PV device consisted of an UC material, synthesised by co-doping a 100 µm thick vitroceramic with Yb^{3+} as the sensitiser and Er^{3+} as the activator, attached to the rear of a substrate-free GaAs solar cell. This also included an Au back reflector to reduce UC photons escaping from the rear of the device, shown in Figure 2.5. The device was characterised via 1.391 eV excitation and exhibited green and red UC emission. This of course would not be possible with c-Si device due to its strong absorption at this photon energy. Results showed that using a Ti-sapphire laser with an irradiance of 25.6 Wcm^{-2}, an efficiency of 2.5% with a quadratic dependence on input power [70] was observed. The UC emission process was attributed to ETU, the most efficient UC mechanism. However, due to the limited enhancement from the UC layer the device was deemed not to be efficient enough for PV application by the authors. Furthermore, as the ETU process is due to the resonance between the $^2F_{5/2}$ (Yb^{3+}) and $^4I_{11/2}$ (Er^{3+}) manifolds which implies that GSA/ESA in the Er^{3+} ion could also be a possible contribution. It is worthy to note here that a Bragg reflector, another term for a 1-D photonic structure, was also proposed as a possible technique to improve absorption in the device. The use of photonic structures is only now becoming a popular area of research for the enhancement of UC-PV devices [74, 75] and is discussed in more detail in Section 2.6.5.

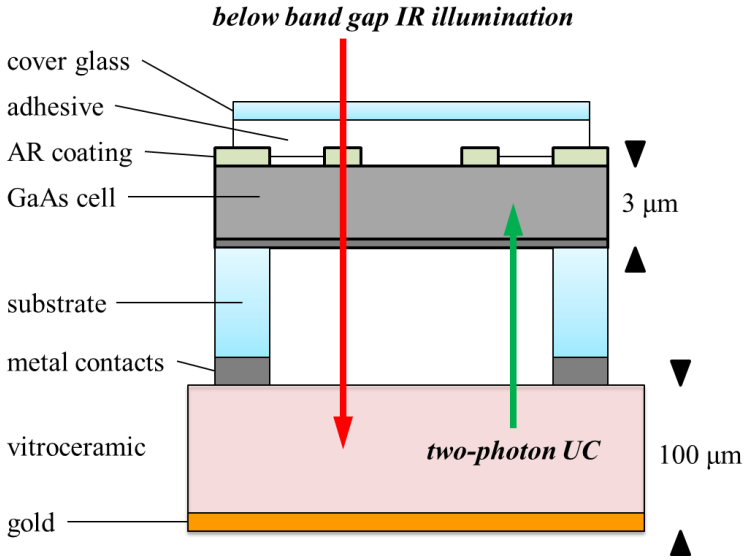

Figure 2.5 Schematic representation of the first UC-PV device adapted from Gibart *et al.* [70]. The PV device includes a cover glass adhered to the anti-reflection (AR) coating of a 3µm thick GaAs cell. The UC vitroceramic is attached after the metal contacts and has a gold reflector at the rear.

The next notable investigation in this area was not until 2005, when Shalav *et al.* [53] reported on the use of Er^{3+} doped β-$NaYF_4$, an UC phosphor for enhancing NIR response of a BF Si solar cell for the first time, see Figure 2.6. The micro-crystalline host lattice was chosen because it is optically inactive and acts to control the phonon energy related to NR decay. Hence, a reduction in NR decay in comparison to an oxide host would be expected. This material further enhances UC by reducing saturation effects, such as CR, by decreasing clustering of Er^{3+} ions while improving its absorption through higher doping ratios. Measurements focused on determining the absorption coefficient of the phosphor and the external quantum efficiency (EQE; defined by the number of electrons generated to the number of incident photons) of the UC-PV device as a function of wavelength and pumping power. Excitation was in the wavelength range below the band gap of Si and lying in the absorption band of the $^4I_{15/2} \rightarrow {}^4I_{13/2}$ manifold of the Er^{3+} ion. Two excitation sources were required to cover the Er^{3+} absorption spectrum; a QTH lamp between 1480-1580 nm and from 1510-1590 nm a tuneable laser was used with the additional benefit of achieving higher powers. It was shown that the wavelength dependent excitation spectra, up to a five-photon process using a tuneable laser, matched well with the absorption shape of the $^4I_{15/2} \rightarrow {}^4I_{13/2}$ transition; supporting the conclusion that ETU is the dominant UC mechanism in Er^{3+} doped β-$NaYF_4$ as otherwise a convolution of the GSA and ESA line shapes would have been observed [55]. This was further supported by the quadratic relation,

determined at lower powers, between I_{sc} and pump power showing a two-step UC process. The device was calculated to have an EQE of 2.5% at an excitation wavelength of 1523 nm with an incident power of 5.1 mW. Moreover, it was also determined by eye that 3-step upconversion with green emission was onset >2.2 mW excitation power. This is confirmed by the deviation of the quadratic relation with regards to the incident power. However, it is essential that the area of illumination should be characterised to determine the irradiance due to the non-linear nature. This work was developed further with results presented by Shalav *et al.* [54] where an increase in efficiency to 3.4%, compared to previous work, attributed to a better back reflector material, host matrix material embedding and attaching the UC layer to the front of the BF cell which had an intrinsically higher efficiency. The latter increase, however, is impractical for a working device as the layer should always be placed at the rear; although this indicated the importance of the cell to efficiently receive the UC emission and for good optical coupling.

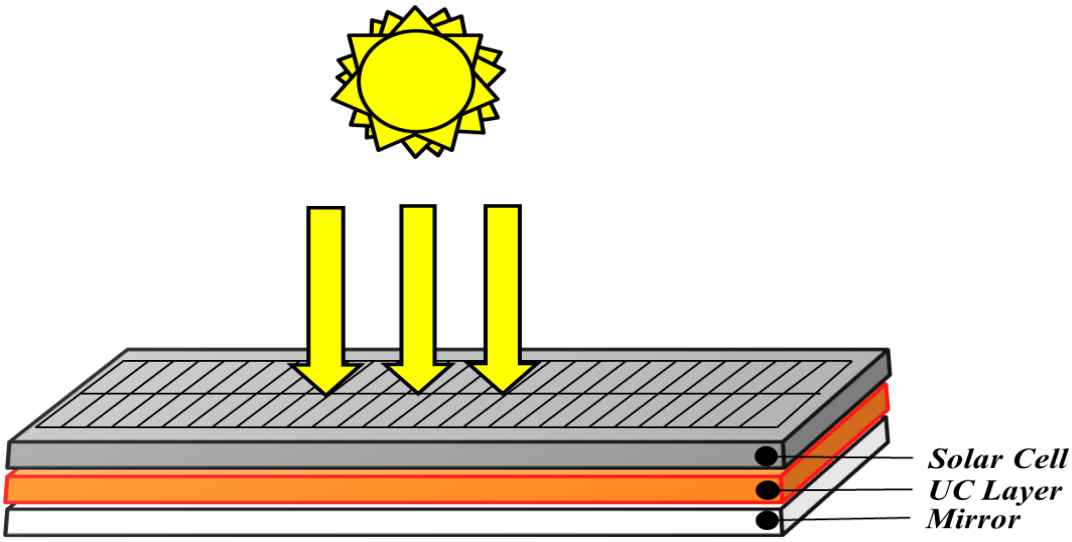

Figure 2.6 A schematic diagram of UC-PC device used by Shalav and Richards, adapted from[56].

The work of Shalav *et al.* [53, 54] initiated a renewed interest in the field UC-PV due to the improvements made in system design which, stimulated further advancements and understanding. The detailed balance analysis of Trupke *et al.* [68] , discussed in section 2.4.1, was developed further by Trupke *et al.* [76] taking into consideration AM1.5G (rather than the ideal 6000 K blackbody) illumination and UC robustness with increasing AM up to 10. The performance of the UC system improved with modelling of a more accurate incident spectrum. Comparisons were also made with intermediate

band solar cells, which can be described by the same equations of detailed balance theory. UC was shown to be significantly more efficient as a third generation technology both theoretically and through best experimental results. This work was further supported by Richards [56] where it was shown that UC can outperform tandem stack devices at higher AM values due to the red shift in the solar spectrum. Further results on applied UC-PV devices in collaboration with Shalav also showed that intermediate band solar cell efficiencies achieved to date were a factor of five lower in relation to UC-PV [77].

Work conducted by Fischer *et al.* [57] has shown one of the most comprehensive studies to date in relation to an actual working device using β-$NaYF_4$ as the crystal host for Er^{3+}. Electrical characterisation of the UC-PV device was conducted with the luminescent properties extrapolated with a detailed consideration of all the possible loss mechanisms. Fischer *et al.* also achieved the highest UC EQE at the time (0.34% under 1090 Wm^{-2} at 1522 nm) in relation to the excitation intensity used which is 0.03 cm^2W^{-1} and approximately 2.2 times greater than that achieved by Shalav. Although in absolute terms this is less than what was achieved by Shalav, a suggestion of defining efficiency in relation to incident power does make this more "efficient". The reason this value is used is to help compensate for various materials under different levels of irradiance since the UC process is non-linear. Fischer *et al.* [57] extrapolated the UC quantum efficiency that would be achieved for 1523 nm excitation wavelength (0.27 cm^2W^{-1}) with 1880 Wm^{-2} intensity to be 5.1%. These results were not measured directly but were calculated by taking into account reflection at the solar cell, reflection of the UC light, non-uniform illumination, nonlinear response of UC (< 0.5 Suns) and the absorption and processing of the binding material. Experiments were also conducted on the dependence of excitation wavelength and power on the UC efficiency. This analysis showed that 810 nm and 660 nm, which are two and three-photon processes, respectively, are only present under excitation powers greater than 100 and 250 Wm^{-2} respectively. However, it is still apparent that low absorption of the Er^{3+} is a major factor in NIR UC performance.

Research was later conducted into the use of other host materials for Er^{3+} such as the fluorozirconate (FZ) glass by Ivanova and Pellé [78, 79]. The FZ glass exhibits relatively low phonon energy (500 – 600 cm^{-1}) and an inhomogeneous broadening of the absorption band due to its amorphous structure. These are important characteristics

to reduce NR decay and to improve absorption of the IR radiation as well as an increased overlap in the ETU energy levels. Although other glasses such as bromides (175 - 190 cm^{-1}) and chalcogenide (200 - 300 cm^{-1}) also have lower phonon energies to reduce NR decay [36], fluorides are more easily processed in the lab with greater long term stability. The concentration of Er^{3+} that were studied were 2 and 5% which are 10 or 4 times less than that studied by Shalav *et al.*, respectively, [53] which would lead to lower absorption. This has the advantage of reduced clustering of ions and therefore reduced quenching of luminescence. Using experimental results combined with theoretical analysis it was shown that the upper efficiency limit for 5% Er^{3+} doped FZ glass as a material for IR enhanced solar cells would be 12.7% with 44% absorption of incident light at 1532 nm [78]. Although this paper reported good progress in the understanding of UC-PV devices it was later criticised by Liao [80] for using concentrations of light far beyond the physical limit possible (> 46 $x10^3$ Suns). Liao also showed an alternative to the classification of UC materials in their application to PV. It was proposed by Liao that different UC materials may perform differently under different concentration conditions where one is not a prerequisite for the other. This supports that the performance of these materials and their characterisation must be normalised to the solar concentration used for excitation first suggested by Auzel [37].

2.4 Material Optimisation

For the realisation of a successful technology it is essential to optimise the system to achieve the best performance. As UC is a non-linear process the doping of the active Er^{3+} ion is critical in this regard. The luminescent species dictates the absorption of IR excitation and the UC mechanisms to achieve spectral conversion. The first investigations to determine the optimum Er^{3+} concentration in β-$NaYF_4$ host lattice for Si PV devices under monochromatic excitation was conducted by Shalav *et al.* [55]. Although, the concentrations measured were 2%, 20%, 50%, 100% Er^{3+} and even included co-doping with Yb^{3+}, this cannot be considered systematic in determining the optimum doping. The optimum doping of 20% Er^{3+} was determined through EQE measurements by coupling the UC material within a transparent rubber matrix to the front of a BF Si solar cell. It was demonstrated from the samples studied that 20% Er^{3+} had the highest EQE of 3.4% for 1523 nm excitation at 6 mW and an equivalent IQE = 5.7%. Since that initial study, it was widely accepted that β-$NaYF_4$:Er^{3+} is the material of choice and 20% Er^{3+} the optimum concentration for PV applications [57, 81]. However, there was no detailed investigation to see if this could be optimised further.

This was until recently, when Ivaturi *et al.* investigated a wide range of concentrations from 5-75% Er^{3+} under monochromatic excitation to determine both the *iPLQY* and external photoluminescent quantum yield, *ePLQY*, which is defined as the number of photons emitted to those incident [66]. Further to this, the ratio of phosphor to host matrix was also varied to determine an optimum loading. This work showed that 25% Er^{3+} at an irradiance of 970 Wm^{-2}, when embedded within a fluorinated polymer host, exhibited the highest *iPLQY* and *ePLQY* with values of 8.4%, equating to a normalised efficiency of 0.86 cm^2W^{-1}, and 6.5% (0.67 cm^2W^{-1}), respectively. Due to the non-linear nature of the UC process it is important to normalise all values of efficiency to the irradiance used in excitation [37, 57].

In a separate study, Fröhlich *et al*. measured the *ePLQY* under broadband illumination for concentrations between 5-40% Er^{3+} using a halogen lamp [82]. This was an important advancement in the optimisation of this material using an excitation spectrum better matched to that of the sun. However, the dependence of *ePLQY* on the irradiance was only conducted for β-$NaYF_4$: 20% Er^{3+} while 25% Er^{3+} was determined to be the optimum. There was also no further analysis conducted to determine why 25% Er^{3+} was found to be the optimum concentration. Unfortunately, it was not possible to determine the absorption of the materials investigated due to the use of broadband excitation which meant *iPLQY* values were not reported, which is often the case. The importance of broadband excitation and its effect on sample optimisation will be reviewed in section 2.5.2.

In the case of organic upconverters, where UC is achieved through triplet-triplet annihilation (TTA) for PV devices, it has been presented that both the incident power and the concentration of the fluorophores are the key parameters to improving efficiency [83]. The UC materials used in this study were palladium porphyrin sensitisers (PQ_4Pd and PQ_4PdNA) with rubrene as the emitter. Although the dependence on incident power was not investigated, a 300-fold increase in the brightness of the upconverter was calculated by increasing the concentration by a factor of 100. In practicality, increasing the concentration by a factor of 100, which is equivalent to a reduction in sensitiser distance of a factor of 4 – 5, is not possible due to aggregation and crystallisation of the porphyrins. These studies show the increasing importance of determining the optimum concentration of the doped upconverter and its potential for enhancing the spectral response of the overlying PV device. Moreover, the

optimisation of the active UC phosphor should always be evaluated in regards to the irradiance of excitation for the comparison of normalised results.

2.5 Upconversion Characterisation

2.5.1 Optical Characterisation: internal Photoluminescent Quantum Yield

The determination of the internal photoluminescent quantum yield (*iPLQY*) – defined as the fraction of emitted photons to those absorbed for luminescent species, also known as absolute or total *PLQY* or even *QY*– is an important photophysical parameter in the evaluation of many optically active materials. Knowledge of the *iPLQY* value is required to determine the optical efficiency of LEDs, colour displays [84, 85], bio-labelling [86], lasers [87], as well as spectral conversion processes for solar energy harvesting [88-91]. The definition of the *iPLQY* requires the accurate and precise measurement of the number of emitted and absorbed photons for a given optical process. Hence, the *iPLQY* is often measured under monochromatic excitation or at least at low bandwidths to reduce uncertainties in determining the absorbance fraction. In the field of UC-PV, this parameter determines the upper limit in performance of the UC layer in regards to the maximum efficiency of 50%. Therefore, the UC phosphor can be optimised within the host matrix and various phosphors can be compared on this merit. The *iPLQY* also determines the maximum optical efficiency and therefore indicates the necessary improvements within the UC-PV device to reach this value. As this is a critical parameter in the evaluation of the UC phosphors used within the PV device this will be discussed in detail below.

The calculation of *iPLQY* is a dedicated task that involves a detailed characterisation of the material under investigation as well as the optical system used for such a measurement. Any factor which may influence the intensity, spectral shape and position of the absorption and/or luminescence spectra must be considered. Therefore the errors and uncertainties associated with these measurements should be evaluated and accounted for. A detailed review of the many factors involved in achieving a reliable measurement can be found by Crosby and Demas [92]. The determination of the *iPLQY* with optical techniques can be measured using a relative method [93], requiring a standard reference material, or absolute method [94]. The former requires a detailed knowledge of the conditions under which the *iPLQY* of the standard was measured, such as 1) the properties of the solvent/matrix host, 2) temperature, 3) concentration of

the luminescent material, 4) accurate and reliable literature values for reference, 5) relative luminescent and absorption spectra at the defined wavelength of excitation. Due to the necessity of a reliable standard this method has been restricted to the visible range, around 300-700 nm; however, this has recently been extended up to 1000 nm [95]. Furthermore, this method is often used for dilute transparent solutions where emission is assumed to be isotropic. Hence, additional computation would be required to account for solid films were wave-guiding, selective alignment of the dipole emitter [96] and significant scattering can occur. This challenge can be more easily overcome with the use of an integrating sphere removing the anisotropy of emission. Combining the integrating sphere with a spectrofluorometer, see Figure 2.7, also negates the use of a standard reference for determining the *iPLQY*, Therefore, an absolute measurement is achieved because both the number of absorbed and emitted photons can be measured directly. However, the spectral response of the integrating sphere and averaging of the emissive intensity must be accounted for. With these considerations in mind an absolute value of *iPLQY* can be measured.

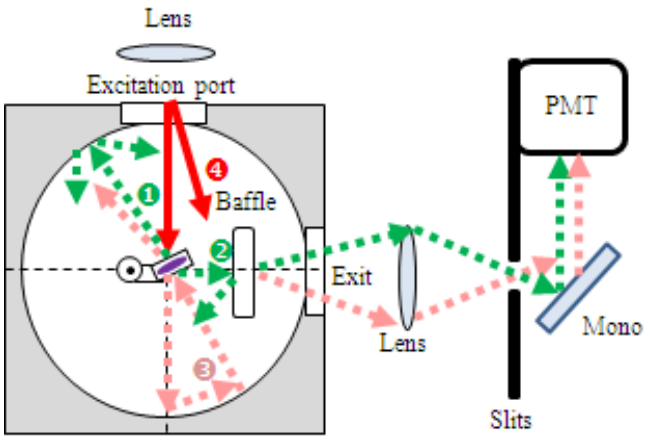

Figure 2.7 Top view of a typical integrating sphere cross section with the sample (purple disk) and sample holder positioned in the centre. The sample is positioned at non-normal incidence to reduce luminescence escaping out the excitation port (arrow ❶) and a baffle is used to remove direct observation of the sample (arrow ❷). Lenses are used to focus the excitation light and in conjunction with motorized slits they are used for spectral bandwidth selection. Furthermore, a monochromator is used for spectral selectivity in the measurement using a detector such as a photomultiplier tube (PMT).

An experimental technique to determine the *iPLQY* of highly scattering samples with anisotropic emission using an integrating sphere has been detailed by de Mello *et al.*

[94]. This method has made it possible to determine *iPLQY* for solid films and powders. Therefore, the range of materials that can be characterised has been broadly increased. One of the most important factors in the absolute method is the requirement of the integrating sphere to have a high diffuse reflectivity, for which the inside is usually coated with Spectralon [97], to reduce the loss in signal and spectral consistency from multiple reflections within while providing an output signal that is an average over all the emission directions from the sample. Figure 2.7 shows a plan view for the experimental set-up of an absolute method using an integrating sphere for the determination of *iPLQY*. This includes a baffle at the excitation port, necessary to remove any preferential observation of the solid angle associated with the anisotropic emission of the sample [98] (Figure 2.7, ray ❷). Furthermore, the sample is positioned at an angle to the incident light to reduce emission and reflection from the front surface escaping from the entrance port of the sphere (Figure 2.7, ray ❶). The *iPLQY* is obtained by the triple measurement procedure conducted with: (a) an empty sphere; (b) the sample present, but not in the excitation path (e.g. arrow ❹ in Figure 2.7); and (c) the sample under direct illumination. This is to take into account additional factors such as illumination from reflections from the sphere walls either from scattered light, transmitted followed by reflected light from the sphere walls (e.g. arrow ❸ Figure 2.7) and also light not incident on the sample (for example, due to the excitation source spot size being greater than that of the sample), which can be absorbed after these events. The formula for the luminescent efficiency is,

$$iPLQY = \frac{P_b - (1-A)P_c}{L_a A} \qquad \text{Equation 2.1}$$

$$A = \left(1 - \frac{L_b}{L_c}\right) \qquad \text{Equation 2.2}$$

where P_b and P_c are the emission of the sample when, firstly, directly illuminated by the excitation and, secondly, illuminated from all angles due to the reflection from the internal sphere walls. The parameter L represents the excitation spectrum when the integrating sphere is empty (L_a), when the sample is directly illuminated (L_b), and when the sphere is illuminated first (L_c). This method was both shown to be suitable for solid and liquid samples. A more recent investigation by Faulkner *et al.* [99] compared the above method with a two measurement procedure, negating the requirement for the measurement of emission and absorption with the sample in the sphere but not under

direct illumination. There it was demonstrated that the above formula can be reduced to [99],

$$iPLQY = \frac{P_b}{L_a - L_b} \qquad \text{Equation 2.3}$$

$$L_b = f\ 1 - A\ L_a + (1 - f)(1 - \mu)L_a \qquad \text{Equation 2.4}$$

where *f* is the fraction of excitation photons which are incident on the sample directly, and μ is the fraction that is absorbed by the sample but after reflection from the sphere. From comparison of the two methods it was shown that there was a very good agreement in the results obtained [99]. However, it was also highlighted, that there are three main issues that should be addressed to determine the absolute *iPLQY* values. First issue being the error associated with the fraction *f*, that can be reduced further by using a lens to focus the excitation beam so that (*f = 1)* all photons are primarily incident on the sample. Secondly, optimization is required so that one can balance low emission, due to dilute concentration and possible weak absorption of the luminescent species, which affects the signal-to-noise ratio (SNR). Third issue is self-absorption, also termed inner-filter effect, which has been shown to influence *iPLQY* values at high concentrations at values typically above an absorbance of 0.1 of the active luminescent species [44, 100]. Self-absorption is also more prominent for materials such as fluorescent organic dyes that exhibit lower Stokes shifts and hence exhibit a greater overlap in the absorption and emission spectrum. This process occurs when an emitted photon is re-absorbed by the sample (one or multiple times) via radiative energy transfer and can therefore reduce the *iPLQY* in the case of a non-unity value. A method on the calibration of self-absorption has been addressed by Wilson and Richards [88], where the emission spectra of a range of fluorescent organic dyes doped in polymer slabs at low concentrations are scaled to match the long wavelength tail, where self-absorption of the emission does not occur, of the red-shifted emission spectra from higher-doped samples. This method has shown excellent agreement for determination of the *iPLQY* of optically dense samples >1000 ppm with their unaffected dilute counter parts of a few ppm [88]. Traditionally, in the measurement of *iPLQY* for organic luminescent materials, with a large overlap in emission and absorption, it is advantageous to excite the sample in a region where there is no overlap between absorption and emission spectra as it is difficult to define absorption if the sample emits in the same region. As

organic luminescent materials have a linear dependence of *iPLQY* with irradiance and it is independent of the radiation wavelength absorbed known as the Kasha-Vavilov rule, it is not necessary to excite such materials at the peak resonant wavelength of excitation.

The measurements of *iPLQY* for solid films has been discussed in relation to materials that respond linearly to irradiance using monochromatic sources of excitation where emission is Stokes shifted to longer wavelengths. This method has also been developed for non-linear processes like anti-Stokes emission through UC. A study by Boyer and van Veggel [101] reported *iPLQY* of UC nanoparticles in comparison to the bulk material for the first time. They used a commercially available spectrofluorometer and integrating sphere of 150 mm in diameter from Edinburgh Instruments to determine the *iPLQY* in conjunction with the method developed by de Mello *et al.* [94]. The values measured were in good agreement with previous reports for the bulk material in the literature [102], which validates this technique for NIR UC. However, there has been increasing interest in moving away from traditional monochromatic illumination towards more solar-like broadband excitation and characterisation of non-linear materials for the enhancement of PV devices through UC of sub-band gap photons.

Ln^{3+} materials with very discrete energy levels have narrow and also weak absorption cross sections due to their parity forbidden transitions. Hence, their optical properties are often defined at the strongest resonant wavelength of excitation. This is compounded by the fact that the *iPLQY* of upconverted light also shows wavelength dependence of *iPLQY*; thus, the traditional motivation to use monochromatic excitation. However, lanthanides such as ytterbium (Yb^{3+}) and erbium (Er^{3+}) can absorb radiation in the broad wavelength range of 900-1050 nm and 1450–1600 nm, [103] respectively. For solar applications it is important to understand the UC efficiency of such materials under broadband excitation similar to the sun. This presents a new challenge in the characterisation of the *iPLQY* as there is a greater overlap between the excitation, absorption and emission of the sample.

2.5.2 Broadband Characterisation

Recently, focus of the UC-PV community has moved towards using broadband excitation to understand the efficiency of UC materials and devices under conditions closer to their application in PV. The first to suggest broadband excitation of UC was Baluschev *et al.* [104] through TTA with organic compounds. In this study the

compound, 9,10-diphenylanthracene (DPA), sensitized with 2 wt% (2,7,8,12,13,17,18-octaethyl-porphyri-nato) Pd(II) (PdOEP) was used. The sensitiser PdOEP are a type of metallated porphyrin macrocycles (MOEP) which are chosen due to the heavy metal centre that increases spin-orbit coupling and thus UC emission[105]. These authors presented no measurements of *iPLQY* for broadband excitation from non-coherent sunlight however; an *ePLQY* of 1% was estimated for broadband excitation at 532 nm with an irradiance of 125 Wcm^{-2}. It is worthwhile to note that the emitter concentration of 2 wt% was optimised in regards to *ePLQY* for reasons discussed earlier. A refined method was presented later [106] which did report *iPLQY* values including optimisation of upconverter concentration. Baluschev *et al.* used MEOPs as sensitisers, similar to co-doping RE^{3+} fluorophores, blended with blue emitters such as polyfluorenes (PF) under broad excitation of ~80 nm and non-coherent sunlight. Although this UC process was suggested as a possible application for PV the absorption band of the system was around 700 nm with emission in the blue, which limits its combination with the most common PV materials such as Si. A quantum tield of 3.2% was measured under low excitation power, around 10 Wcm^{-2} [106] hence, would be more suitable for achieving UC under low solar concentration values which is beneficial to the overall system.

More specifically, using Er^{3+} for c-Si devices, recent work on the EQE of an UC-PV device showed a considerable increase in EQE from 0.71%, at 1523 nm, to 1.07% using a xenon (Xe) lamp for broadband excitation [81]. However, a detailed description of the illumination spectrum was omitted and no extrapolation of *iPLQY* was performed. Therefore, there exists a lack of basic understanding of UC through analysis of *iPLQY* under a controlled broadband excitation spectrum in order to more fully evaluate the potential of UC for Si PV devices under concentrated sunlight. For example several papers have been published on the enhancement of singularly doped β-$NaYF_4$: Er^{3+} [81, 89], as well as co-doped β-$NaYF_4$: Er^{3+},Yb^{3+} [107] and Er^{3+},Yb^{3+} -doped gadolinium oxysulphide (Gd_2O_2S) [108] under broadband excitation. Most of the reported research has focused on the short circuit current (I_{sc}) generation within the PV device [81, 109], the sub-band-gap enhancement of the external quantum efficiency (EQE) [81, 109], or determination of the *ePLQY* of the phosphor [82]. However, the *iPLQY* under monochromatic excitation is rarely reported and even less so for broadband illumination [89]. Therefore, a detailed investigation on both the *iPLQY*, to determine the internal processes and the maximum efficiency possible, and the *ePLQY* for evaluating the overall UC-PV device performance is required to understand the efficiency limits of the

material over a wide range of Er^{3+} doping concentrations. Moreover, as the *iPLQY* of these materials is both power and wavelength dependent, characterisation under broadband excitation is important. The measurement of the *ePLQY* allows the evaluation of reflection, scattering, and transmission, as well as the prediction of the end performance of a complete device. However, the information gained from *iPLQY* is invaluable to understand the internal processes, what limits the performance, and how this can be overcome. Comparisons between these types of measurements illustrate how both *iPLQY* and *ePLQY* are required for a holistic understanding.

2.6 Advanced UC-PV Systems

2.6.1 Secondary Optics

Research in to the application of UC has so far shown that large solar concentrations are necessary to increase the irradiance, and proportionally, the *iPLQY*. The UC-PV device would hence be part of a CPV system to achieve this. A solar concentration of 100 Suns for c-Si devices have been used since an increase in series resistance and associated losses dominates at higher concentrations. Contrastingly, UC-PV research has only seen moderate efficiencies of the UC system at $10^3 – 10^5$ Suns, which leads to a mismatch in the desirable illumination conditions. Therefore, secondary optics, placed between the solar cell and the UC layer has been suggested to allow more common devices to be used. This was possibly first suggested by Strümpel [110] in 2007 by using a slanted rear reflector to focus the light on UC layer with a concentration factor of 2. This was mainly suggested to avoid shading losses from the metalised grid at the rear of the BF cell by selectively localising the UC material which meant the added solar concentration was not the main focus but a serendipitous consequence. A more deliberate optical design involved embossing the rear reflector with Si microspheres to create micro reflectors to focus the light on to the UC layer [111]. This proof-of-principle approach showed a small increase of 20% in comparison to a flat reflector using an organic UC system although; greater improvements of around a factor of 9 would be expected for an optimised design through ray-tracing software. A more relevant investigation using the efficient β-$NaYF_4$: 25% Er^{3+} phosphor carried out a detailed investigation on various types of secondary concentrators such as; objective lens (×100), parabolic (× 2.3) and tapered optics (×28 and ×34), see Figure 2.8 for schematic [112].

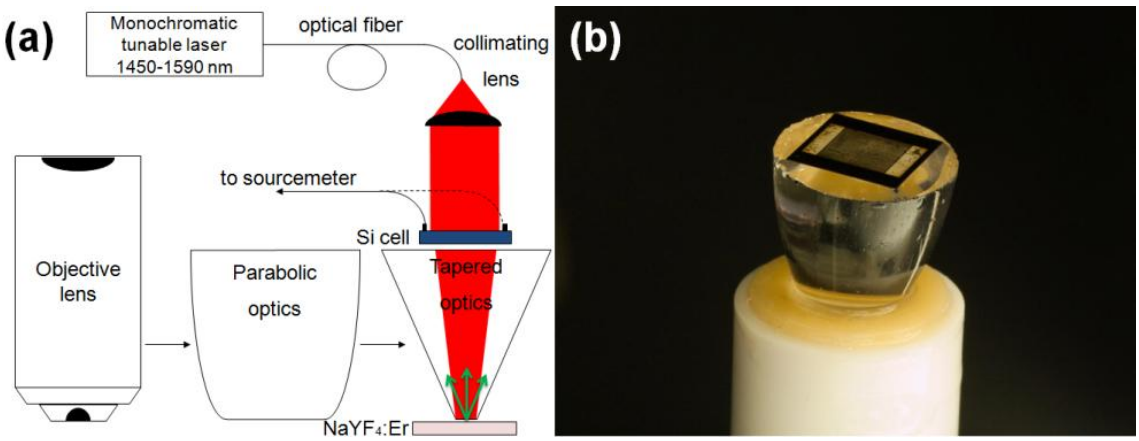

Figure 2.8 Experimental set-up of the UC-PV system under investigation with the range of secondary optics experimented (a), and a picture of the actual system (b) adapted from [112].

The highest performance was achieved with the parabolic reflector, followed by the objective lens, which appears contrary to the hypothesis that the highest concentration would achieve the greatest increase in the coupled Si cell. The transmission properties of the concentrators, in regards to both the excitation spectrum and the emission spectrum, were detailed as the main reason for this difference. This effect is also compounded by the number of reflections undergone between the cell and the UC layer. However, an enhancement in the EQE of 0.075% or equivalently, when normalised to the power of excitation, 3.38×10^{-2} $cmW^{-1,}$ shows the promise of this approach as a technique to overcome the non-linear response.

2.6.2 Spectral Concentration

One of the limiting factors associated with using Ln^{3+} as the UC ions is the narrow absorption range (~100 nm) and low absorption cross section which reduces the fraction of sub band gap photons available for UC. Current work [113, 114] is now focusing on improving the absorption of Er^{3+} via the use of nano quantum dots (QD) such as lead sulphide (PbS), lead selenide (PbSe) or combinations of which are used in core-shell QD's. These have beneficial properties as they have an absorption range from the UV to IR with a relatively narrow emission band (~100 nm). Other important properties such as high quantum yields (~80%) with electronic characteristics that can be tuned by varying their size in the fabrication process also make them suitable candidates for luminescence applications. It has been proposed that QD's can be used to absorb most of the light between the Si band edge and the absorption edge of Er^{3+} which are then re-

emitted in the absorption range of the upconverter [113]. This is shown schematically using the AM1.5G spectrum in Figure 2.9. This has the additional benefit that the QD's can be incorporated into a fluorescent solar concentrator (FSC) which can add geometrical concentration in addition to spectral concentration.

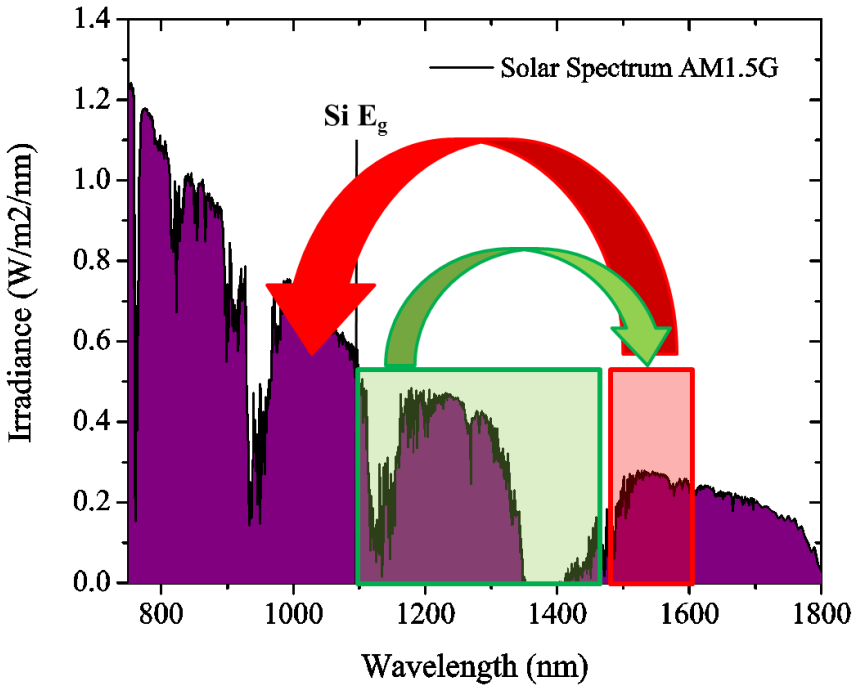

Figure 2.9 The AM1.5G spectrum is plotted showing the *Eg* of Si where all photons with energy below this are transmitted by the cell. Spectral concentration is achieved by using the QD's to absorb the green region and to emit in the red absorption region of the Er^{3+} ion. This can then be upconverted and directed back the Si solar cell.

However, environmental stability is a major issue as these materials are photo and oxygen sensitive. Therefore, they can degrade under illumination and over time when exposed to the environment which is expected in regards to their application as a UC-PV device. Results have already been published on their combined use with Er^{3+} as the UC ion by Pan *et al.* [114, 115]. An EU FP7 project, headed by Fraunhofer ISE, is also looking at the realisation of enhancing UC through the use of these nano particles [116]. Although, only limited enhancements have been demonstrated which is most likely due to coupling losses from additional layers and the low *iPLQY* of the QD's used in the investigation.

2.6.3 Absorption Broadening

Spectral concentration, discussed above, uses two luminescent species separated in space to effectively broaden the absorption range available to the upconverter. However, the focus of this section is on the modification of the UC species itself to broaden the absorption range and therefore the available photons for this process. The use of UC for the enhancement of NIR response for PV device has been conducted for a-Si:H cells [58] and was briefly reviewed in previous sections. The UC-PV device used co-doped β-$NaYF_4$:18%Yb^{3+} , 2%Er^{3+} as the UC phosphor which has one of the highest UC efficiencies reported [117] when excited at 980 nm, as this is not as well absorbed compared to c-Si devices due to a higher band gap. This exploits the higher absorption coefficient of Yb^{3+} which is used as a sensitizer to absorb the incident 980 nm excitation and transfer this non-radiatively to the Er^{3+} acceptor to achieve UC emission in the visible and UV. The sensitization of co-doped RE^{3+} via non-radiative energy transfer has been known since the wok of Auzel in 1966 [118]. In regards to PV applications, this material will benefit from both the absorption of Er^{3+} around 1523 nm and that of Yb^{3+} at 1000 nm and the effect of this can be determined by dual excitation. The absorption range is increased by co-doping but still remains relatively narrow with respect to the solar spectrum transmitted by the coupled solar cell.

The technique has further been advanced through the use of organic ligands used as "antennas" which, via fluorescent resonant energy transfer, FRET, also known as Föster resonant energy transfer, can broaden the absorption range of UC species even further. A recent paper by Zou *et al.* [107] used dye sensitisation in the NIR to broaden the absorption of β-$NaYF_4$:18%Yb^{3+} , 2%Er^{3+} NP's to utilise a greater fraction of the sub band gap photons. When NP's are synthesised they already have ligands attached to the surface, which are usually hydrophilic or hydrophobic to allow dispersion within a chosen solution or matrix. However, with further processing these ligands can be chosen to fulfil a beneficial photophysical process to enhance UC process. This is not a novel method and has been used extensively in other systems such as for DS, DC and in DSSC. Zou *et al.* used a commercial cyanine dye (IR-780) as the antenna (see Figure 2.10) due to its broad absorption range with an absorption coefficient ~5 $\times 10^6$ greater compared to Yb^{3+}. The results showed that the number of antennas needs to be optimised to both increase the absorption without luminescent quenching due to dye-dye interactions. Finally, the integrated UC emission between 720 – 1000 nm of the dye-sensitized NP compared to the unsensitised NP was ~3,300 times greater. Most

organic dyes work in the region around 250 – 800 nm which means this technique is suitable only for large band gap devices such as a-Si:H or GaAs. There is now a growing interest for these antennas to work in the IR (1000- 2000 nm) in areas such photonics, telecommunications and of course PV [119] although these are less common compared to dyes which work in the visible range. Organic dyes have been used as variable optical attenuators for telecommunications at 1550 nm [120], so this is entirely possible for UC-PV devices using Er^{3+}

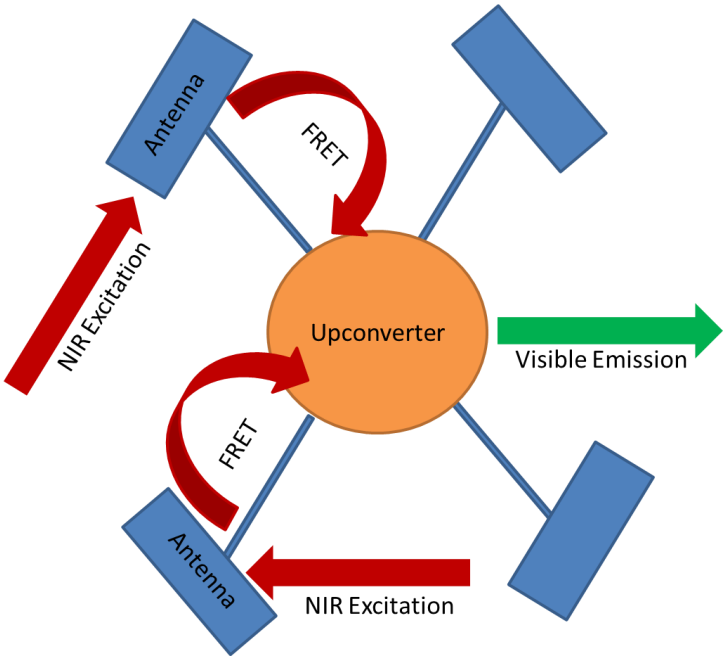

Figure 2.10 Schematic diagram of a β-$NaYF_4$:18%Yb^{3+}, 2%Er^{3+} NP functionalised with a commercial cyanine dye (IR-780). The IR-780 acts as broader and stronger absorbing species which transfers the energy to the UC NP through fluorescent resonant energy transfer (FRET) to achieve UC emission.

2.6.4 Plasmonics

The fundamental challenges of using RE^{3+} as the UC species *viz.*, the non-linear behaviour with irradiance, narrow and weak absorption could be improved through the use of plasmonics [121]. Plasmonics is concerned with the confinement of electromagnetic radiation on a scale smaller than that of the wavelength of interest and can be grouped in to two main areas; surface plasmon polaritons (SPP) and localised surface plasmons (LSP). This effect is seen for noble metallic particles, which are smaller than the resonant wavelength hence, the conduction electrons are confined. When the electrons are in resonance with the incident electromagnetic field this can

create significantly high irradiances near the metallic particle and increase absorption and scattering processes [122]. The resonant conditions can be controlled by the choice of conductive material, the shape and interaction between neighbouring plasmonic structures. The high intensity near field effect can therefore be used to improve non-linear phenomenon such as UC but this effect is only possible at short distances no greater than 10 nm. Hence, this requires the upconverter to be of the nano scale so as to best benefit from the enhancement.

Research conducted by Zhang *et al.* [123] used disk-coupled dots-on pillar antenna array to allow the resonance to be controlled by both the disc radius and the pillar with the latter giving more freedom to align the plasmonic resonance with the desired energy level of the $NaYF_4$: Er^{3+}, Yb^{3+} NP's. An enhancement by a factor of ~310 was achieved and also a reduction in the lifetime of the emitting state by a factor of 8 attributed to the manipulation of the photonic density of states (pDOS) was demonstrated. Such a large improvement compared to earlier studies was attributed to an optimised plasmonic structure, correct alignment of the plasmonic resonance and a reduction in the parasitic quenching due to the metal. However, more research is necessary to increase the UC-plasmonic interaction as PV devices are on the cm scale. Using NP's also has its disadvantages as they have a *iPLQY* that are an order or two lower than their bulk counterparts [101], which means that the plasmonic enhancements only cover the losses compared to bulk crystals.

2.6.5 Photonics

Many avenues are being investigated to gain the most out of Er^{3+} and its use as a UC material for PV devices. Most of these are focused on combination with other materials and how these can work synergistically to improve efficiencies. However, all are concerned with the manipulation of light and how to better control its interaction with the UC material for which photonic crystals (PhC) have a vast application. A PhC is defined as a structure with a spatially periodic variation in refractive index (n) on a scale relative to the desired wavelength. This can be in 1, 2 or 3 dimensions giving a multitude of optical applications. The materials, or more specifically their refractive index, used in creating the PhC and the scale of the periodic variation determine the optical properties.

In solar cell applications, photonic structures can be used to maximise efficiency by reducing escape cone losses and increasing absorption via selective filters and diffraction patterns respectively. There have been many papers on the use of selective filters for improving PV devices and for LSC's [90, 124]. In the study by Goldschmidt *et al.* [90] measurements showed a 20% relative increase in EQE for a LSC with a selective filter. However, most other research is theoretical, such as studies on intermediate selective filters for Si tandem devices [125], which predict a factor of 1.3 improvement in absorption of the upper cell. PhC's have also shown theoretical potential as diffractive structures for increasing the absorption of thin film a-Si [126]. At longer wavelengths near the band edge of a-Si:H light is absorbed poorly, due to an indirect band gap but, can still create electrical carriers important for performance. The absorption of these wavelengths is thus limited by the thickness of the cell which has been reduced to lower material costs, improve carrier collection and lower entropy. Using a periodic structure of binary material at the back of the cell will lead to the coupling of diffractive modes into greater angles of propagation and hence increase the path taken inside the cell. With large increases in output power between, 24 - 31% depending on PhC structure, projected [126], processing and experimental characterisation looks to be fruitful. The introduction of disorder within the periodic variation of *n* creates localised modes, or an increase in the pDOS, that relate to the geometry of the defect [127-129]. The defect introduces a phase slip allowing for Bragg resonance of the desired mode [127]. It should be noted that different effects arise when either adding dielectric material or removing it from the unit cell and will induce modes either near the long or short wavelength edge of the photonic band-gap (PBG), respectively [129]. By varying the modulation in *n* this can be tuned to any part of the band gap [129, 130]. This effect is used in dielectric mirrors, however it has also been theorised to increase absorption of PV devices although with a bandwidth of 15% and an acceptance angle of 50° this does not equate well with the solar spectrum [131] but ideal for a material such as Er^{3+}. It was proposed by John in 1987 [127] that this effect could also be a trigger mechanism for non-linear effects such as that encountered with UC-PV.

It is apparent that UC via RE^{3+} for PV devices is limited by their weak interaction with light and non-linear properties. The use of PhC however, has shown that these limitations can be improved by modulating the surrounding dielectric and thus optimising their environment. As mentioned, due to the size and effects of a PBG

embedded with a luminescent species, RE^{3+} and their complexes allow for better control. Yang *et al.* [132] described inverse opals doped with an UC material using a sol-gel method and demonstrated the suppression of the spontaneous emission of visible light of an efficient UC nano-crystal (NC) $YbPO_4:Er^{3+}$. An important result was to show UC enhancement by overlapping the emission edge with the longer wavelength band edge of the PhC. UC enhancement was ascribed to Bragg reflections, which is supported by Li *et al.* [133] as the effect was removed when the periodic structure was destroyed. This was for excitation in the NIR (2 W at 980 nm) followed by two photon UC for red and green emission and is thus still relevant to a-Si devices. Moreover, there is nothing to suggest this could not be applied to the 1523 nm levels of Er^{3+} for enhancement of 980nm emission and subsequent absorption of a coupled device. Alternative research is being carried out looking at using PhC as selective filters for UC layer at the rear of PV device that traps light within the UC layer for better overall performance. This process is also improved by the use of QD's which have been discussed in section 2.6.2 [114]. The spectral concentration of the QD's is estimated to be a factor of 10 and hence aims to improve the non-linear response. Other applications such as a periodic diffraction pattern at the back of a UC doped substrate is another possibility for increasing UC effects. When light is diffracted into modes it is observed that local field enhancement takes place which would be compatible with the non-linear effects of UC ions. The effect of increasing path length also partially addresses the poor absorption of the UC phosphors.

2.6.6 Solar Cells

It is often considered that the UC system can be optimised independently of the solar cell as these are only optically coupled and not electronically. However, an optimised high efficiency c-Si solar cell is designed to best convert the photons with energy above the band gap with little consideration necessary for the photons which are transparent to the device. Optical and electronic techniques, such as an AR coating or a fully contacted metallic rear surface, are used for improving carrier collection and reflection of long wavelength IR light, respectively. Unfortunately, this leads to a reduction in the intensity of the photons suitable for UC due to reflections at these boundaries. The use of BF cells has been the obvious choice for UC-PV devices as they have been designed for illumination from the front and rear surfaces, yet they have lower efficiency than the standard devices. Research at the Fraunhofer Institute ISE has started to look at how to reengineer the NIR optical properties of the cell so that they can work more holistically

with a coupled UC layer [134]. However, this generally involves degrading the overall cell efficiency to add little gain from the UC process.

2.7 Summary

The theoretical efficiency limit for an ideal UC-PV device can surpass the S-Q limit, which makes UC an attractive option for reducing intrinsic transmission losses. UC is possible with the use of RE^{3+} ions, specifically Er^{3+} for c-Si solar cells; however low absorption cross section and narrow bandwidth of excitation pose challenges in realising an efficient UC-PV system. Moreover, UC is a non-linear process which requires high irradiances to achieve better efficiencies. This has led to the characterization of these materials to be predominantly conducted with monochromatic high power lasers, which are rather dissimilar to the broad solar spectrum encountered in their applications. Therefore new characterization methods using broadband excitation is necessary to better understand the performance of these materials and to determine their optimum photophysical properties.

CHAPTER 3 - MATERIALS AND METHOD

3.1 Introduction

Within this chapter, the synthesis procedures of the UC materials investigated and characterised in Chapters 4, 5 and 6 will be reviewed. The most extensively studied UC phosphor β-$NaYF_4$:Er^{3+} is a micro-crystalline powder and is therefore embedded within a polymer host. A number of polymers and binding agents were considered however discussion will focus on the final chosen matrix, PFCB. The optical methods for assessing their performance will be discussed including the excitation sources, optical equipment and detectors. As the UC process is non-linear, dependent on the irradiance of excitation, the methods for determining these properties are reviewed in detail.

3.2 Materials

3.2.1 Hexagonal Erbium-doped Sodium Yttrium Fluoride (β-$NaYF_4$:Er^{3+})

One of the most efficient UC phosphors from the literature was chosen in this thesis due to its high performance within UC-PV devices [55, 57]. The material, β-$NaYF_4$ doped with Er^{3+}, was synthesised solely at the University of Bern following the procedure by Krämer *et al.* [135]. Samples with 10 to 75 mol% Er^{3+} were synthesized according to the formula β-$NaY_{1-x}Er_xF_4$ (x= 0.10, 0.15, 0.20, 0.25, 0.30, 0.35, 0.40, 0.50, 0.75). Herein, the commonly used simplified nomenclature, such as β-$NaYF_4$:10% Er^{3+} instead of β-$NaY_{0.9}Er_{0.1}F_4$, is used throughout this thesis.

This phosphor is synthesised as a micro-crystalline powder to achieve the more efficient hexagonal phase. Although a bulk crystal would not require a matrix to bind the phosphor, with the additional benefit of reduced scattering, this has only been achieved for the cubic phase. Therefore to apply this micro-crystalline UC material to a solar cell it requires embedding within a host matrix. The host matrix should have desirable properties such as; i) low parasitic absorption in the range of excitation, ii) low absorption in the range of UC emission, to reduce quenching, iii) a refractive index matched to that of the phosphor to reduce scattering, iv) a relatively high loading factor to embed sufficient UC phosphor to achieve complete absorption of the sub-band gap photons. A range of host matrices were assessed in this regard and will be discussed briefly in Chapter 5. The chosen matrix was a fluorinated polymer, perfluorocyclobutyl (PFCB, Tetramer Inc., USA). The phosphor powders were embedded with a 55.6

w/w% ratio of UC phosphor in a PFCB matrix and cured at 160 °C for 18 hrs. This was conducted under vacuum to remove any air bubbles which could cause scattering of the excitation source. The samples were then cut into discs of 12.5 mm diameter, 1 mm thickness and polished to a good optical finish. The dimensions were chosen with regards to that of the sample holder used for *iPLQY* measurements. The fluorinated polymer chosen here has been shown to have a reduction in C-H bonds [136] which absorb in the same range as UC ion, therefore suitable for this application. A further benefit such as the preservation of high *iPLQY* of other embedded luminescent species is also a desirable property [137]. In addition, investigations carried out at Heriot-Watt University (HWU) have shown that large phosphor/matrix loading ratios are feasible to achieve higher absorption and increased *iPLQY* [66].

3.2.2 Transparent Glass Ceramics: Erbium-doped Yttrium Fluoride (YF_3:Er^{3+})

Although β-$NaYF_4$:Er^{3+} has been shown to be one of the most efficient for UC-PV applications to date this does not mean that other materials do not have the potential for use within PV applications. The material (β-$NaYF_4$:Er^{3+}) is synthesized as a micro-crystal and has particle sizes of 10's of microns. This means that light is scattered strongly unless a suitable index matching material, in the desired wavelength range, is used as the host matrix. Another problem is the loading of the material into the host; this requires subsequent machining for optical finishes. Other methods or materials could be used to prepare upconverters which are nm's in size and can be synthesized within the host leading to good optical surfaces, low scattering with high chemical and mechanical stability.

There has been an indication from the literature that FZ glass ceramics can achieve high UC efficiencies [78], [121]. This is due to active Er^{3+} being doped within a highly crystalline environment with low phonon energies to reduce NR decay. Interaction with the amorphous environment also helps to broaden the absorption of the excitation spectrum, important for broadband irradiance. Furthermore, scattering has been suggested as a contribution to the reduction in successful UC of the excitation spectrum [54]. Therefore the synthesis of nano-crystalline precipitates within an amorphous host could also reduce scattering leading to improved performance. The upconverter, potentially interesting for PV applications, doped within an oxyfluoride transparent glass ceramics (TGC) have been prepared at the Fujian Institute of Research into the Structure of Matter (FJIRSM) by melt-quenching. The samples were then subsequently

heated for 2 hours at temperatures ranging from 630 – 710 °C, depending on the sample. The composition of the precursor glass is $44SiO_2$-$28Al_2O_3$-17NaF-$11YF_3$ (in mol %), doped with 1 mol% active Er^{3+} ions which are introduced in the form of ErF_3. The doping concentration of the NC's is closer to 10% as the Er^{3+} ions reside within the YF_3 which accounts for 11% of the bulk ceramic. Due to a difference in temperature this leads to a different degree of segregation, where the fluoride ions present in the melt tend to form small fluoride NC inside the silica-based matrix [138]. A range of temperatures was chosen to determine the optimum conditions for the synthesis of the UC layer.

3.3 Characterisation Methods

3.3.1 Scanning Electron Microscopy

Scanning electron microscopy (SEM) was conducted at HWU and was used to observe the β-$NaYF_4$:Er^{3+} micro-crystalline phosphor doped within the PFCB host matrix. The model used was a Quanta 3D FEG SEM which has suitable resolution (0.8 nm at 30 kV under vacuum) to observe samples on the micron scale.

3.3.2 X-ray Diffraction

It is well known for $NaYF_4$:Er^{3+} that the hexagonal or β-phase shows over a magnitude higher efficiency than that of the cubic or α-phase. Therefore it is important to know the crystal structure of the prepared UC materials to maximize their performance or improve the synthesis conditions. Analysis on the crystal structure of the synthesised TGC was conducted at the Chinese Academy of Sciences (CAS), Fuzhou, China. Measurements were made using X-ray diffraction (XRD) with a powder diffractometer (DMAX2500 RIGAKU) using CuKα radiation (λ=0.154 nm). The measurements also allowed calculation of the YF_3:Er^{3+} NC average size using the Scherrer equation, discussed further in Chapter 5. XRD analysis was also conducted at the University of Bern for the determination of the achieved phase for $NaYF_4$:Er^{3+} micro-crystalline powder.

3.3.3 Transmission Electron Microscopy

Transmission electron microscopy (TEM) is often used for the characterisation of materials of the nano scale which require greater resolution than a SEM. TEM was used to observe YF_3: Er^{3+} precipitated NC's within the TGC samples. This was carried out

using a JOEL JEM-2010 at the CAS, Fuzhou, courtesy of the resident technicians. The TEM also facilitated the use of energy dispersive X-ray spectroscopy (EDS) for determining the composition and concentration of the prepared NC's. The images produced were then analysed using software to determine crystal size, size distribution and Er^{3+}, for example.

3.3.4 Absorption Measurements

The absorption properties of the UC materials are an important parameter in determining the *iPLQY* and evaluating their performance in regards to their application within PV devices. In the absence of scatter (I_s) and reflection (I_r) the absorption of a material can be determined by the reduction of the incident intensity (I_o) after passing through a distance *x* within the material. This is known as the Beer-Lambert Law,

$$I = I_o e^{-\alpha x} \qquad \text{Equation 3.1}$$

were α is defined as the absorption coefficient and is valid for monochromatic excitation at low irradiances. However, the micro-crystalline $NaYF_4$:Er^{3+} powder leads to scattering of the excitation spectrum due to the mismatch in refractive indices with that of the host matrix. This therefore makes it difficult to determine the path length, or distance *x*, the excitation radiation has transitioned through the sample. This can be estimated through modelling using the Kubelka-Munk theory as has been conducted by Fischer *et al.* [61] for β-$NaYF_4$:20% Er^{3+}. However, this is only necessary when determination of the transition cross section (σ(*v*)) is required and is not the case for evaluation of the *iPLQY*. Herein, absorption is calculated by removing the fraction of radiation transmitted (*T*), reflected (*R*) and scattered (*S*) from the fraction of incident radiation ($I_o / I_o = 1$) and is defined as the absorptance (*A*) or the fraction of absorbed photons (Equation 3.2).

$$A = 1 - T - R - S \qquad \text{Equation 3.2}$$

The absorption of all the samples was measured in a UV/vis/NIR spectrophotometer (Perkin-Elmer, Lambda 950) using the integrating sphere method. The integrating sphere was supplied by Perkin-Elmer with the standard 150 mm diameter. In the integrating sphere configuration the detector will measure *T, R* and *S* and therefore can

be subtracted from unity to determine *A*. The Lambda 950 can measure from 175 nm – 3,300 nm with resolution as low as 0.20 nm in the NIR and 0.05 nm in the visible. Excitation is from a deuterium and tungsten lamp for short and long wavelengths, respectively, and a double holographic grating monochromator for wavelength selection. The detector in the NIR was a Peltier-cooled PbS version and for the UV/vis a photomultiplier R6872. All scans conducted here were with a 1 nm resolution and a 1 $sec.nm^{-1}$ integration time. Un-doped samples were used as reference to remove any absorption caused by the host lattice or matrix material. Absorption spectra of β-$NaYF_4$:Er^{3+} in the PFCB matrix were also validated by measuring in the integrating sphere of the spectrofluorometer via synchronous scans of the excitation and emission monochromator. Further to this, all measurements were conducted at room temperature.

3.3.5 Photoluminescent Quantum Yield

Luminescence is defined as "*Spontaneous emission of radiation from an electronically excited species or from a vibrationally excited species not in thermal equilibrium with its environmen*t" [139]. Luminescence is a general term which includes fluorescence and phosphorescence for example; however, photoluminescence is luminescence which occurs directly from excitation due to the absorption of a photon. Due to the long lived excited states of the RE^{3+}'s, and more specifically Er^{3+}, we are concerned with phosphorescence which is characterised by a lifetime greater than fluorescence. Therefore the "photoluminescent quantum yield" determines the probability that the absorption of a photon (quanta) leads to emission and is here defined as the internal photoluminescent quantum yield (*iPLQY*; discussed in Chapter 2). The external photoluminescent quantum yield (*ePLQY*) can be determined using the same spectra measured for determining the *iPLQY*. However, without the requirement for determining the absorption is thus much more easily quantified.

The *iPLQY* measured herein was obtained using a calibrated spectrofluorometer from Edinburgh Instruments (FLS920) shown in Figure 3.1. Detection was achieved in conjunction with a Hamamatsu NIR photomultiplier tube (R5509-72) cooled to -80°C with liquid nitrogen and an integrating sphere from Jobin-Yvon (150 mm diameter). All measurements were conducted at room temperature. Only the emission from the $^4I_{11/2}$ level, with peak resonance at 980 nm, was considered for measurement of the *iPLQY* as higher photon UC processes are of an order of magnitude lower and would only increase the *iPLQY* marginally [64]. To avoid saturation of the detector, neutral

density (ND) filters where used in the emission arm of the spectrofluorometer and calibrated for accordingly. Each measurement was conducted ten-fold to reduce any noise and to give a reasonable average of the photon counts measured. A spectral resolution of the emission monochromator of 1 nm and dwell time of 1 sec. (integration time) was used for all measurements. For every series of irradiance measurements, the stability of the excitation source was measured over an extended period (typically two hours) prior to any measurements to be within an error of ± 2%. To ensure the methodology yielded repeatable results, the *iPLQY* measurement at full power was always conducted prior to any other power. The uncertainty due to the calibration of the various spectra and the integrating sphere, which is quoted by the manufacturer, is ±10%. Further analysis was performed due to the range of concentrations measured, the irradiance, and the bandwidth of the excitation; a correction method to account for the re-emission in the absorption spectra was also undertaken. A detailed discussion of the correction method can be found in Chapter 4. However, the additional error constitutes both the noise to signal ratio, which was determined to be in the range of 1 - 25% depending on the irradiance of excitation and emission of the various concentrations, and the uncertainty inherent to the equipment used. All errors were summed in regards to the method for the propagation of errors in quadrature. The measurement of the irradiance incident on the sample was characterised independently of the *iPLQY* therefore, these errors are estimated separately. Measurements were not conducted for irradiances less than 0.05 ± 0.01 MWm^{-2} as the SNR of the emission was then too low for a valid determination of the *iPLQY*. The values of *ePLQY* were obtained with exactly the same procedure without the requirement to determine the absorptance. The above method to determine the *iPLQY* is considered absolute and therefore does not require calibration using an *iPLQY* standard. This is because the use of an integrating sphere eliminates the anisotropy of emission viewed by the detector. Further to this, combining the integrating sphere with a spectrofluorometer negates the use of a standard reference for determining the *iPLQY*. Therefore, an absolute measurement is achieved because both the number of absorbed and emitted photons can be measured directly. A detailed explanation of these differences has been explained in Section 2.5.1. However, it was considered prudent to do so. Hence, measurements were conducted on styryl-13 (Laser Physics, Exciton LDS925), which has been utilized as a standard for NIR measurements [140]. The *iPLQY* was measured to be 2.4 ± 0.2% under monochromatic excitation at 625 nm and emission around 940 nm, which is in fairly good agreement with the literature value of 2.0 ± 0.2% [140].

Figure 3.1. A standard FLS920 spectrofluorometer with a single excitation and emission monochromator and Xe lamp at the rear. Significant modifications to the standard set-up have been made and are discussed in detail within Chapter 3.

Broadband excitation was achieved using a white light supercontinuum (SC) laser from Fianium, 6-400-PP, with 6W average power; see Figure 3.2. The SC laser has an 80 MHz repetition rate with a pulse width of ~70 ps and a spectral output from 400-2600 nm. The fibre optic output was then connected to a NIR high power acousto-optical tuneable filter also from Fianium (AOTF-HP) which allowed a maximum bandwidth of 80 ± 1 nm in the desired range of excitation. The broadband excitation spectrum was aligned to be symmetric around the strongest resonant wavelength at 1523 nm. In Chapter 5 excitation was conducted using free space propagation after the AOTF-HP which allowed higher irradiances to be achieved. For the results in Chapter 6 the output of the NIR AOTF-HP was coupled into a multi-mode fibre to homogenise the beam spatially and a fibre collimator was used to launch the beam into free space. Various ND filters (Andover, 130FA46-25) were used to vary the irradiance by reducing the maximum power. However, this only allowed two orders of magnitude variation in irradiance due to a reduced SNR of emission at lower powers. Furthermore, a 1300 nm long pass filter was used to remove any higher harmonics from the diffractive optics and to represent the transmission of a Si PV device.

Figure 3.2 Picture of the Fianium, 6-400-PP, 6W supercontinuum laser with fibre and collimator output, which allows good optical coupling to the AOTF-HP (not shown here).

3.4 Excitation Characterisation

3.4.1 Irradiance

As UC photoluminescence is non-linear with excitation power it is essential to thoroughly characterise the irradiance incident on the sample. In Chapter 5 the irradiance was measured using a calibrated germanium (Ge) photodiode (Newport, 818-IR) and an IR imaging camera (Electrophysics MicronViewer 7290A), with beam diagnostic software to determine the area from the FWHM. The combined error of the calibration and the uncertainty associated with a digital display with respect to irradiance is ± 4.4%.

In Chapter 6 the irradiance was measured by placing a three-axis translation stage at the sample position and using a knife-edge to scan the beam area in the *x*- and *y*-directions. This was performed for various values of *z* to determine the beam waist at the focus. Therefore, the maximum possible irradiance incident on the sample was determined. This alternative method, in comparison to that used in Chapter 5 was preferred due to the improved accessibility within the optical enclosure and the precision achieved in the *z*-direction. The area was defined by the FWHM of irradiance of the beam to allow consistency with previous investigations from literature. Moreover, the power was measured using a thermopile detector (Thorlabs, S302C), which had a flat broad spectral response suitable for the excitation used and calibrated by the manufacturer. Figure 3.3 shows a topographical view of the apparatus used in the characterisation of irradiance which includes in clock-wise order from the top; the excitation lens, collection lens, power meter and three-axis stage with attached knife edge. The

measured values of power were also compared to a calibrated germanium photodiode (Newport, 818-IR), used in Chapter 5, which exhibited a precision within 2% absolute. The combined error associated with the calibration, stability, and reading error for the irradiance values was determined to be ± 12.3%.

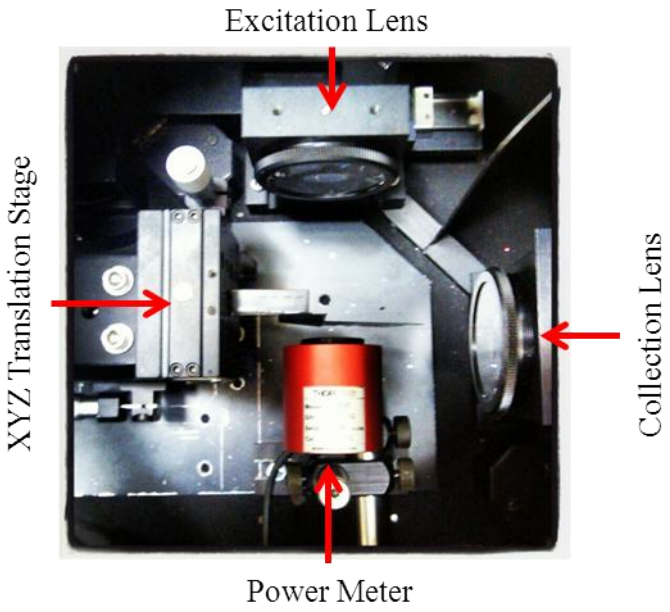

Figure 3.3 Topographical view of the sample chamber during characterisation of irradiance. In clock-wise order from the top; the excitation lens, collection lens, power meter and three-axis stage with attached knife edge.

For monochromatic excitation, the slit width of the excitation monochromator was kept constant, 20 nm, as this determines the area of illumination. This ensured that the beam area, which was determined to be square, was identical for all the measurements. In addition, due to the top hat distribution, the area was characterised accordingly. The beam size was measured using an IR imaging camera (Electrophysics MicronViewer 7290A) and a beam diagnostic software. A total of 238 camera shots were taken and the average beam size was determined as 10.5×10^{-4} cm^2 with an uncertainty of 0.03%. The beam power was measured by a calibrated germanium photodiode (Newport 818-IR) positioned at the focus of the excitation spot with a 1 µm resolution XYZ stage. The calibration error of the photodiode detector is ± 3%. The combined error of calibration of the photodetector, uncertainty associated with the irradiance which includes both measured power meter readings and the measured area, is ± 4.4%.

3.4.2 Solar Concentration

Previous work in this field has only shown analysis in relation to the AM1.5G spectrum [55, 77, 81], which is the standard spectrum for characterizing PV devices under non-concentrated sunlight. However, terrestrial concentrator cell and module efficiencies are measured under the air-mass direct beam (AM1.5d, ASTM G-173-03) spectrum at an intensity of 900 W/m^2 and a cell temperature of 25°C. With respect to the intensity required for UC-PV, it is proposed that the AM1.5d spectrum should be the standard method of reporting as an UC-PV device is expected to operate under a concentrated solar spectrum. The broadband irradiance used here therefore requires additional analysis in determining the solar concentration and a new method of reporting this value more accurately. Moreover, this also aids in clarifying the difference between additional power under monochromatic excitation and increased power due to a larger bandwidth. The method used was to determine the FWHM of the excitation spectrum from the AOTF for bandwidths between 12 – 80 nm and compare this to the same bandwidth of the AM1.5d with the same central wavelength, λ_c. Additional measurement of the irradiance for each bandwidth of excitation, allowed for the calculation of the solar concentration as described in Equation 3.3:

$$Solar\ Concentration = \frac{Excitation\ Irradiance\ (FWHM, \lambda_c)}{\int_{\lambda_1}^{\lambda_2} AM1.5d\ Irradiance\ (\lambda) \cdot \delta\lambda} \qquad \text{Equation 3.3}$$

Where, $\lambda_1 = \lambda_c - (FWHM / 2)$ and $\lambda_2 = \lambda_c + (FWHM / 2)$ are the limits of integration. Therefore, all measurements are normalised to the solar spectrum, making increased bandwidth independent of increasing spectral irradiance which allows analysis of performance in intuitive units. As these measurements were performed with a 1 nm resolution including the data for the AM1.5d spectrum an absolute uncertainty of ± 0.5 nm in relation to the FWHM, associated with the irradiance for a given excitation, under one sun with an integrated irradiance of 900 Wm^{-2} applies.

3.5 Summary

The UC materials that have been investigated in Chapters 4, 5 and 6 were described in detail. Important considerations, such as the desirable properties of the host matrix for the micro-crystalline powder, β-$NaYF_4$:Er^{3+}, and the crystal phase of the UC phosphor have also been reviewed. Various methods have been used to characterise the physical attributes of these phosphorescent species such as SEM, TEM and XRD due to the

effect this has on the UC efficiency. More importantly, the optical methods to investigate the photophysical properties such as the absorption and *iPLQY* have been discussed. This has included the equipment used, apparatus for the experimental set-up, and the analysis of errors associated with the reporting of the results. However, the standard method for measuring the *iPLQY* under broadband excitation will be shown to be inadequate, due to the effect of re-emission in determining the absorption of the UC material. Therefore, the standard method has been further developed, over a wide range of Er^{3+} concentrations and irradiances, to account for this error. This is essential for determining values of the *iPLQY* under broadband excitation, important in the analysis of UC-PV devices, which will be examined in the following chapter.

CHAPTER 4 - BROADBAND CHARACTERISATION METHOD FOR INTERNAL PHOTOLUMINESCENT QUANTUM YIELD

4.1 Introduction

The internal photoluminescent quantum yield (*iPLQY*) – defined as the ratio of emitted photons to those absorbed – is an important parameter in the evaluation and application of luminescent materials. The *iPLQY* is rarely reported due to the complexities in the calibration of such a measurement which have been discussed in detail in Chapter 2, Section *2.5.1*. An experimental method is proposed here to correct for re-emission, which leads to an underestimation of the absorptance of UC phosphors under broadband excitation. Although traditionally the *iPLQY* is measured using monochromatic sources for linear materials, this advancement is necessary for non-linear materials with wavelength dependent *iPLQY*, such as the application of UC to solar energy harvesting. The method requires an additional measurement of the emission line shape that overlaps with the excitation and absorption spectra. Through scaling of the emission spectrum, at the long wavelength edge where an overlap of excitation does not occur, it is possible to estimate the value of *iPLQY*. The method has been evaluated for a range of Er^{3+} concentrations within the β-$NaYF_4$ host and under various irradiances to analyse the boundary conditions that favour the proposed method. Use of this extended method is important for a reliable measurement of *iPLQY* under a broad illumination source such as the sun. The discussion of this method is a prerequisite in understanding how the UC materials are characterised in Chapters 5 and 6.

4.2 Explanation of Method

It is necessary to discuss here what procedure will be required to determine the *iPLQY* under broadband excitation. This will be based on the currently accepted method, discussed at length in Section *2.5.1 Optical Characterisation: internal Photoluminescent Quantum Yield*. Herein the discussion will focus on the additional considerations for determining the *iPLQY* under broadband excitation. Thus the additional correction, due to the overlap in absorption and re-emission, required under broadband excitation, will be evaluated. The particular focus within this chapter is the determination of the *iPLQY* of upconverting materials under broadband excitation. However the wider applicability of this method, to that of other luminescent species and their applications, is inferred.

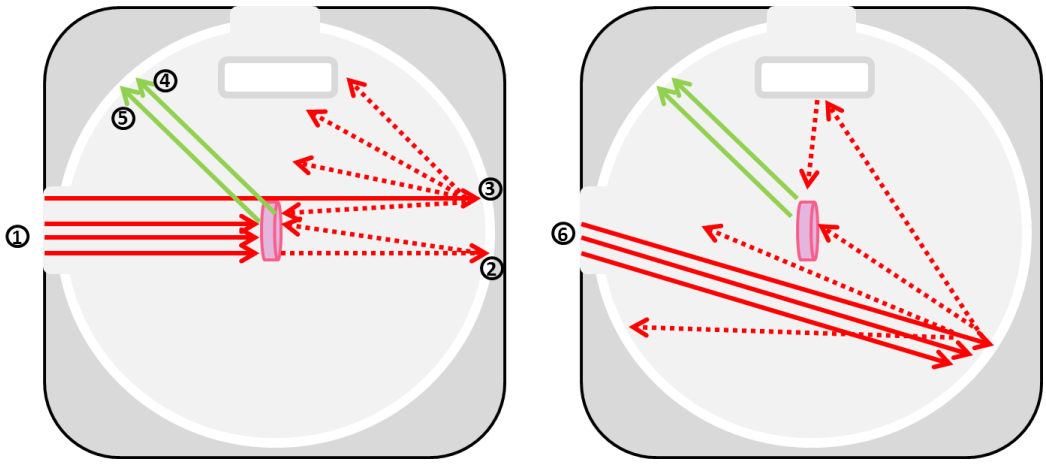

Figure 4.1 Schematic diagram of an integrating sphere used for measuring *iPLQY*. The various sources of excitation and emission have been labelled; ① is the direct excitation (L_a), ② and ③ are excitation photons which have been reflected from by the sphere wall (L_c), ④ represents the emission from the sample due to excitation from the sphere wall (P_c) and ⑤ is the emission of the sample under direct excitation (P_b). The second measurement procedure is the method for removing the effect of P_c. Here, ⑥ is the same excitation as ① but is not exciting the sample directly.

To determine the *iPLQY* two values must be known; 1) the absorptance (A) and 2) the emission of the sample (P_b; see ⑤ in Figure 4.1). The absorptance is the fraction of photons which are absorbed divided by those that are incident on the sample. As mentioned previously, the *iPLQY* for a non-linear process, such as the evaluation of UC, is dependent on the irradiance. Hence, any photon incident on the sample primarily from the excitation source (① in Figure 4.1) or after a secondary process can alter the *iPLQY* (② and ③ in Figure 4.1). Therefore, any photons reflected from the internal surface of the integrating sphere, after initially being transmitted by the sample, have the potential to be absorbed, affecting the *iPLQY*. The surface of the integrating sphere scatters photons diffusely. Hence, the scattered excitation spectrum (L_c) will be significantly lower in irradiance compared to that of direct excitation (L_a). Due to the weak absorptance of the Ln^{3+} materials this will not affect the *iPLQY* and it can be assumed that $\mu = 0$. μ are the fraction of excitation photons that are absorbed by the sample but after reflection from the internal sphere wall ($\mu = L_c / L_a$). Thus, an experimental measurement of the UC emission (P_c; see ⑥ in Figure 4.1), with the sample present but not directly illuminated (L_b), will confirm this assumption. This means that the emission from the sample due to scattered light from the sphere wall can

be assumed to be zero and removed from the calculation. In the experimental set-up used here, a lens is used to increase the irradiance, leading to an area of illumination much smaller than the sample area. This has the consequence that the fraction of photons, which are primarily incident on the sample (*f)*, is equal to one. This is an important consideration for the reliable measurement of the *iPLQY* as discussed by Faulkner *et al.* [99] and reviewed in section 2.5.1. Hence, using the method of de Mello [94] the formula for *iPLQY* can therefore be calculated as follows,

$$iPLQY = \frac{P_b - (1-A)P_c}{L_a A} \qquad \text{Equation 4.1}$$

where,

$$A = \left(1 - \frac{L_b}{L_c}\right) \qquad \text{Equation 4.2}$$

$$P_c = 0 \qquad \text{Equation 4.3}$$

$$L_c = L_a \qquad \text{Equation 4.4}$$

$$iPLQY = \frac{P_b - (1-A)P_c}{L_a\left(1 - \frac{L_b}{L_c}\right)} = \frac{P_b}{L_a - \frac{L_a L_b}{L_a}} = \frac{P_b}{L_a - L_b} \qquad \text{Equation 4.5}$$

equivalent to the two measurement procedure [99] discussed previously in Section *2.5.1*. Finally, it should be noted that the measurement of L_a is performed with a reference sample (undoped β-$NaYF_4$ powder in PFCB) so as to account for absorption of the host and matrix material. Further to this, any emission from contamination of impurities can be removed by determining any emission when the reference sample is present (P_a). These are known as blank measurements and have been discussed within Chapter 3.

Figure 4.2 shows the excitation spectrum, L_a, referred to henceforth as the reference scatter (**—**), of the AOTF-HP in conjunction with the SC laser source. This is used for broadband excitation of the β-$NaYF_4$: Er^{3+} series, with the 25% Er^{3+} emission spectra used for illustration in Figure 4.2. The bandwidth of excitation at FWHM is 80 ± 1 nm

with an irradiance of 1.97 ± 0.24 MWm^{-2}. This is the maximum irradiance achievable with this set-up which is used to achieve the best SNR of the measured spectra. After the reference scatter has been obtained the same measurement is performed for the sample in the integrating sphere (L_b, sample scatter; ▬▬). This allows the latter spectrum to be subtracted from the former hence, determining the number of absorbed photons (measured absorptance; ▬▪▬).

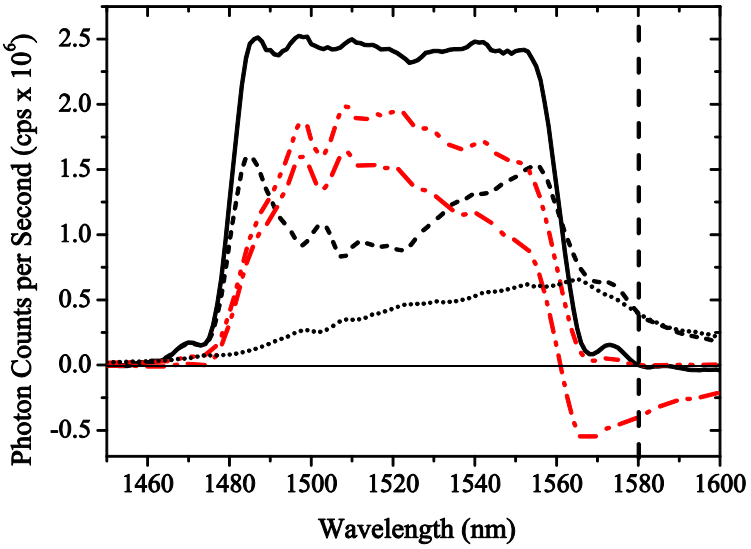

Figure 4.2 Spectra required to determine the corrected iPLQY; the reference scatter (▬), sample scatter (▬▬), absorptance (▬▪▬), re-emission from the sample in the region of excitation (▪▪▪▪▪) and the calibrated absorptance (▬▪▬).

It is clear to see that there is a negative contribution for wavelengths above 1560 nm in determining the number of absorbed photons. This artefact therefore leads to an artificial increase in *iPLQY* because of a lower value of the integrated absorptance (*A*). The presence of these negative integrals is due to photons present in the sample scatter which are not present in the reference scatter (comparison of the ▬▬ and ▬ lines, respectively); thus, can only be attributed to re-emission (▪▪▪▪▪ line) of the sample in the observed range (1450-1600 nm). This is more significant at longer wavelengths as emission is Stokes-shifted in comparison to the absorption for the transitions associated with the same energy levels. The measurement thus contains both information on the number of absorbed and re-emitted photons. To determine the absolute *iPLQY*, deconvolution of these spectra is necessary. Hence, to determine the actual spectral shape of emitted photons, that cause a systematic error in the calculation of *iPLQY*, the long wavelength edge of the sample scatter was used. This is because the photons in

this range can be attributed to re-emission only. The vertical line in Figure 4.2 shows where there are no photons present in the reference scatter; hence the long wavelength tail can be used for fitting an emission curve to account for the error of re-emission. This method follows a similar technique presented by Wilson and Richards [88], which was derived from the work of Ahn *et al*. [100], to account for re-absorption of highly doped (>1000 ppm) linear materials. It is important to note here that the spectral range of the NIR PMT is limited to 1600 nm. This is due to non-linear response of the NIR PMT with the corresponding instrument correction at the edge of the detector response. Although the re-emitted photons (Figure 4.2, ····· spectrum) can be seen to go beyond this limit this does not affect the correction of the absorptance which can only occur in the range of excitation. Attempts were made to measure the full emission spectrum using an InGaAs detector from Hamamatsu (G8372-03). The detector included an integrated lock-in amplifier and was cooled with liquid nitrogen. However, the response of the detector was too weak to give a measurable spectrum. Instead, Lorentzian peaks can be fitted to predict the spectral shape of the emission beyond 1600 nm if the *iPLQY* of the Stokes shifted emission from the $^4I_{13/2}$ level is of importance. This may be of interest in determining the *iPLQY* of other luminescent materials used for solar applications under broadband excitation, such as in LDS or DC, but has no effect in regards to upconverted photons and the method presented here.

The Er^{3+} doped β-$NaYF_4$ series, for all concentrations, was then measured in the range 1450-1600 nm to determine the emission line shape when excited at 980 nm. These spectra were required to account for the re-emission of the samples which overlap with the absorption. This was conducted using the integrating sphere to calibrate for the optical and detector system as well as to remove any preferential observation of emission from each sample. The area under the emission curves was then normalized so that a comparable scaling factor could be determined for later analysis. The emission spectrum was scaled so as to achieve the greatest overlap with the long wavelength edge of the sample scatter, which can be seen in Figure 4.2. The scaling process was performed by determining the maximum value of best fit (R^2) by varying the scaling factor from 0 to 60 in steps of 0.1. The final part to the procedure was to combine the measured number of absorbed photons with the scaled emitted photons. The spectrum of the measured absorbed photons plus the emitted photons, now defined as calibrated absorptance, can be seen in Figure 4.2 with the trend ▪···.

4.3 Results and Discussion

As a first evaluation, the method would appear to be a valid estimate due to the removal of any negative area as was associated with the un-calibrated absorption spectra shown in Figure 4.2. Moreover, the outer nodes associated with the transmissive properties of the AOTF-HP are also replicated indicating a suitable removal of the re-emission spectra. The calibrated absorptance line shape was then compared to the monochromatic absorption, which was measured using a spectrophotometer; although this cannot give any quantitative analysis this serves an illustrative purpose in understanding any differences, see Figure 4.3. The monochromatic absorptance was determined by normalising the curve to the measured absorptance value at 1498 nm (one of the resonant peaks) and then multiplying this by the reference scatter to determine the equivalent counts per second (cps). Attempts were made to normalise the monochromatic absorption further into the blue end of the spectrum to reduce the effect of re-emission. However, scaling to a slope led to significant random error in the number of absorbed photons. Both trends in Figure 4.3 are for the 25% Er^{3+} sample under an irradiance of 1.26 ± 0.15 MWm^{-2}, which gives a good representation of all measurements in regards to different irradiances and a higher SNR for clarity. Comparisons of these spectra differ slightly for low concentrations where broadband excitation shows a higher estimate of absorbed photons compared to monochromatic excitation. The reciprocal of this is also observed where large concentrations indicate higher absorptance for the monochromatic spectra. Overall, the monochromatic absorption line shape and that of the calibrated absorption agree well. The calibrated absorption spectrum shows a homogeneous broadening compared to the normalised monochromatic absorption. This indicates saturation and a more equal contribution of all wavelengths to the UC process. The observed broadening has also been indicated by experiments conducted by Shalav [141], which looked at various powers of white light biasing on measurement of EQE for a UC-PV device. Although the calibrated absorptance preserves the resonant peaks associated with the Stark splitting of the $^4I_{13/2}$ there is a reduction in the magnitude of the peak resonance at 1523 nm. In the case of the normalised monochromatic absorption, which is estimated with regard to the broadband excitation spectrum, the resonant peak at 1523 nm also appears to have been reduced. This affect can therefore be partially attributed to the convolution of the incident photons of excitation (reference scatter) and the absorption line shape as the maximum photon counts have approximately a ± 5% variation.

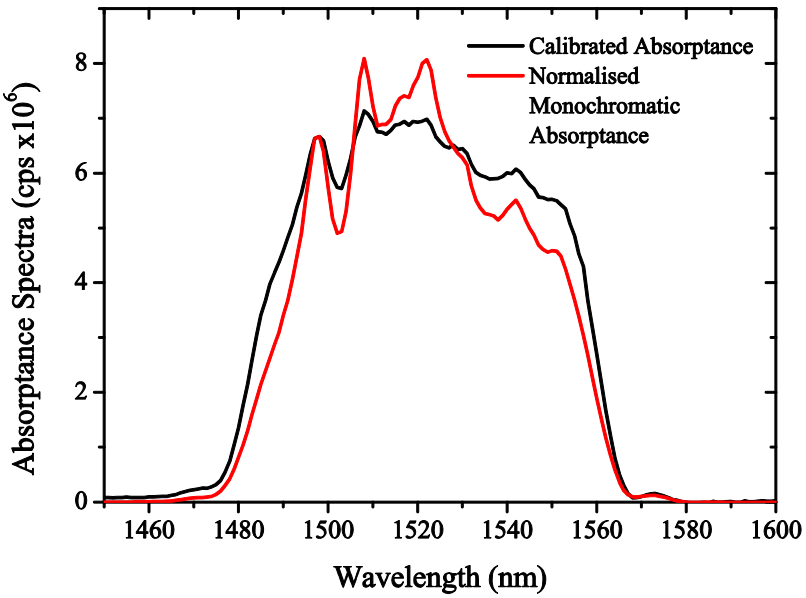

Figure 4.3 Comparison of the corrected absorptance spectra due to re-emission with the normalized and scaled absorptance spectra for 25% Er^{3+} measured using a spectrometer. Although the broadband absorption shows homogeneous broadening and higher absorptance the lineshape is well preserved except for saturation of the 1523 nm peak.

A closer analysis of the calibrated absorptance spectrum was carried out by normalisation of the curve to the peak value, shown in Figure 4.4(a). This was then carried out for the scaled monochromatic absorption for comparison, as plotted in Figure 4.4(b). In both Figure 4.4(a) and (b), only selected concentrations have been shown for clarity. Figure 4.4(a) shows that there is a significant broadening of absorption into the long wavelength edge and somewhat into the blue edge, which is also supported by that measured using the spectrophotometer for monochromatic excitation. It is also apparent that the absorption spectrum for broadband excitation is generally flatter in regards to the sharp peaks seen for the monochromatic equivalent which has been discussed above. This is further supported by Figure 4.2 where a normalised absorptance spectrum in regards to the excitation photons also shows much broader features due to the convolution of the two. Although the broadening of the absorption spectra, for increasing Er^{3+} concentration, is greater under broadband excitation this shows good agreement with the trend and standard method for measuring absorption under monochromatic excitation. Furthermore, it is possible to see clearly the resonances at 1498 nm and 1508 nm in both spectra, however for broadband excitation the resonant peaks at 1523, 1531, 1544 and 1551 nm are less dominant but still present.

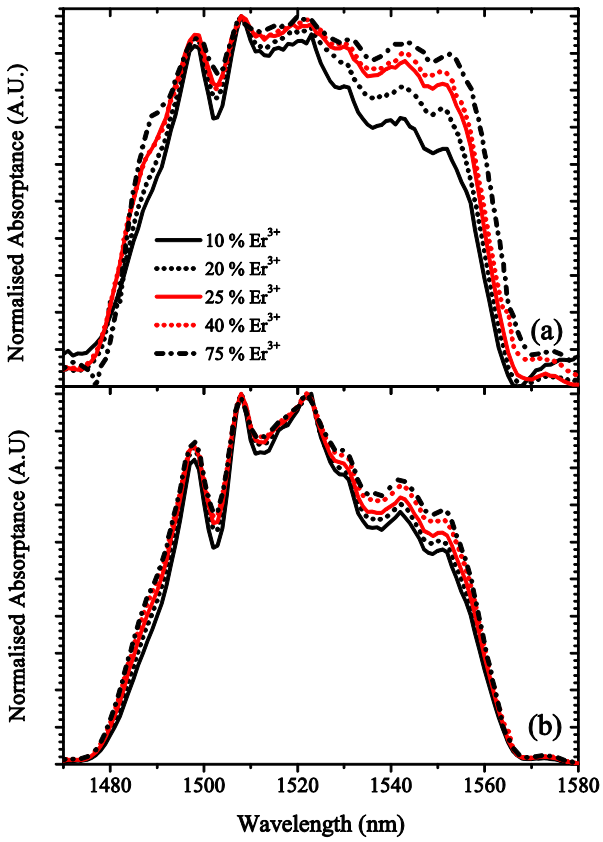

Figure 4.4 Normalised calibrated absorptance spectra under (a) broadband excitation for the highest irradiance and (b) the monochromatic absorption measured with the spectrometer. Both spectra are normalized to the peak value and only selected concentrations are shown for clarity.

The "corrected" *iPLQY* values were then calculated using the integral of the calibrated absorptance data and compared to the previous values as can be seen in Figure 4.5. The correction due to re-emission of photons in the range between 1450-1600 nm is most prominent at lower concentrations. As the highest concentration shows very little re-emission and a close match to the uncorrected value this can be proposed as a point of reference. The effect of re-emission is therefore intrinsically linked to the samples inability to upconvert the absorbed photons as well as the UC mechanisms responsible for this phenomenon. Both absorptance and the UC mechanism are concentration dependent and hence a reflection of this in the calibration should be expected, and is thus observed.

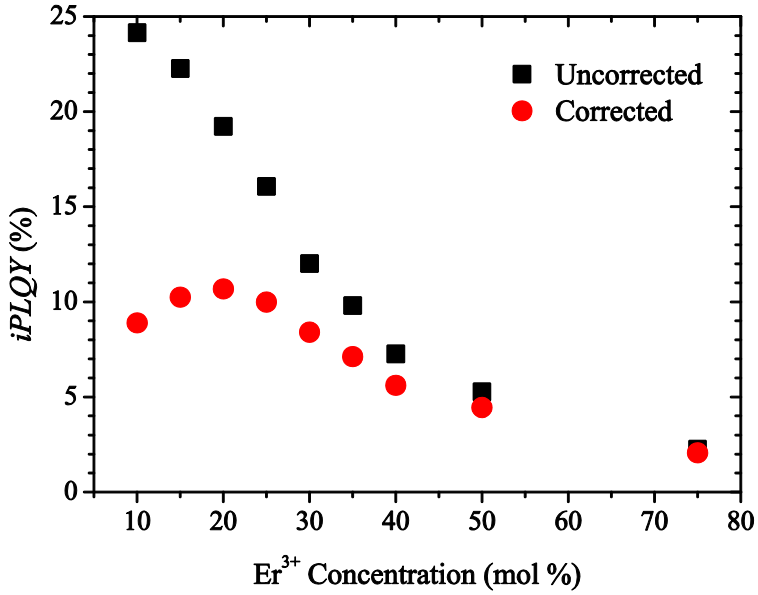

Figure 4.5 Comparison of the uncorrected iPLQY (black squares, ■) and the corrected iPLQY (red dots, ●) in regards to re-emission at an irradiance of 1.97 ± 0.24 MWm^{-2}. The difference is seen to be concentration dependent with high concentrations being the least affected.

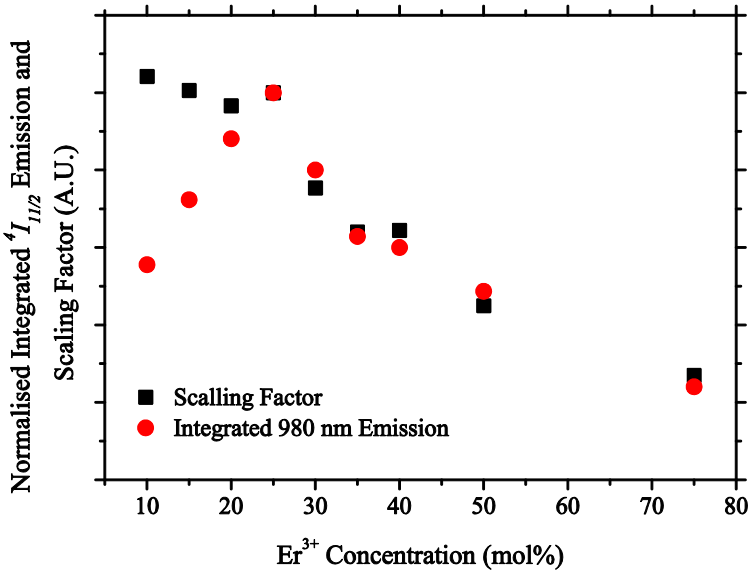

Figure 4.6 Correlation between the scaling factor, which is proportional to the emission from the $^4I_{13/2}$ level, and the integrated emission of the $^4I_{11/2}$ which have both been normalised to the 25% Er^{3+}values. Good agreement is seen for Er^{3+} greater than 25%, however divergence in this trend is seen at lower concentrations.

Analysis on the scaling factors in relation to the integrated emission of the $^4I_{11/2}$ level was also conducted. As the re-emission curve was estimated by scaling the emission from 1450-1600 nm under excitation into the $^4I_{11/2}$ there should be some correlation

between the two. Figure 4.6 shows normalised values for the scaling factor and integrated emission for the range of Er^{3+} concentrations. From 25% to 75% Er^{3+} there is a very good correlation of these values; however this correlation breaks down for concentration between 10 - 20%. This proposed relationship is also less apparent at lower irradiances where the ion population is expected to be in the lowest energy levels. It is suggested that these calibrated values may diverge at lower concentrations and irradiances as the re-emission between 1450-1600 nm is more proportionally due to decay between $^4I_{13/2} \rightarrow {}^4I_{15/2}$ rather than from the $^4I_{9/2} \rightarrow {}^4I_{13/2}$ or $^4I_{11/2} \rightarrow {}^4I_{13/2}$ levels, however these cannot be detected with the current NIR PMT. Lower energy transfer and energy migration due to lower concentrations may also lead to a change in the re-emission spectrum and an incorrect scaling factor applied.

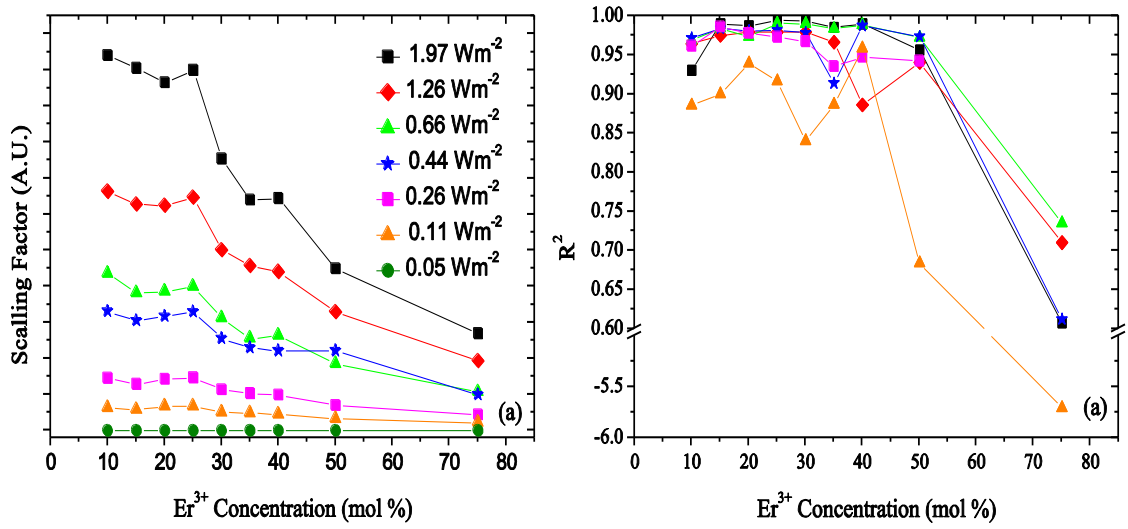

Figure 4.7 (a) shows the scaling factor for each concentration and irradiance in regards to the re-emitted photons with a consistent trend. In (b) it can be seen that the R^2 values are close to 1 for high irradiances and low concentrations however a good fitting is not achieved for the lowest powers and highest concentrations. The scaling factor for the irradiance of 0.05 Wm^{-2} was close to zero hence, these have been omitted from the calculated R^2 values.

Further analysis in Figure 4.7(a) shows the scaling factors, which are proportional to the number of re-emitted photons between 1450-1600 nm, used in the fitting process for calibration of the *iPLQY*. The trend in the concentration dependence is fairly consistent for all irradiances. The concentration dependence of the re-emission is preserved; however this is amplified by the increase in irradiance. The scaling factor tends to increase for lower concentrations where emission from $^4I_{13/2} \rightarrow {}^4I_{15/2}$ will be more

probable and is also supported by the line shape of the emission spectrum. The R^2 values can be seen in Figure 4.7(b) which displays the general trend that the re-emission effect is better matched for the highest irradiances and lowest concentrations. This is because at higher concentrations and lower irradiances there is less of an effect from re-emission and subsequently a poorer fit of the calibration curve. In other words, this is due to the fact that re-emission is less dominant for high concentrations and low values of irradiance. The emission of the $^4I_{13/2}$ level is linear with irradiance and will therefore increase at higher pump rates. Furthermore, the emission from this level is also reduced by higher rates of energy transfer for greater concentrations of Er^{3+}. As the irradiance increases the emission from $^4I_{13/2} \rightarrow {}^4I_{15/2}$ will increase which overlaps with the absorption spectra and will contribute to re-emission. Furthermore, when populations of higher energy levels are greater, the rate for stimulated emission will increase especially for broadband excitation with a greater overlap with the transition line shape. In the case of higher concentrations of Er^{3+}, equivalent to reduced ion spacing, ETU processes dominate and an increased absorption also leads to population of higher excited states at lower irradiances. For higher concentrations, the emission from the transitions around 1450-1600 nm ($^4I_{13/2} \rightarrow {}^4I_{15/2,}$ $^4I_{11/2} \rightarrow {}^4I_{13/2}$, $^4I_{9/2} \rightarrow {}^4I_{13/2}$) do not contribute as significantly due to saturation and higher photon UC.

4.4 Conclusions

An experimental method has been proposed for the correction of the fraction of absorbed photons detected under broadband excitation of an UC sample. This is a necessary procedure for determining the *iPLQY* for the evaluation of spectral converters, especially upconverters, in the field of solar energy harvesting. The systematic error associated with the estimation of the absorptance has been attributed to re-emission which exhibits a spectral overlap with both the broad excitation spectrum and the absorption line shape. Through scaling of the $^4I_{13/2} \rightarrow {}^4I_{15/2}$ emission to the uncorrected absorptance spectra in the long wavelength edge, which is out with the range of excitation, a corrected absorptance spectrum has been determined. This has been validated via comparison of the standard monochromatic absorption and previous observations which show an observed broadening of the line shape under broadband excitation. The method has been tested for a wide range of active ion concentrations and irradiances which shows that re-emission artefacts have a greater influence at higher irradiances and lower concentrations. Although this experimental study has been applied specifically to upconverters for use under a broad excitation such as the sun, due

to the determination of the absorptance and *iPLQY* under broadband excitation being of increased importance; it is also beneficial to a wide range of spectral converters in solar energy applications. More significantly, this effect will also be present under monochromatic excitation of UC materials, although has never been observed or quantified to the authors knowledge. Due to the nature of monochromatic excitation a scan of the excitation spectrum over a short bandwidth would make it difficult to observe any modification due to re-emission. The effect of re-emission has been shown to be dependent on irradiance, of which, can be achieved more readily with the high power and broadband excitation of the SC laser used here. Nonetheless, this indicates that values of *iPLQY* measured under monochromatic excitation have been overestimated, especially at low concentrations of the doped upconverter and high irradiances of excitation. Finally, the method that has been developed within this chapter is now used in the following Chapters 5 and 6 to determine the *iPLQY* under broadband excitation. Thus, the effect of broadband characterisation with regards to the evaluation of performance of an UC layer within a UC-PV device will now follow.

CHAPTER 5 - BANDWIDTH DEPENDENCE OF UPCONVERSION MATERIALS

5.1 Introduction

In this chapter, the importance of using broadband excitation as a method to characterise UC materials is investigated. In addition, the possible benefit of this method for evaluating the performance of the UC layer, within an UC-PV device, is demonstrated. Herein, two promising materials for such an application are measured by comparison of photoluminescent properties under different excitation bandwidths. The first is an oxyfluoride transparent glass ceramic (TGC) with embedded YF_3: 10% Er^{3+} nano-crystals (NC); where the material properties are examined in Section 5.2. The UC emission of the TGC with embedded YF_3: 10% Er^{3+} NC, under broadband excitation with 12 nm and 38 nm FWHM, is presented in Section 5.3 of this chapter. A characterisation method was used to measure the photoluminescence where the increase in excitation bandwidth was independent of spectrally dependant irradiance. The irradiance was normalised to the air mass 1.5 direct (AM1.5d) solar spectrum for the first time. This allows for a more intuitive understanding of the excitation conditions necessary. This is because the wider PV community is unfamiliar with the available irradiance conditions at wavelengths outside the working range of the device. Normalising to the most appropriate solar spectrum is thus less clandestine. This makes for a clearer evaluation of the potential for UC in regards to its application within a working UC-PV device. The experimental results show that increasing the bandwidth of excitation by a factor of 3.17, led to a 55 fold increase in emission for the same solar concentration. This is equivalent to achieving the same level of emission with a factor of 7.6 less Suns. However, due to the low absorption and emission of the TGC samples, it was not possible to investigate the *iPLQY* dependence on the bandwidth of excitation which is necessary to quantify their potential efficiency within an UC-PV device. Hence, the more optically efficient β-$NaYF_4$: 10% Er^{3+} embedded in PFCB was measured using the method presented in Chapter 4. The material properties of the β-$NaYF_4$: 10% Er^{3+} phosphor doped in PFCB and *iPLQY* under broadband excitation, with FWHM ranging from 12 to 80 nm, are discussed in section 5.5. The measurements reveal that by broadening the excitation spectrum a higher *iPLQY* can be achieved at lower solar concentrations. The *iPLQY* of 16.2 ± 0.5% was achieved at 2270 ± 100 mW mm^{-2} which is the highest ever measured.

5.2 Material Characterisation of TGC doped with YF_3: 10% Er^{3+} NC's

The physical properties of the upconverter material have a strong effect on the UC mechanisms; therefore, should be characterised to understand their performance. Important characteristics such as crystal phase, particle or crystal size, concentration and host material can influence UC process [142]. The TEM images of the TGC with embedded YF_3: 10% Er^{3+} NC's is given in Figure 5.1 for the range of annealing temperatures investigated. The homogeneous dispersion of NC's can be seen clearly, with increasing size due to higher annealing temperature (Figure 5.1 (a)-(e)). Figure 5.1(f) demonstrates the low scatter and absorption of visible light of the sample with dimensions of 10×10×2 mm. From the TEM images a statistical analysis of the size distribution of the NC's for different annealing temperatures was performed (Figure 5.2). The size of the NC's, for samples annealed in the range 650-710°C, was calculated to be 30 nm, 45 nm, 55nm and 70 nm.

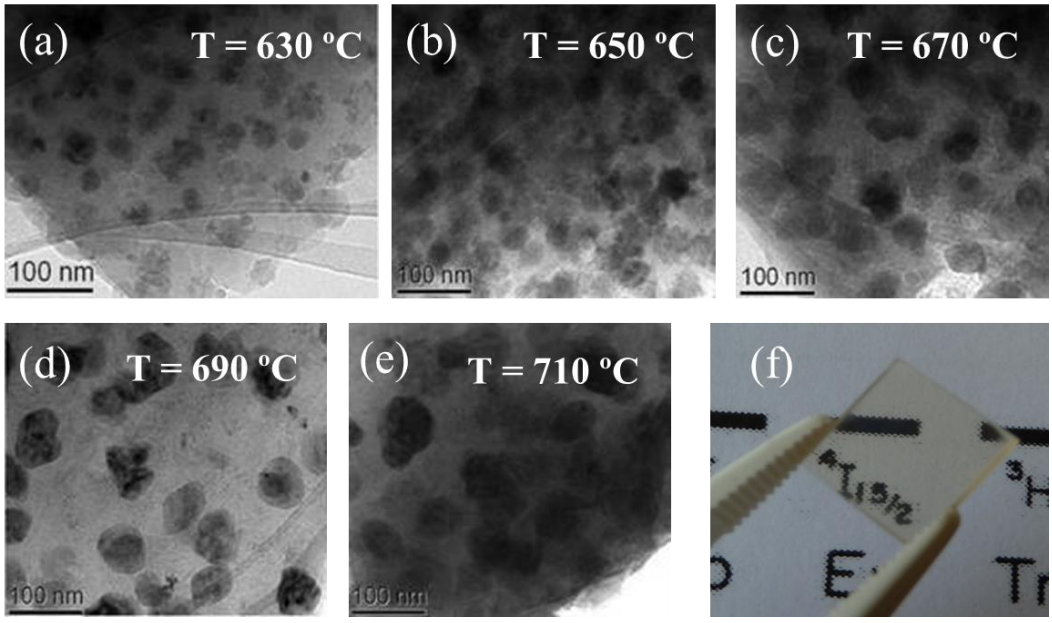

Figure 5.1 TEM images of the TGC samples annealed in the range 630-710°C, (a)-(e). (f) Shows there is very little scattering of visible light and low absorption. Courtesy of Daqin Chen at the Chinese Academy of Science, Fuzhou.

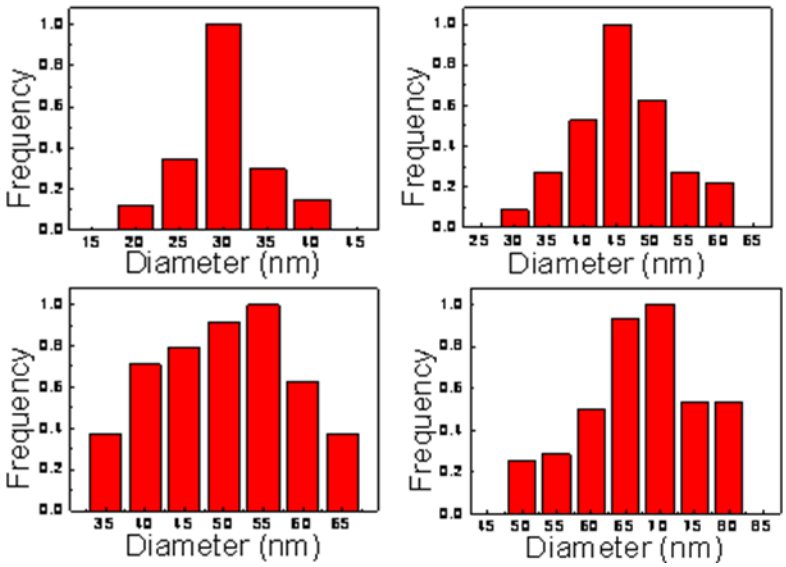

Figure 5.2 Size distributions for TGC samples annealed at temperatures of (a) 650°C, (b) 670°C, (c) 690°C and (d) 710°C. Higher temperatures lead to larger NC's with a broader distribution of size.

The phase of the NC's was measured through XRD which shows a transition in the phase from mixed hexagonal and orthorhombic to pure orthorhombic phase at temperatures > 650 °C (Figure 5.3). The diffraction peaks in the XRD confirm the formation of YF_3 NC's within the TGC. The size of the NC's can be calculated using the width of the diffraction peaks in the Scherrer equation (Equation 5.1) which gives sizes of 14 nm, 28 nm, 42 nm, 50 nm and 65 nm, with increasing temperature, respectively.

$$\Delta = \frac{\kappa\lambda}{\gamma \cos\theta} \qquad \text{Equation 5.1}$$

Here, Δ is the average crystal domain size, κ is a shape factor parameter which is dependent on the shape of the measured NC, λ is the wavelength of excitation, γ is dependent on the FWHM broadening of the diffraction peak (after removing the instrument response) and θ is the angle at which the diffraction peak occurs. This method is limited to NC particles < 100-200 nm and hence is suitable for the material measured here. These results match well with the statistical analysis from the TEM images discussed above. Analysis of the particle size is important as this parameter directly influences the *iPLQY*. This interdependency has been attributed to increasing surface to volume ratio with a greater number of surface defects leading to NR decay

[143]. Finally, EDX was also performed to determine the successful doping and precipitation of Er^{3+} within the TGC (Figure 5.4) which was calculated to be 10% Er^{3+}. The successful incorporation of Er^{3+} within the ordered precipitated NC's is desired as the phonon energies and defects are reduced in comparison to glass; hence, parasitic processes such as MPR and NR decay are reduced.

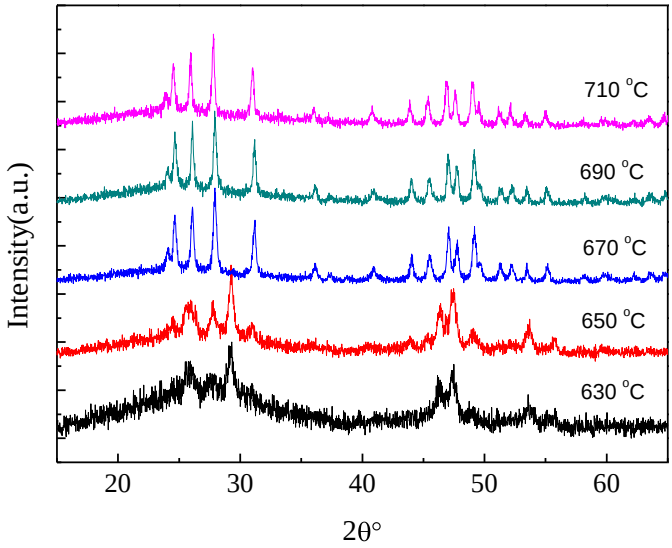

Figure 5.3 XRD analysis of the annealed samples showing the transition from a mixed hexagonal and orthorhombic to pure orthorhombic phase at temperatures > 650°C.

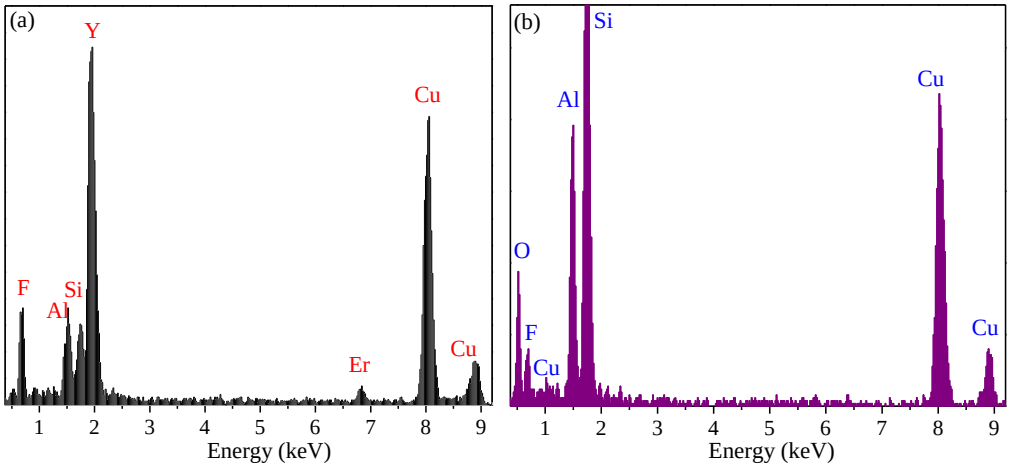

Figure 5.4 EDX of (a) the YF_3: 10% Er^{3+} NC doped TGC and (b) un-doped oxyfluoride TGC. The image shows successful incorporation of the doped NC's. The Cu component is due to the copper sample grid.

5.3 Bandwidth Dependent Photoluminescence of YF_3: 10% Er^{3+}

The absorbance of the TGC samples prepared at a temperature of 630-710 °C can be seen in Figure 5.5. The absorbance of the $^4I_{15/2}$ level shows a maximum peak at 1523 nm for all samples. Thus, the central wavelength of the excitation bandwidth was chosen in accordance with this. The sample annealed at 630°C was selected for photoluminescence measurements due to its higher absorption at the range of excitation. The spikes in the spectrum near 800 nm are due to inherent system artefacts which arise from the higher spectral correction at the limit of the monochromator within the UV-VIS spectrometer.

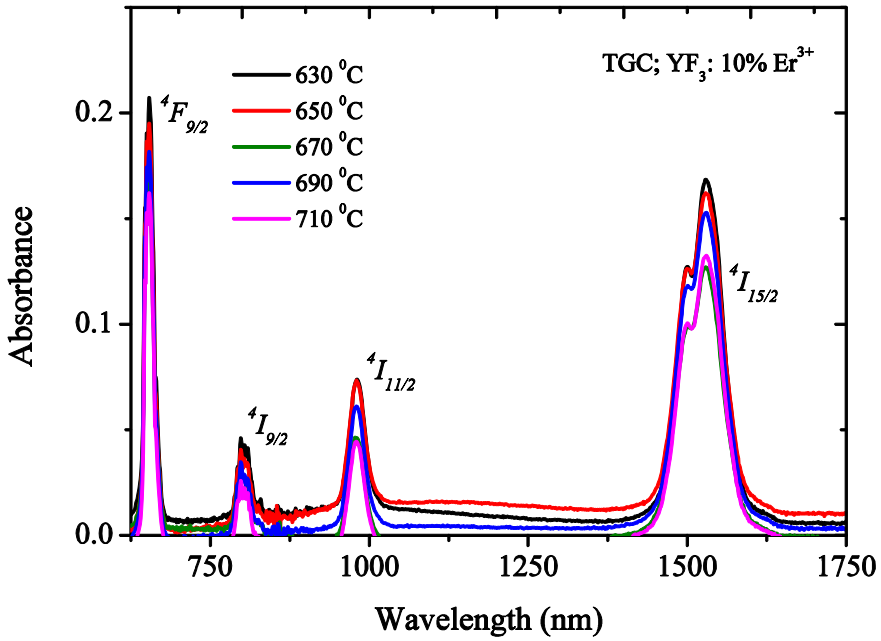

Figure 5.5 The absorbance properties of the YF_3: 10% Er^{3+} NC's within an oxyfluoride host for the sample processed at a temperature of 630-710°C. The energy levels are also shown for each absorption peak.

The UC photoluminescence measurement of the sample processed at 630°C has peak emission at 981 nm when excited with a 12 nm bandwidth centred at 1523 nm; as expected the host lattice has very little effect on the *4-f* shell, see Figure 5.6. To evaluate the effect of using broadband excitation the emitted UC light was measured and integrated to determine the total number of photons emitted per second (also referred to as counts per second (cps)). The emission was then compared to the irradiance and with respect to the bandwidth of excitation which was either 12 or 38 nm. Due to the non-linear properties of the UC material the photons emitted (P_{out}) are proportional to the square, for a two-step UC process, of the photons in (P_{in}). This can

be more generally described as the amount of UC photons emitted is proportional to the irradiance, raised to the power of the number of photons involved in the process (*n*):

$$P_{out} \propto P_{in}{}^{n} \qquad \text{Equation 5.2}$$

Consequently, when the results are plotted in a log-log plot, for example, a gradient of two is observed for emission from the $^4I_{11/2}$ level (980 nm) in the low pump regime as a minimum of two photons are required. As the pump power increases so does the population of the $^4I_{11/2}$ which therefore increases the probability of absorption, or energy transfer, of a third photon to a higher energy level. Other factors such as cross relaxation also increase at higher powers which lead to depopulation of the energy level. Hence a deviation from a straight line until saturation of emission is reached. Furthermore, higher photon UC will increase, such as green ($^4S_{3/2}$) and red ($^4F_{9/2}$) emission which also conspires to depopulate lower energy levels.

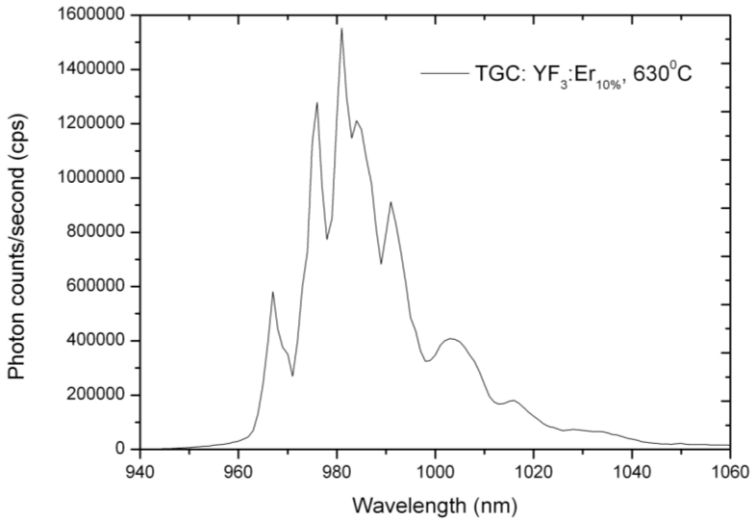

Figure 5.6 Emission spectrum of the $^4I_{11/2}$ level, under 12 nm bandwidth excitation centred at 1523 nm, of the TGC doped with YF_3: 10% Er^{3+} NC's which was processed at a temperature of 630°C.

Figure 5.7 shows that there is a strong enhancement of UC emission, representative of the total integrated emission of the $^4I_{11/2}$, due to an increase in excitation bandwidth. It is apparent that spectrally broader excitation, from 12 nm to 38 nm (a ratio of 3.17), leads to over a ~55 fold increase in UC emission. This enforces the fact the UC-PV has more potential than previously reported for monochromatic excitation. Coincidently

this also means that at least a factor of 7.6 less suns is necessary to achieve previous calculations of performance enhancement by increasing the bandwidth by a factor of 3.17. The implication for a practical system increases the likelihood of utilising standard cells rather than cells suitable only for high solar concentrations. The discussed improvement is shown for an increase in bandwidth from a FWHM of 12 nm to 38 nm allowing for significantly larger bandwidths to be used in the future with the current method, which will be investigated further in Chapter 5 and 6. This can be increased further to include all wavelengths of absorption in the excitation range leading to UC emission, negating the need for such high excitation intensities used currently. It should be noted that the absorption of this wider spectrum will become significantly less compared to the peak value at 1523 nm.

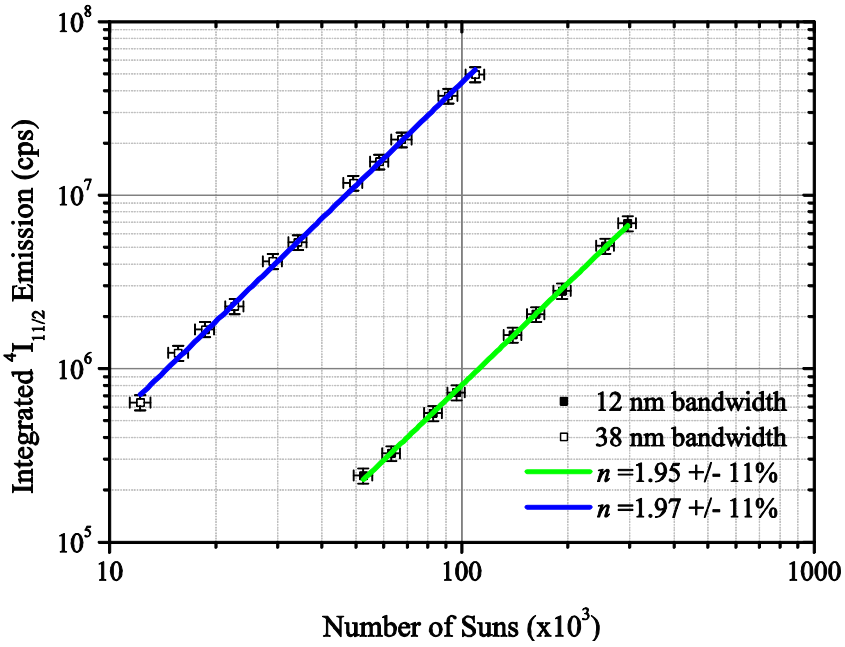

Figure 5.7 The integrated two-photon UC emission (counts per second) in relation to incident power flux for various powers between 10-300 $\times 10^3$ Suns concentration is shown. The log-log plot shows that the P_{out} vs. P_{in} has a gradient of just fewer than two which is close to the theoretical value.

It can also be seen in Figure 5.7 that the 12 nm and 38 nm bandwidth excitation gradients are equal to 1.95 and 1.97, respectively. This shows good agreement with theoretical predictions given by Equation 5.2. Although this value is below what would be expected it is well within experimental error. Measurements were conducted with different excitation spectra and irradiance therefore; the agreement of both the plotted lines reinforces the quality of these results. In addition, this value implies that UC of

the YF_3: 10% Er^{3+} doped NC's is due to a two-photon process; however time resolved measurements are necessary to determine whether this is due to GSA/ESA or ETU, which is not possible with the available set-up. The linear fit for both 12 nm and 38 nm excitation means that these samples are still in their low pump regime as a deviation from a straight line is not observed. It is apparent from the graph that a high level of solar concentration is needed to achieve good UC emission of these samples; a factor of 110 $\times 10^3$ Suns with a bandwidth of 38 nm used in excitation of the sample shows the highest emission. Although this is more than double the concentration limit achievable on Earth (46 $\times 10^3$ Suns) due to the angle subtended by the sun; this does mean that these samples show good stability under high power excitation.

5.4 Measurement Challenges

Attempts were made to measure the signal of the sample at lower excitation powers and to determine the *iPLQY*. However a couple of factors made this difficult which will now be discussed. The first is due to the noise associated with the measurement system, more specifically the NIR-PMT, that makes detection of UC light difficult at low irradiances. These can occur from various sources such as unwanted NIR emission from the environment and electrical noise within the equipment. Another problem which arises when conducting photoluminescent measurements is artefacts such as Lorentzian peaks and ghost effects. Lorentzian peaks are usually low in intensity and are due to scattered light passing through the emission monochromator. These can be reduced or removed by using; longer focal length monochromators, dual monochromators or filters to reduce the amount of scattered light entering the system. However, ghosts are due to periodic defects in the monochromator which cause large peaks at non-integer multiples of the excitation wavelength. These effects are present in the reference scatter, which in most cases can be used to remove them, however due to absorption of the excitation light in the sample being greater than the reference these peaks are smaller in the former. It was verified in this instant that the artefact peaks were due to excitation light scattered into the detector at given angles of the emission monochromator. The artefact present in the reference spectrum could therefore be normalised to the peak in the sample emission to be effectively removed.

The effect of aggregation is also present in the photoluminescent measurements as different orientations of the sample leads to variations in the peak counts of the UC light. Therefore the sample had to be handled carefully so that the same area and

surface was illuminated each time. Consistency was achieved by always using the maximum irradiance for alignment to replicate the peak emission counts before altering the power. The challenge of aggregation would therefore have to be overcome to gain a more consistent and repeatable performance, which would be necessity in a commercial UC-PV device.

The relative bandwidth dependent photoluminescent measurements of YF_3: 10% Er^{3+} are affected by many challenges although a qualitative comparison has been given. To quantify the effect of bandwidth dependence on UC it is necessary to evaluate the absolute value of *iPLQY*. Unfortunately, due to the compounding effects of both a low efficiency of the YF_3: 10% Er^{3+} NC's and the challenges mention above it was not possible to reliably measure the *iPLQY* under various bandwidths of excitation. Hence, the more efficient β-$NaYF_4$: 10% Er^{3+} phosphor was used to quantify the absolute enhancement of bandwidth dependence and will now be discussed in the following section 5.5.

5.5 Material Characterisation: β-$NaYF_4$: 10% Er^{3+} doped in PFCB

For the investigation of the *iPLQY* dependence on the bandwidth of excitation the UC phosphor measured in this section is β-$NaYF_4$: 10% Er^{3+}. As has already been discussed it is important that $NaYF_4$ host is of the efficient hexagonal phase which has been shown to be over an order of magnitude greater in efficiency than alpha phase. This can be determined via XRD analysis, performed at the University of Bern, which can be seen in Figure 5.8. The XRD measurements confirm that the phosphor is of the efficient β-phase as the peaks in the X-ray counts are aligned with the standard spectra shown as the dashes at the bottom of the graph.

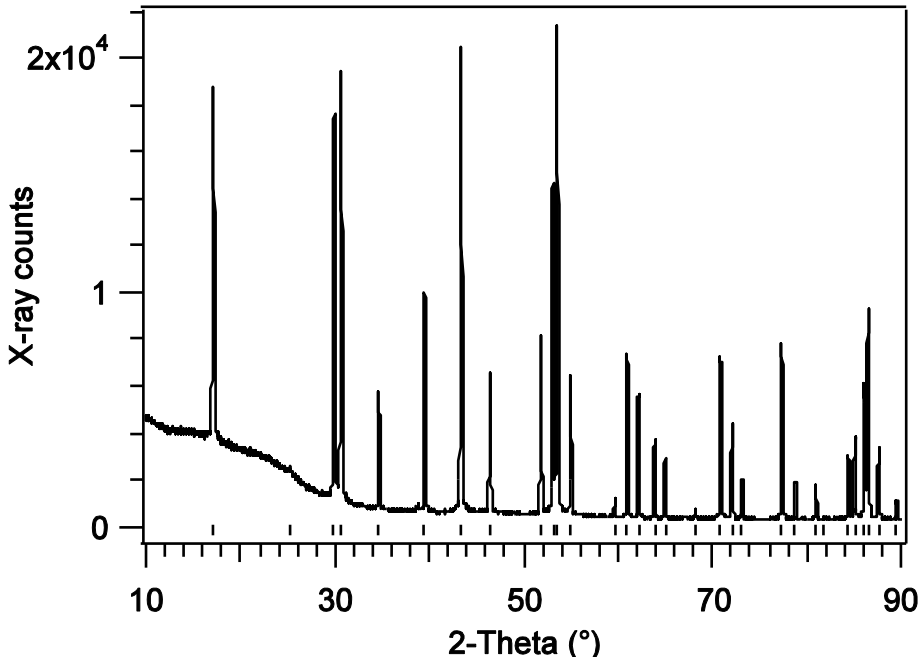

Figure 5.8 XRD analysis of the $NaYF_4$:Er^{3+} phosphor which clearly shows that the sample is of the more efficient hexagonal phase. Measurements were performed at the University of Bern courtesy of Karl Krämer.

The β-$NaYF_4$: 10% Er^{3+} phosphor is synthesised as a meso-powder, hence a binding matrix is required to hold the powder together. Various polymers, used in optical applications or in PV devices, were considered which will now be discussed. Ethylene-vinyl acetate (EVA) was investigated due to its use as an encapsulation material for Si solar cells [144] and luminescent solar concentrators [145]. A proven lifetime equal to that of a PV module as well as desirable optical properties for standard devices could make it a suitable polymer matrix. Another encapsulation material used in PV devices is poly (dimethylsiloxane) (PDMS). Thus for the reasons given above, this material was also given consideration as a possible matrix. Other polymer samples investigated were poly (methylmethacrylate) (PMMA, also known as Plexiglas®) and poly urethane (PU) which have been used in CPV design [10]. Finally, a fluorinated polymer, PFCB, was investigated due to a reduction in C-H bonds which are known to absorb in the NIR. Furthermore, PFCB has also shown to have desirable properties in conserving *iPLQY* of other luminescent species [137]. As can be seen from Figure 5.9, PFCB showed the best transmission in both the absorption and emission range of Er^{3+} doped β-$NaYF_4$ thus was chosen as the preferred matrix material.

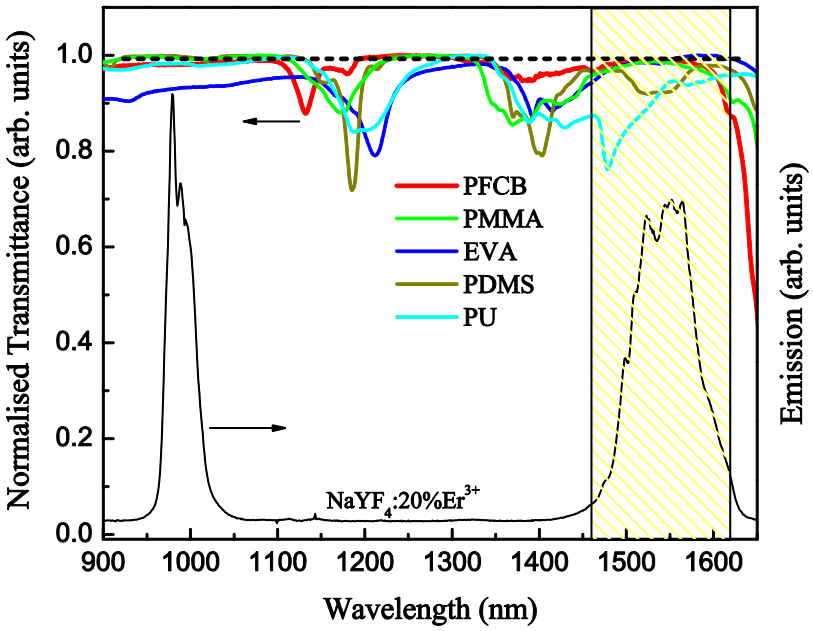

Figure 5.9 Normalised transmission in the absorption and emission range of the various polymers considered for the matrix material to bind the UC phosphor. The fluorinated polymer PFCB was chosen due to its superior performance

The β-$NaYF_4$: Er^{3+} embedded within the PFCB matrix with a 55.6%w/w ratio can be seen in the Scanning electron microscope (SEM) images in Figure 5.10. The phosphor powder β-$NaYF_4$: 10% Er^{3+} was prepared as described in Chapter 3. The final sample was polished to a good optical finish with dimensions of 1 mm in thickness and a diameter of 12 mm, which is confirmed from the cross section image in Figure 5.10. Figure 5.10 demonstrates the spatial separation of the phosphor and PFCB in host matrix used to bind the UC material. The inset Figure 5.10 shows the porous phosphor with a grain size of less than 5 µm. Therefore, it can be confirmed that the β-$NaYF_4$: 10% Er^{3+} was successfully embedded within the preferred fluorinated polymer PFCB, with a 55.6 w/w% phosphor to polymer ratio.

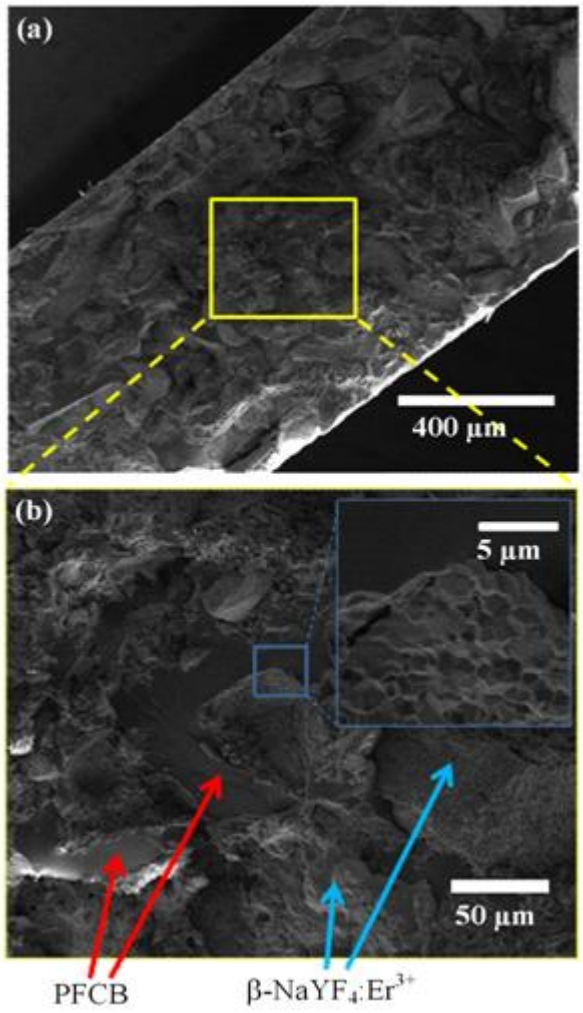

Figure 5.10 Scanning electron microscope (SEM) cross-section image of the UC phosphor (β-$NaYF_4$: 10% Er^{3+}) embedded in the PFCB matrix with a 55.6% w/w ratio with a thickness of 1mm and polished to a good optical finish (a). Magnification of the sample displays the spatially separated phosphor and host matrix PFCB regions (b). Inset in (b) shows the smaller porous grain size (< 5 µm) of the β-$NaYF_4$: 10% Er^{3+}.Courtesy Aruna Ivaturi.

5.6 Internal Photoluminescent Quantum Yield of β-$NaYF_4$: 10% Er^{3+}

The β-$NaYF_4$: 10% Er^{3+} UC phosphor embedded within the fluorinated polymer PFCB, with a 55.6 w/w% was measured under broadband excitation with FWHM ranging from 12 to 80 nm to determine the *iPLQY*. Figure 5.11 displays the excitation spectra used and how each channel is added to achieve greater bandwidths in an asymmetric/symmetric sequence, such that even channels increase bandwidth into the short-wavelength and odd channels into the long-wavelength end of the spectrum. The interplay of channel addition on peak photon counts makes it difficult to produce a flat top profile; however, the channel with the greatest variation in peak counts is within ±

5.5% relative to its average. Furthermore, all the individual channel maximum peak counts are within 2.6% of the average of all the channels. This allows the effect of bandwidth to be determined independently of any change in intensity at a given wavelength. It can also be seen that the long and short wavelength FWHM points are well matched in relation to channel addition (Figure 5.11). The AM1.5d spectrum in the wavelength range 1460 – 1600 nm has been plotted so as to allow one to compare the bandwidth used in excitation. Although there is a close match in the spectra used; for bandwidths greater than 61 nm the peak photon counts are less in the AM1.5d at wavelengths shorter than 1490 nm.

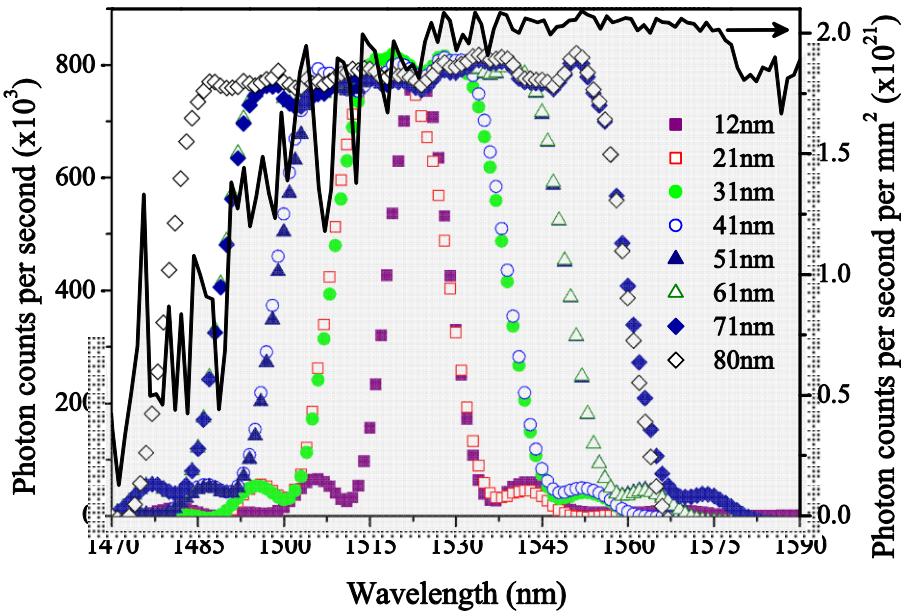

Figure 5.11 Excitation scatter spectra used to achieve UC emission at 980 nm. The broadening of the spectrum due to additional channels from the AOTF-HP can be seen as well as the asymmetric/symmetric sequence. The AM1.5d solar spectrum (grey shaded area) is also plotted against the secondary y-axis.

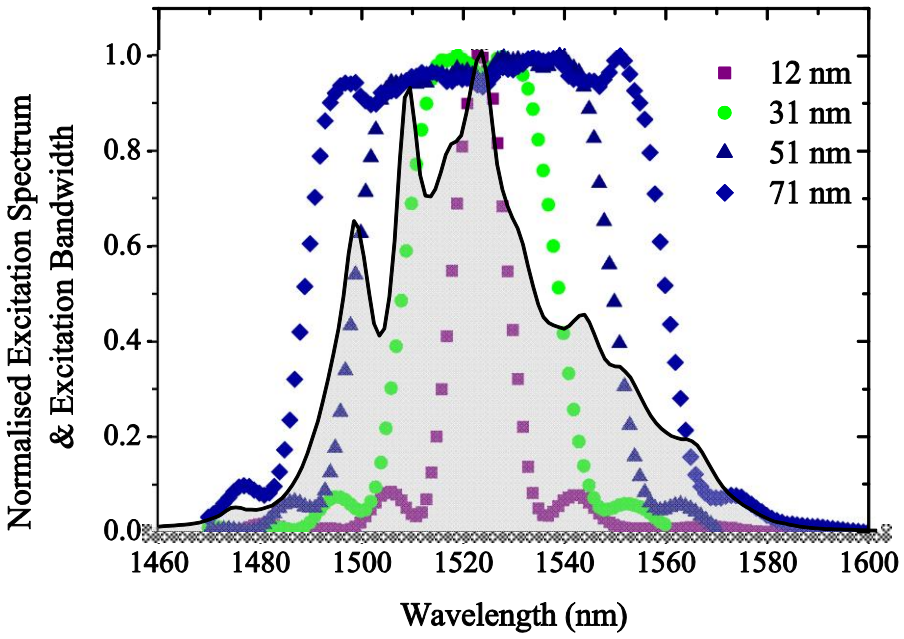

Figure 5.12 Excitation wavelength dependence of achieving 980 nm UC emission with clear resonant peaks at 1523, 1509 and 1498 nm as shown by the grey shaded area. Increasing bandwidths encompass a larger portion of the excitation spectrum.

An excitation scan was performed to determine the most efficient wavelength range at which to excite the β-$NaYF_4$: 10% Er^{3+} to achieve emission at 980 nm, shown in Figure 5.12 as the grey shaded area. The excitation intensity for odd channels is shown to describe how the broadening of the spectrum encompasses a greater number of resonant peaks.

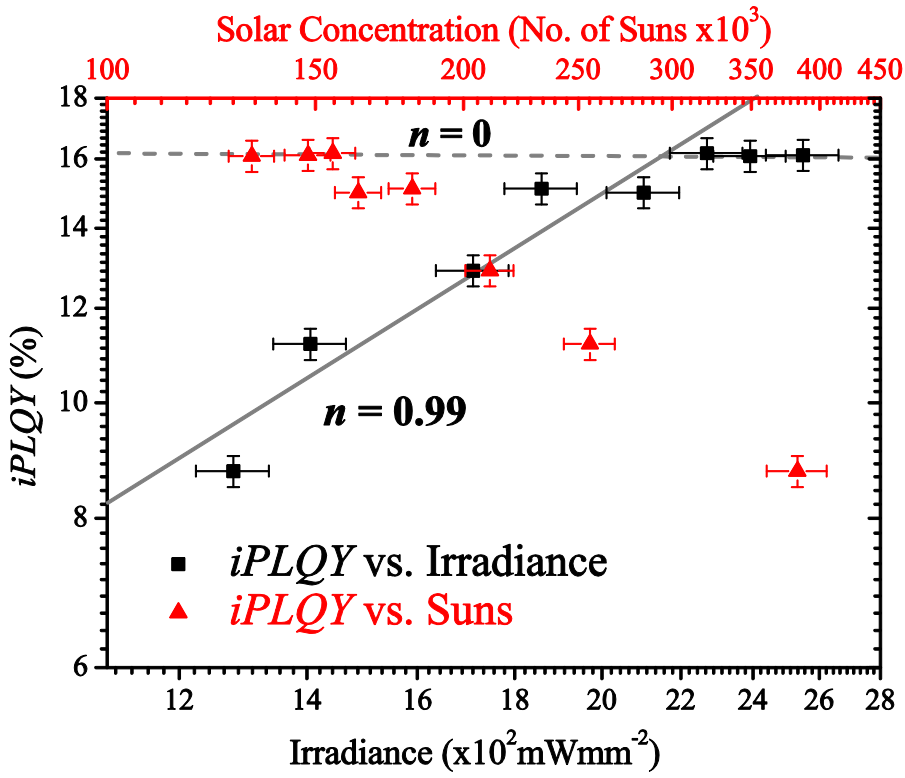

Figure 5.13 The standard reporting method is shown (black squares, ■) in comparison to the suggested "suns" method for broadband excitation (red triangles, ▲). These results show very high efficiencies, which improve with lower solar concentrations.

The results in Figure 5.13 show the comparison of broadband excitation in relation to irradiance and the proposed method of solar concentration to define the *iPLQY* of the UC sample. In Figure 5.13, it can be seen that the *iPLQY* increases with higher power (■) due to the non-linear nature of the two-photon UC process. The *iPLQY* for the narrowest FWHM = 12 ± 1 nm is 8.7 ± 0.3%. As the channel addition follows an asymmetric/symmetric step there is a large increase in *iPLQY* followed by a smaller increase, respectively, until saturation at 16.2 ± 0.5% is reached. This can be explained by the excitation spectrum, which shows greater resonance and larger peaks on the shorter wavelength side of the maximum at 1523 nm (Figure 5.12). Similarly, a lower resonance at longer wavelengths leads to a smaller increase in *iPLQY*. Therefore, a broadening into the short-wavelength range encompasses a larger portion of the excitation spectrum and subsequent higher population of the $^4I_{13/2}$ level (GSA), a prerequisite for UC emission. It has been shown previously that ETU is the dominant mechanism for high concentrations of Er^{3+} (>2%) within the $NaYF_4$ host under monochromatic excitation [53]. However, due to the broadband nature of the excitation spectrum, it is reasonable to assume that ESA has a higher contribution due to the

presence of a wider range of resonant photons. Therefore, in comparison to monochromatic excitation, where the highest efficiencies are reported at the greatest resonant wavelength; the synergistic effect of exciting multiple resonant peaks associated with the individual transitions ($^4I_{15/2} \rightarrow {}^4I_{13/2}$ and $^4I_{13/2} \rightarrow {}^4I_{9/2}$) leads to an improved performance. Validation of the contribution from ESA requires careful analysis of photoluminescence decay measurements and is not possible with the current set-up. Once the bandwidth increase surpasses these peaks (> 61 nm) there is a reduction in this effect, hence the *iPLQY* saturates with the only variation due to experimental error. The *iPLQY* of 16.2% is the highest value reported in the literature for an UC material known to the author. This value was measured at 61 ± 1 nm bandwidth with a central wavelength of 1519 nm and a power of 2270 ± 100 mW mm^{-2}. It should be noted that an *iPLQY* of 16.2% represents the conversion of over 32% of the absorbed photons. The absorption of the sample was measured to be on average 20.8% in this region. This equates to an *ePLQY*, a ratio of emitted photons to incident photons, of 3.4%. The previous highest *iPLQY* was for an Er^{3+} doped ZBLAN glass investigated by Ivanova and Pellé [78] with an *iPLQY* of 12.7%. The result achieved in this work is also slightly higher to the *iPLQY* of 16% which was measured for an organic upconverter [146], however with absorption at 670 nm this does not apply to Si devices. To make some reference to monochromatic excitation, as this is not possible with the AOTF-HP the same sample was measured using a tuneable laser (HP Agilent, 8168F) with a power of 38 ± 2 mWmm^{-2} at the absorption peak of 1523 nm. The attained efficiency was 1.1 ± 0.1%. However, due to the limited power from the tuneable laser this does not make for good comparison for the value of irradiances under broadband excitation. As the measurements saturate at a consistent value this validates the repeatability of these results for β-$NaYF_4$: 10% Er^{3+} through broadening of the excitation spectrum. Figure 5.13 is displayed in a double logarithmic plot, which allows the linear relation between *iPLQY* and irradiance to be observed (Equation 5.3 and 5.4).

$$No.\ of\ Photons\ Emitted \propto I_o^2 \qquad \text{Equation 5.3}$$

$$iPLQY \propto \frac{No.\ of\ Photons\ Emitted}{I_o} \propto I_o \ \therefore \log\ iPLQY \propto 1 \cdot \log(I_o) \qquad \text{Equation 5.4}$$

The gradient is calculated to be n = 0.99 for the data before saturation, which agrees with the theoretical value n = 1. Therefore, increasing bandwidth of excitation, while

keeping the intensity per nm constant, follows the same relation to increasing power. For applications where a high *iPLQY* is required one could use spectrally broader sources rather than increasing power at a given wavelength. Equivalently, the same *iPLQY* can be achieved with a factor of 1.9 less power with an increase in bandwidth by a factor of 5.1. The implication of this is that previous efficiencies for UC-PV devices could be achieved at lower powers or enhanced when illuminated by a broader spectrum.

When the *iPLQY* is normalized to the irradiance required, a value of 7×10^{-4} cm^2 W^{-1} was calculated. This is a reporting method suggested by Auzel [37] to account for higher efficiencies at higher irradiances due to the non-linear behaviour of upconverter. However, this analysis is limited at higher irradiances where the *iPLQY* saturates and hence the normalised value decreases. This value is significantly lower than that reported by Fischer *et al.* [57], with a normalized efficiency of between 0.27-0.03 cm^2W^{-1}. Furthermore, it is also one order of magnitude lower than the result calculated by Richards *et al.* [77] of 0.07 cm^2W^{-1} for an extrapolated efficiency of 16.7% although their measurements were performed with a higher Er^{3+} concentration (β-$NaYF_4$: 20% Er^{3+}).

The results in Figure 5.13 are significant when presented in the new "Suns" method, which accounts for a broadband excitation spectrum (▲). When the same values of *iPLQY* are plotted in relation to the solar concentration defined by Equation 3.3, corresponding to the equivalent irradiance for a given bandwidth, an inverse relation is observed. As the bandwidth is increased so does the power due to the addition of further channels; however, an increase in bandwidth in relation to the solar spectrum also increases the irradiance. For the bandwidths measured between 12 – 80 nm the irradiance used increases by a factor of 2. Equivalently, in relation to the AM1.5d spectrum, a factor of 5 increase is observed over the same bandwidth. This means that although the irradiance is increased, the actual solar concentration is reduced leading to an enhanced performance at a lower number of suns. Thus, the use of broadband excitation increases the available power without increasing the solar concentration. With comparison of the results achieved here, one can increase the *iPLQY* by a factor of 1.9 with a reduction in solar concentration by a factor of 2.9 via utilisation of a broader spectrum. This emphasises the importance of the proposed method for excitation and understanding the true potential of UC-PV devices.

Although the solar concentrations used in these measurements are beyond the diffraction limit achievable on Earth (45×10^3 suns limit [147]), they were performed on a sample that has neither been optimized in Er^{3+} concentration with the β-$NaYF_4$ host nor the loading factor of the phosphor within the polymer matrix. A study conducted by Ivaturi *et al.* [66] has shown that increasing the loading of the phosphor can improve the *iPLQY* further. A relative increase in *iPLQY* of 47% is possible when increasing from 55.6w% to 84.9w%. In addition, with the increased interest in the field of UC-PV and recent publications on the use of NIR quantum dots (QD) as spectral concentrators [114], it has been shown that performance of UC-PV devices can be improved. This can be achieved by absorbing the photons between the band edge of Si and the absorption range of Er^{3+} using QD's, which then emit in the range of the upconverter [113]. Moreover, the use of a PFCB host in the present study has the additional benefits when encapsulating NIR emitting QD's, with investigations indicating preservation of *iPLQY* and homogeneous dispersion [137]. The addition of these spectral concentrators would therefore make the efficiencies reported herein more practically achievable. Further investigation into the use of photonic structures for increasing the local electric-field surrounding the UC will also allow for greater intensities to be achieved under a lower factor of suns. A recent paper by Johnson *et al.* [74] modelled a 1-D photonic structure (commonly used as an anti-reflection coating) to determine the enhancement of excitation light. Simulations showed that an enhancement factor between 2 and 18 could be achieved for 10 and 40 layer structures, respectively. Nevertheless, as the enhancement factor increases the relative bandwidth decreases, which implies that optimisation would be needed for broadband excitation. Moreover there is a large potential for the use of plasmonics for increasing the intensity of incident spectrum through localised and propagating surface plasmons with possible enhancement factors of 450 times [148]. With these new advances in nano-materials and structures, in conjunction with analysis under broadband excitation, it is promising that the high *iPLQY* reported here can be achieved under more realistic conditions. This is an important consideration in the potential dissemination of this technology.

5.7 Conclusions

The TGC was prepared by melt quenching to produce active YF_3: 10% Er^{3+} NC's within an oxyfluoride host material processed at 630°C. Investigation of the effect on UC emission due to broadband excitation showed that for a factor 3.17 increase in spectral irradiance lead to a ~55 fold improvement in UC emission. In relation to the

performance previously reported in the literature, this could suggest a factor of 7.6 less Suns would be required through broadening of the excitation spectrum by a ratio of 3.17. This means the characterisation of UC materials for PV through broadband excitation is required to determine their true potential to enhance the collection of sub-band gap photons. Although ultra-high irradiances were used in these measurements, in relation to the AM1.5d spectrum, the UC process was shown to follow close to a quadratic dependence alluding to the sample still being in a low irradiance regime. Broadening the spectral content and using higher irradiances would determine the optimum pump regime for the TGC's. Improvements in performance could be achieved by increasing the concentration of the active UC and that of the NC's to increase the probability of ETU and the absorbance of light. Unfortunately, it was not possible to determine a reliable value for the *iPLQY* mainly due to the weak absorption of the sample. Therefore, to investigate the effect of broadband excitation on the *iPLQY* a more efficient UC phosphor was used.

One of the most efficient UC materials from the literature was chosen to further investigate the effect of broadband excitation on the *iPLQY*. This is the first time that β-NaYF4:Er^{3+} has been measured within PFCB and for any UC material under broadband excitation to determine the *iPLQY*. The *iPLQY* has been shown to increase from 8.7% to 16.2% by increasing the bandwidth from 12 nm to 61 nm, at which point the efficiency saturates for higher bandwidths. As this is the first time *iPLQY* measurements have been reported for broadband excitation, a reporting method was developed to present the analysis in an intuitive way through solar concentration. The resulting *iPLQY* of 16.2 ± 0.5% at 2270 ± 100 mW mm^{-2} (7 $\times 10^3$ W^{-1} cm^2) or equivalently (155 ± 7) $\times 10^3$ suns is the highest value reported in the literature. Although this is far beyond the solar concentration achievable on Earth, the measurements reported in the present study were performed on a sample without optimization of Er^{3+} concentration or phosphor loading within the host matrix. With an improved understanding on the limits of UC and in conjunction with enhancement from photonics and nano-materials, one can determine the true potential of UC-PV.

CHAPTER 6 – BROADBAND OPTIMISATION: ER^{3+} CONCENTRATION AND POWER DEPENDENCE

6.1 Introduction

In the field of UC-PV it is imperative to determine the efficiency limits and optimum material for this process to determine the feasibility of this technology. Further to this, the methods used to characterise these properties should best represent those to be expected within its proposed application. Therefore in this chapter, the optimum Er^{3+} doping within the efficient upconverting host material β-$NaYF_4$ is investigated for a wide range of irradiance values while under broadband excitation (80 ± 1 nm). In Section 6.2 of this chapter, measurements of the *iPLQY* have been conducted over two orders of magnitude in irradiance with the corresponding solar concentrations characterised to determine the optimum Er^{3+} concentration. The highest *iPLQY* was for 20% Er^{3+} with a value of 10.7 ± 1.2% equivalent to a normalised efficiency of (5.43 ± 0.90) $\times 10^{-4}$ cm^2W^{-1} at an irradiance of 1.97 ± 0.24 MWm^{-2} ((108 ± 13) $\times 10^3$ Suns). The dominant UC mechanisms are then discussed in Section 6.3. Through analysis of the *iPLQY* dependence of each Er^{3+} concentration in regards to irradiance, their effect on saturation can be deduced. The mechanisms are further explored in Section 6.4 through analysis of the photoluminescence and in comparison to theory. More importantly for application to Si solar cells, the *ePLQY* is discussed in Section 6.5. The highest *ePLQY* was for 25% Er^{3+} and was measured to be 6.6 ± 0.7% ((3.35 ± 0.56) $\times 10^{-4}$ cm^2W^{-1}), which agrees well with monochromatic investigations. The 25% Er^{3+} sample was shown to be more efficient due to an anomalous increase and broadening of the absorption in comparison to lower concentrations which is investigated in Section 6.6. In the penultimate section, energy transfer mechanisms are proposed for the reduced efficiency of higher concentrations and depletion of the upconversion luminescence. Finally, the conclusions are given in Section 6.7 where the importance of these results are interpreted in regards to their application within a UC-PV device

6.2 Power Dependent Internal Photoluminescent Quantum Yield: Optimisation of Er^{3+} Concentration

The *iPLQY* was measured for all Er^{3+} concentrations from 10 to 75 mol.% to evaluate the most efficient doping for the $^4I_{11/2}$ to $^4I_{15/2}$ emission which has been shown to be an order of magnitude stronger than any higher UC emission in this material [64]. All measurements were conducted with a constant bandwidth of excitation (80 ± 1 nm) and

a phosphor doping of 55.6 w/w% within the PFCB polymer matrix for various irradiances of excitation. In Figure 6.1 the concentration dependence of the *iPLQY* for a range of almost two magnitudes in irradiance is shown. The general trend observed is that the *iPLQY* increases with an increase in irradiance, for all individual Er^{3+} concentrations, as expected from the non-linear nature of the UC process. The optimum Er^{3+} concentration of the UC phosphor is always between 20 – 25 mol% within the range of irradiances measured. The highest value of *iPLQY* is 10.7 ± 1.2% for an Er^{3+} doping of 20% at an irradiance of 1.97 ± 0.24 MWm^{-2} (see also *Table 1*).

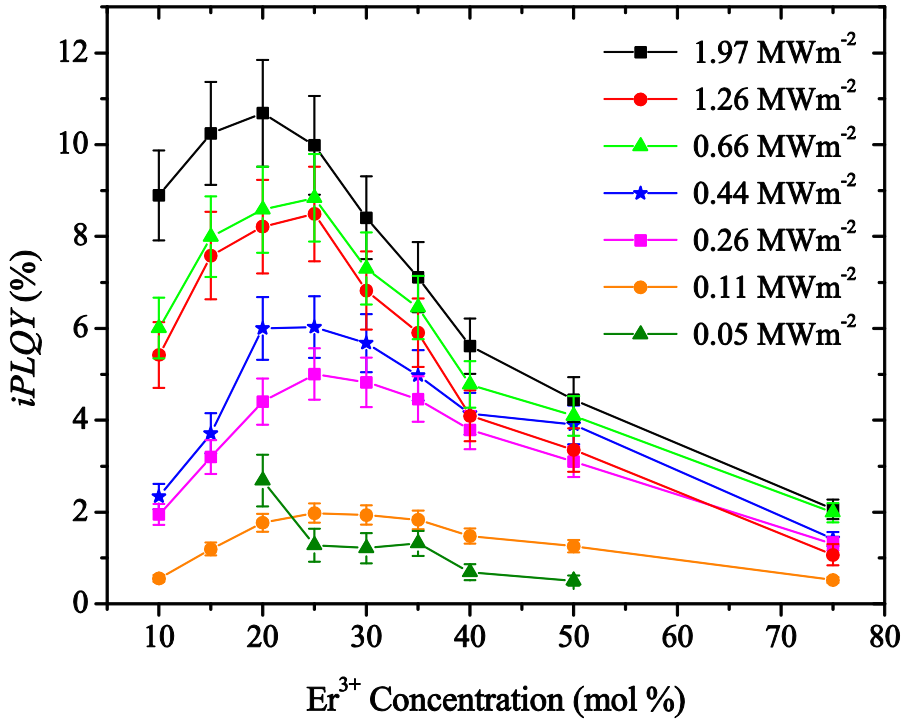

Figure 6.1 iPLQY values of β-$NaYF_4$: Er^{3+} for Er^{3+} doping from 10 to 75% under various irradiances. The optimum concentration is consistently between 20% and 25% for all irradiances measured.

The *iPLQY* normalised to the irradiance, which was suggested by Auzel [37] as means of comparison for different values of irradiance, is (5.43± 0.90) $\times 10^{-4}$ cm^2W^{-1}. This is three orders of magnitude lower than that calculated for the 20% Er^{3+} sample under monochromatic excitation at 970 Wm^{-2} (0.54 ± 0.08 $cm^2W^{-1}$for 55.6 w/w% phosphor loading) [66]. However, the former result was obtained within a high power regime where saturation (see further discussion below) will reduce the value of normalised efficiency. If the *iPLQY* has reached saturation, increasing the power will only reduce the calculated normalised efficiency. Thus comparisons should be conducted for

measurements below saturation only. Hence, an improved comparison before saturation is that of the 25% Er^{3+} sample at 0.26 MWm^{-2}, where a value of (1.92 ± 0.32) $\times 10^{-3}$ cm^2W^{-1} was calculated, with that of the equivalent sample under monochromatic excitation of 0.59 ± 0.08 cm^2W^{-1} [66]. This result means that broadband excitation is less efficient than monochromatic excitation (at the absorption maximum) because the absorption varies over the broadband excitation spectrum. This may appear detrimental to the use of broadband excitation for a UC-PV device, however, it is more important to emit a greater number of photons under an equal magnitude of solar concentration. In regards to the previous results in Chapter 5 on the bandwidth dependence of the *iPLQY* for β-$NaYF_4$:10% Er^{3+}, a normalised efficiency of 7 $\times 10^{-4}$ Wcm^{-2} was measured at a bandwidth of 61 nm and an irradiance of 2.27 MWm^{-2}. This is greater than that measured here at a bandwidth of 80 nm and a power of 1.97 MWm^{-2} which is (4.52 ± 0.78) $\times 10^{-4}$ Wcm^{-2}. In Chapter 5 the 10 mol% Er^{3+} sample was shown to have saturated in efficiency for bandwidths ≥ 61 nm, hence it is difficult to compare the results as although the power is less (improving the normalised efficiency) the bandwidth is greater (reducing the normalised efficiency). It is important to reiterate here that a modification to the experimental set-up (than that used in Chapter 5) with the addition of a multi-mode fibre was made. Homogenisation of the spacial output with the free space propagation of a top-hat distribution, which was determined to be more beneficial to the characterisation of irradiance, was achieved. This has resulted in a lower transmission of power. With these points in consideration, the results of the normalised efficiency agree fairly well within experimental error.

From Figure 6.1, it is apparent that at higher concentrations *iPLQY* reach saturation at lower values of irradiance, as expected. The saturation effect can be explained due to higher absorptance, which is defined as the fraction of the total photons that are absorbed to those incident. This leads to greater population of the intermediate state and increased possibility for energy transfer mechanisms that are determined by ion-ion separation; therefore achieving equilibrium of the dynamics sooner. In the lower irradiance regimes the difference in *iPLQY* is less for concentrations above that of the optimum (30-75 mol% Er^{3+}) whereas for higher irradiances the difference is observed to be greater. Again, the dominance of the energy transfer mechanisms is determined by the Er^{3+} concentration and the population of intermediate excited state due to increased absorptance and irradiance. Therefore, at higher irradiances a non-linear reduction in the *iPLQY* is observed for higher concentrations in comparison to a more linear trend at

lower irradiances. For lower concentrations than the optimum (10-25 mol% Er^{3+}), the reduction of the *iPLQY* can be attributed to lower absorptance of the sample as well as a greater ion separation reducing the effect of the efficient ETU mechanism. The measurements are also consistent with monochromatic measurements on the optimum doping concentration for β-$NaYF_4$:Er^{3+} [66], which demonstrated 25 mol% to be the most efficient, but at an irradiance of 970 Wm^{-2}. With these previous results in mind, β-$NaYF_4$:25% Er^{3+} has been shown to be the most efficient for both monochromatic and broadband excitation for a significant range of irradiances. At the highest irradiance measured the optimum shifts to 20 mol% Er^{3+} which can again be attributed to energy transfer to higher energy levels. This will be discussed in more detail with regards to power dependent measurements in section 6.3.

Table 1 Optimum Er^{3+} concentration within the β-$NaYF_4$ host lattice in regards to both iPLQY and ePLQY for a range of irradiances and the equivalent solar concentration (number of Suns).

Irradiance (MWm^{-2})	**Suns ($\times 10^3$)**	**opt. Er^{3+} conc. (mol. %)**	***iPLQY* (%)**	***ePLQY* (%)**
1.97 ± 0.24	**108 ± 13**	**20, 25**	**10.7 ± 1.2**	**6.6 ± 0.7**
1.26 ± 0.15	**68.8 ± 8.0**	**25**	**8.7 ± 1.0**	**5.7 ± 0.6**
0.65 ± 0.08	**35.5 ± 4.2**	**25**	**8.8 ± 0.9**	**5.8 ± 0.6**
0.44 ± 0.05	**24.0 ± 2.7**	**25**	**6.0 ± 0.7**	**3.7 ± 0.4**
0.26 ± 0.03	**14.2 ± 1.6**	**25**	**5.0 ± 0.6**	**3.2 ± 0.3**
0.11 ± 0.01	**6.01 ± 0.53**	**25**	**2.0 ± 0.2**	**1.2 ± 0.1**
0.05 ± 0.01	**2.73 ± 0.53**	**20, 25**	**2.7 ± 0.6**	**0.3 ± 0.1**

The non-linear response of the UC phosphor makes it important to define the values of *iPLQY* with respect to the irradiance of excitation. Moreover, for UC-PV device applications, it is important to discern what this means in terms of the solar concentration required. A facile method described in Chapter 3 can be used to make a first approximation, see Equation 3.3. The estimate of the number of Suns is given in *Table 1* with the corresponding value of irradiance. For the highest *iPLQY* of 10.7% a solar concentration of (108 ± 13) $\times 10^3$ has been calculated. This high value is more

than double that achievable with regards to the fundamental diffraction limit of 45×10^3 Suns [6]. At lower solar concentrations of $(6.01 \pm 0.53) \times 10^3$, which would be a more feasible level, the maximum *iPLQY* for 25% Er^{3+} has reduced considerably to 2.0 ± 0.2%. Therefore, novel methods are required to reduce the actual incident solar concentration while increasing the irradiance incident on the UC layer to achieve higher efficiencies. These challenges could be met by the proposed use of spectral concentrators such as QD's which can harvest the light between the band edge of c-Si and emit in the range of the UC and would increase the available power flux by around a factor of four for the UC process [113]. Furthermore, greater improvements are expected for the inclusion of the upconverter material within a photonic structure [75] or in conjunction with plasmonic resonators [148]. A combination of these methods could also be used for an advanced UC-PV device to gain from higher intensities at lower solar concentrations.

6.3 Power Dependent Internal Photoluminescent Quantum Yield: Mechanisms and Saturation

The *iPLQY* for the range of Er^{3+} concentrations can also be analysed in relation to the increase in irradiance as displayed in Figure 6.2 (a-d). The non-linear nature of the UC process can be seen due to the linear trend in the log-log scale graph. Only selected concentrations which are representative of the overall trend for Er^{3+} series are shown, all other concentrations can be seen in Figure 6.3 for reference. The relationship between the UC luminescence (L_{UC}) to the incident power (P) can be modelled by an effective three energy level system. The population of the intermediate level (N_2) is dependent on the absorption coefficient (σ_{12}), the incident power or pumping rate (P) and the concentration of the active ions (N_1, population of the ground state) which is described by Equation 6.1. The population of the emitting state (N_3) is proportional to the energy transfer between two intermediate states; hence, it is dependent on the product of the probability of one ion relaxing to the ground state (W_{21}) and transferring its energy to an ion in the excited state (W_{23}), see Equation 6.2. This shows that the population of N_3 is proportional to the square of the incident power. More generally, this can be described by Equation 6.3 where the L_{UC} is proportional to P with an exponent equal to the number of photons required (n) [149]. As the *iPLQY* is the L_{UC} divided by the absorptance (A), hence, its dependence on the incident power is given by Equation 6.4.

$$N_2 \propto \sigma_{12} P N_1 \qquad \text{Equation 6.1}$$

$$L_{UC} \propto N_3 \propto W_{21}W_{23}{N_2}^2 \propto P^2 \quad \text{Equation 6.2}$$

$$L_{UC} \propto P^n \quad \text{Equation 6.3}$$

$$iPLQY \propto \frac{L_{UC}}{A} \propto \frac{P^n}{P^1} \propto P^{n-1} \quad \text{Equation 6.4}$$

Thus, for a two-photon process, the *iPLQY* will show a linear dependence with power (here, *n-1 = m*). The initial gradients of Figure 6.2 (b-c) match well with theory with *m = 1* defining the low irradiance regime (see *Table 2* for all concentrations). In Figure 6.2(a) the 10 mol% Er^{3+} sample shows a super linear trend at lower irradiances which can be ascribed to error as well as the data range used for comparison. The saturation of higher concentrations at lower irradiances is also clearly observed (see *Table 2* for all other concentrations). The reciprocity of this is that concentrations equal to or lower than 25 mol% Er^{3+}, which is the optimum within the range measured herein, can still achieve higher efficiencies under greater magnitudes of irradiance. For Figure 6.2(a) and (b) this is explained by the reduction to a sub linear trend at higher irradiances (*m < 1*, high pump regime) whereas for 25 and 50 mol% Er^{3+} these have almost all but reached saturation (*m = 0*) for the relative irradiances. Saturation is predominantly due to depopulation of the emitting level through higher photon ETU [64] although, it is also affected by all other loss mechanisms. Comparing Figure 6.2(a, b) with (c, d) a transition from the low pump regime (*m = 1* to *m < 1*) is apparent at an irradiance of 0.66 ± 0.08 MWm^{-2} for low concentrations, whereas this occurs at 0.26 ± 0.03 MWm^{-2} for concentrations above 25 mol% Er^{3+}. For higher ion doping a beneficial effect at low irradiance due to higher absorption and ETU is observed, but is deleterious at higher concentrations where higher energy transfer becomes more dominant [64]. The saturation in *iPLQY* of the power dependent results for higher concentrations shows the upper limit achievable under broadband excitation of the $^4I_{15/2}$ level. Therefore advanced technologies to reach higher irradiances (discussed above) in conjunction with lower concentrations would be needed to achieve higher *iPLQY* with broadband excitation similar to the sun.

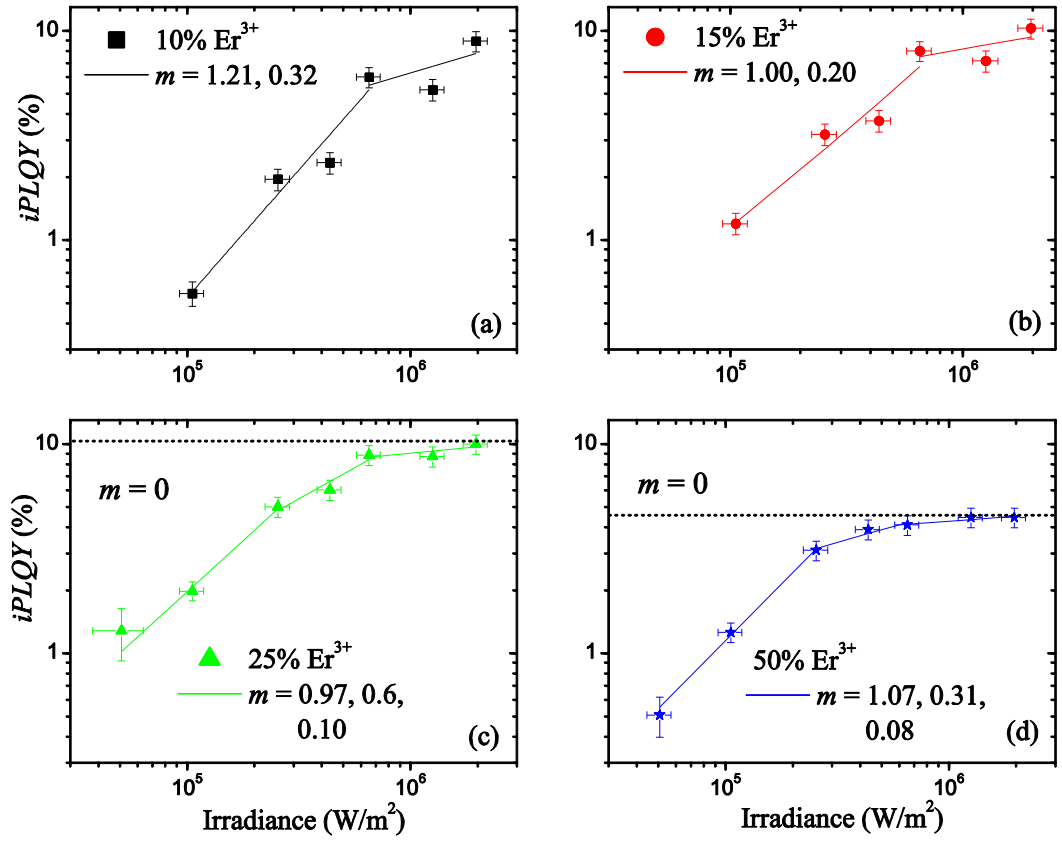

Figure 6.2 Log-log plot of the power dependence of *iPLQY* for concentrations of (a) 10, (b) 15, (c) 25, and (d) 50 mol% Er^{3+} in β-$NaYF_4$:Er, respectively, indicating the non-linear UC process and saturation for higher concentrations. The value (m = n-1) is representative of the log relationship between the *iPLQY* which is proportional to P^m and n represents the number of photons required for emission. The dotted lines represent *m = 0* where saturation is expected.

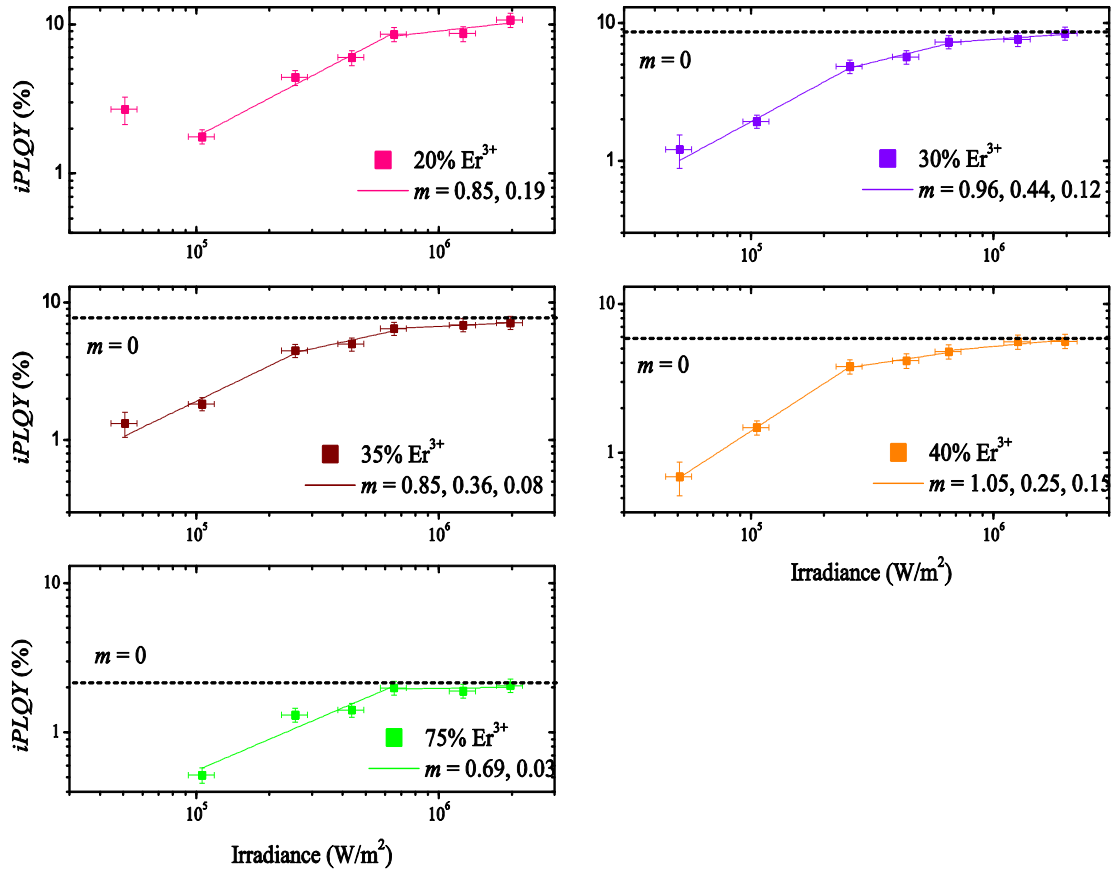

Figure 6.3 Log-log plot of the power dependence of *iPLQY* for concentrations of 20, 30, 35, 40 and 75 mol% Er^{3+} doped β-$NaYF_4$ host lattice, respectively, indicating the non-linear UC process and saturation for higher concentrations. The value (*m = n-1*) is representative of the log relationship between the iPLQY which is proportional to P^m and n represents the number of photons required for emission. The dotted lines represent m = 0 where saturation is expected.

Table 2 The iPLQY dependence on irradiance (the gradient, m = n-1, where n is the number of interactive photons) is listed for all Er^{3+} concentrations for the defined high, intermediate and low pump regimes.

Er^{3+} Concentration (mol %)	High Pump Regime	Intermediate Pump Regime	Low Pump Regime
10	**0.32**	**1.21**	
15	**0.20**	**1.00**	
20	**0.19**	**0.85**	
25	**0.10**	**0.60**	**0.97**
30	**0.12**	**0.44**	**0.96**
35	**0.08**	**0.36**	**0.85**
40	**0.15**	**0.25**	**1.05**
50	**0.08**	**0.31**	**1.07**
75	**0.03**	**0.69**	

6.4 Power Dependent Photoluminescence of β-$NaYF_4$: Er^{3+}

The observation of a non-linear process is also supported by Figure 6.4 (a-d) which displays the relationship between the integrated emission from the $^4I_{11/2}$ level and the irradiance on a log-log plot. Again, selected Er^{3+} concentrations are chosen which are representative of the overall series with other concentrations displayed in Figure 6.5 for reference. The relation between the UC luminescence (L_{UC}) and the pump power (P) is given by Equation 6.3, where n is the number of photons that interact in the process [149]. For 25 mol% Er^{3+} in the lower power regime (between 0.05 ± 0.01 MWm^{-2} and 0.65 ± 0.08 MWm^{-2}) the trend ($n = 2.00$) matches perfectly with theory and is also true when saturation is reached with a transition to a gradient equal to one. It has already been discussed that this saturation in the higher power regime is largely due to higher photon energy transfer [64]. This phenomenon also describes that of the 50 mol% Er^{3+}sample, see Figure 6.4(d), however; as the gradient in the lower irradiance regime is $n < 2$ this indicates an earlier onset of saturation compared to 25% Er^{3+}. This is observed for all pump regimes where higher concentrations show an earlier onset in saturation (comparison of all concentrations are shown in Table 3). Full saturation occurs when the increase in photoluminescence becomes linear and has been indicated in both Figure 6.2(c) and (d). As this has a reciprocal affect for lower concentration (Figure 6.4(a) and (b)) this can be ascribed to the energy transfer mechanism and depopulation of the $^4I_{11/2}$ level which is concentration dependent. With regards to Figure 6.2, it is expected that for increasing irradiance the photoluminescence of lower concentrations will increase at a higher rate. Once saturation has been reached the photoluminescence of all samples will increase linearly ($n = 1$ for the highest emitting state or $n \leq 1$ for any intermediate energy level such as that measured here) at higher irradiances, hence lower Er^{3+} concentrations can overcome that of respectively higher ones.

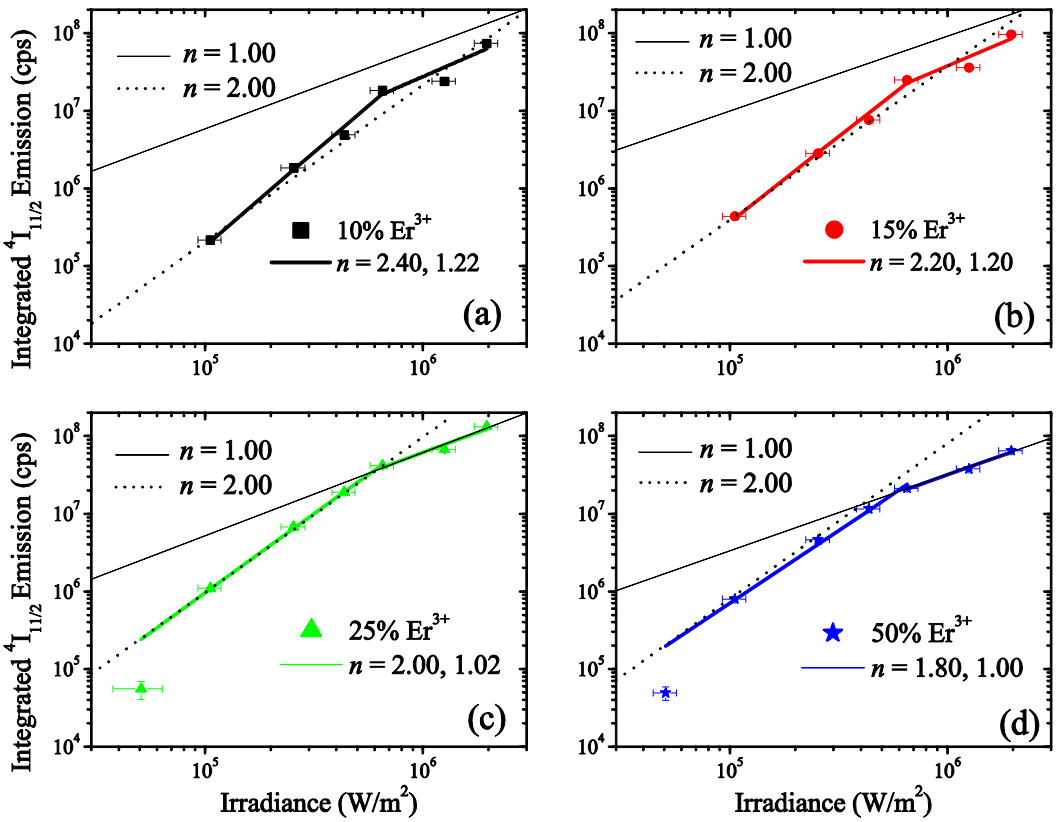

Figure 6.4 Log-log plots of the integrated $^4I_{11/2} \rightarrow {}^4I_{15/2}$ emission with fitted linear trend (n) further supporting observation of a non-linear process for representative concentrations of (a) 10, (b) 15, (c) 25 and (d) 50 mol% Er^{3+} in β-$NaYF_4$:Er^{3+}. All figures have been plotted with the same axis.

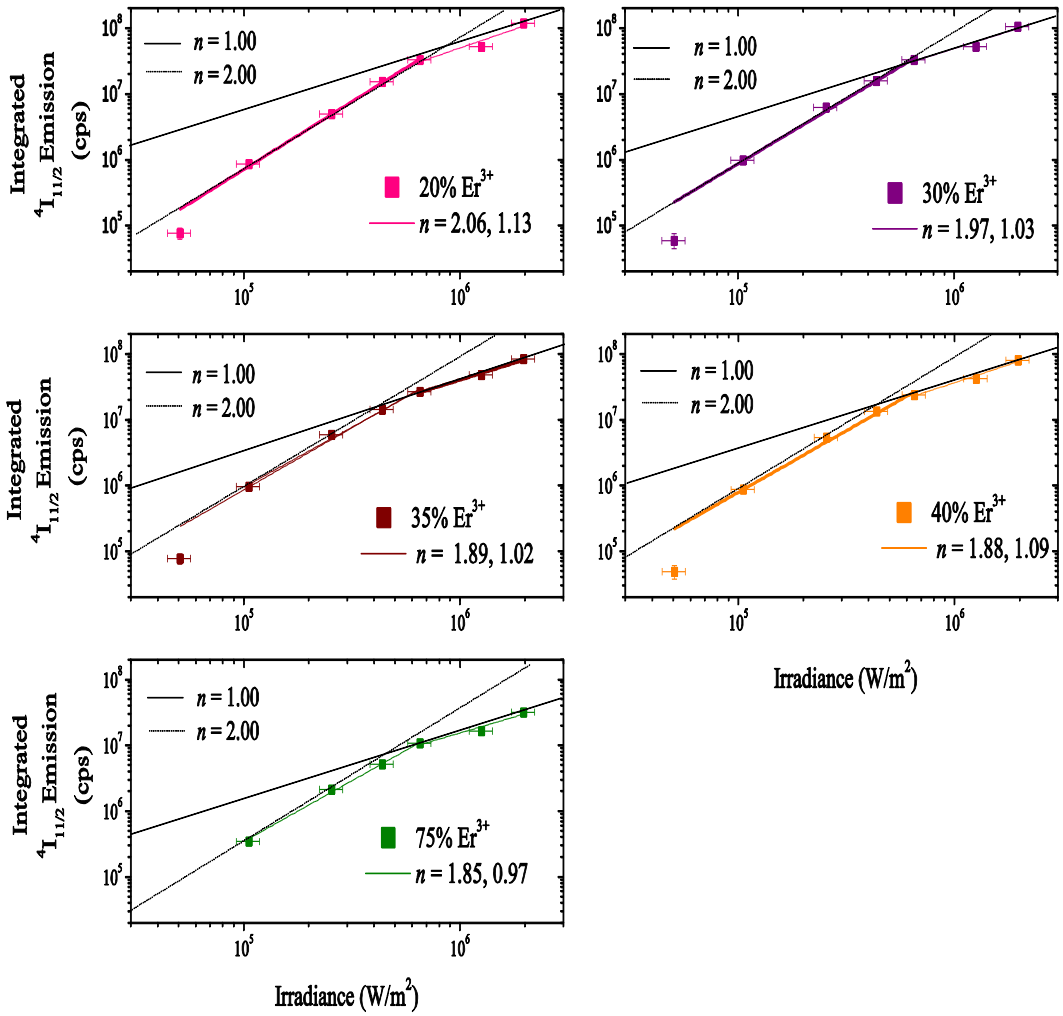

Figure 6.5 Log-log plots of the integrated $^4I_{11/2}$ emission with fitted linear trend (n) further supporting observation of a non-linear process for representative concentrations of 20, 30, 35, 40 and (e) 75 mol% Er^{3+}doped β-$NaYF_4$ host lattice . All figures have been plotted with the same axis.

Table 3 The photoluminescence dependence on irradiance (n, the number of interactive photons) is listed for all Er^{3+} concentrations for the defined high and low pump regimes.

Er^{3+} Concentration (mol %)	High Pump Regime	Low Pump Regime
10	**1.22**	**2.4**
15	**1.2**	**2.2**
20	**1.13**	**2.06**
25	**1.02**	**2**
30	**1.03**	**1.97**
35	**1.02**	**1.89**
40	**1.09**	**1.89**
50	**1.00**	**1.87**
75	**0.97**	**1.85**

6.5 External Photoluminescent Quantum Yield of β-$NaYF_4$: Er^{3+}

The *ePLQY* was calculated for various Er^{3+} concentrations and irradiances as this is the most important photophysical parameter in regards to a UC-PV device. The material which emits the highest number of UC photons has the best application potential since it generates more charge carriers in the overlying PV device. For *iPLQY*, the quantity depends on the emission of photons already absorbed which is a measure of internal efficiency, whereas the definition of *ePLQY* is independent of absorption. In Figure 6.6, the *ePLQY* increases for higher irradiances which is a result of the non-linear behaviour of the phosphor, already shown for both *iPLQY* and photoluminescent measurements. Although there is an appreciable difference in the overall shape of the trends, in relation to *iPLQY* values in Figure 6.1, this is purely governed by the absorptance of the sample. Furthermore, this also makes these measurements independent of the re-emission correction conducted for the *iPLQY* results (discussed in Chapter 4). Here, the optimum dopant concentration is always found to be 25% Er^{3+} independently of the irradiance of excitation. The highest *ePLQY* measured was 6.6 ± 0.7% for 25% Er^{3+} at an irradiance of 1.97 ± 0.24 MWm^{-2}, with respective values for other irradiances found in *Table 1*. This is equivalent to a normalised value of (3.35 ± 0.56) $\times 10^{-4}$ cm^2W^{-1} however, as previously discussed, this is calculated in the saturation regime. Therefore, for comparison with that achieved for monochromatic excitation (0.45 ± 0.06 cm^2 W^{-1} at 970 Wm^{-2}) [66] that measured at the lower irradiance ((1.22 ± 0.20) $\times 10^{-3}$ cm^2 W^{-1} at 0.26 MWm^{-2}) for 25 mol% Er^{3+} is used. Hence, under broadband excitation, it can be concluded that β-$NaYF_4$: 25% Er^{3+} is the most efficient material for the range of irradiances investigated within this thesis. Once again, this is also found for

monochromatic excitation where previous findings showed an optimum concentration of 25 mol% Er^{3+} for the same w/w% of phosphor doping within the fluorinated polymer [66]. These results obviously raise the question why β-$NaYF_4$: 25% Er^{3+} is more effective than the other concentrations investigated.

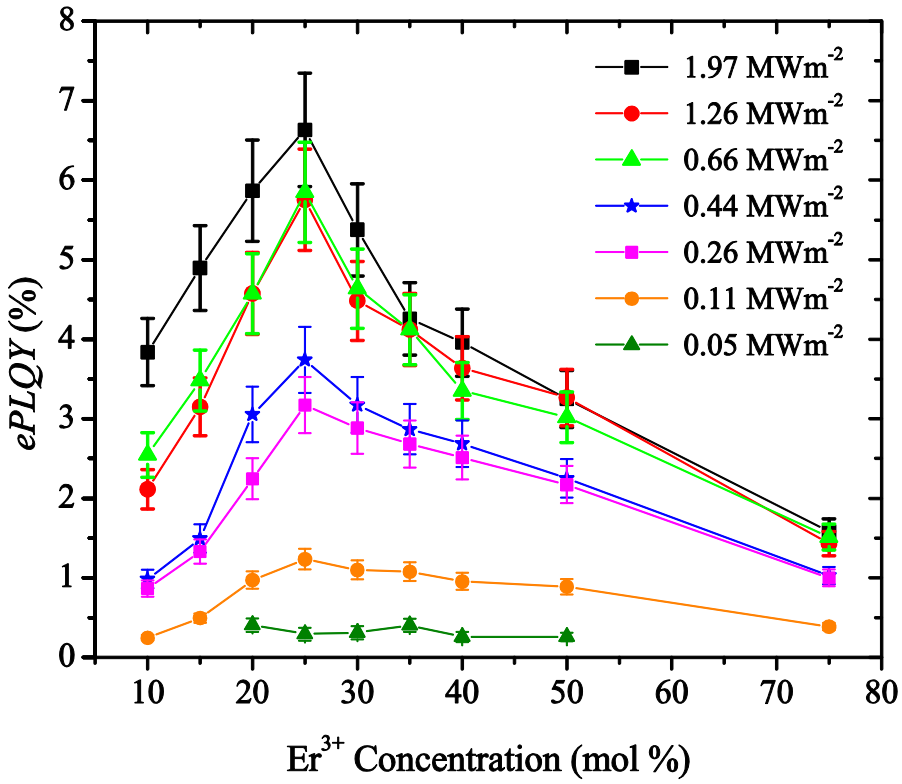

Figure 6.6 Variation in *ePLQY* as a function of Er^3 -doping concentrations under various irradiances. It is evident that 25% Er^{3+} is the optimum doping for broadband excitation in regards to the irradiances used here.

6.6 Absorption and Emission

To investigate this further, it is prudent to first evaluate the absorption of IR radiation in more detail as this is the precondition for the UC mechanism and subsequent emission. Figure 6.7(a) shows the absorptance, calculated with regards to re-emission discussed in Chapter 4, for all different Er^{3+} concentrations under investigation for an irradiance of 1.97 ± 0.24 MWm^{-2}.

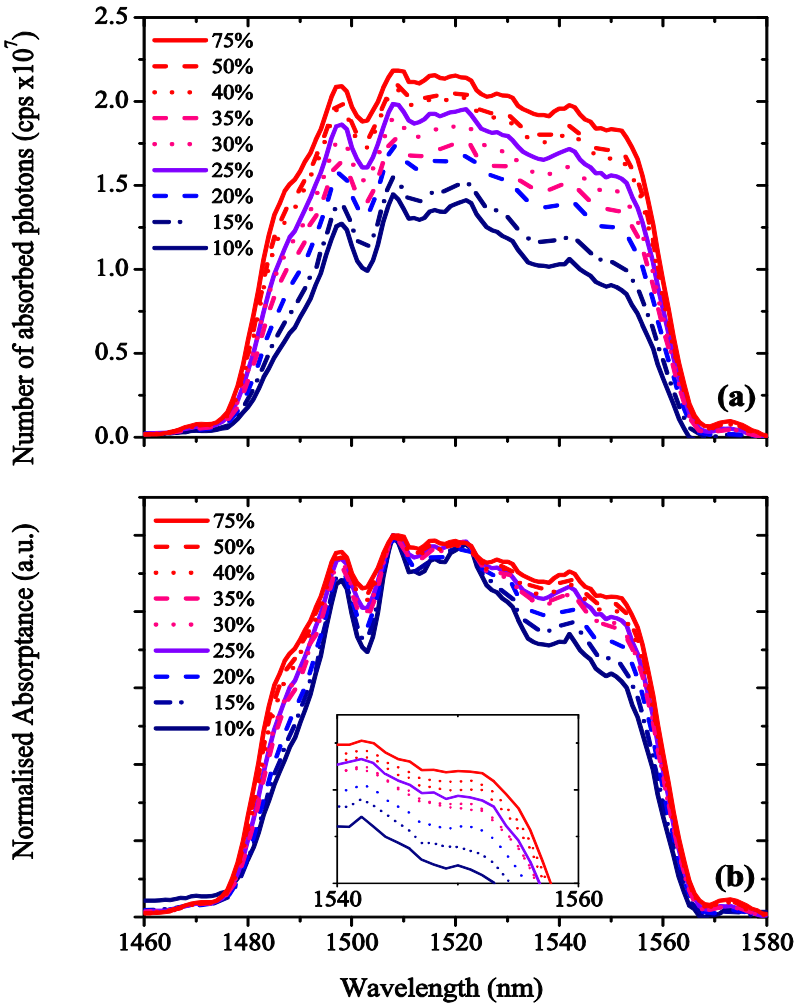

Figure 6.7 (a) Corrected absorptance spectra, for an irradiance of 1.97 ± 0.24 MWm^{-2}. Dotted lines for 30 and 35% Er^{3+} demonstrate the divergence of increasing absorption with concentration; (b) the same spectra normalised to their peak value (1508 nm) and homogenous broadening with increase in concentration. The figure has been partly expanded for clarity.

Only the absorptance spectrum for the highest irradiance is shown here, however this is indicative of all other regimes. In the case of monochromatic excitation under low irradiances, the absorption increases linearly with the concentration of Er^{3+} ions according to Beer-Lamberts Law, Equation 3.1. However, this is not satisfied under the conditions of this study. In Figure 6.7(a) it can be seen that the number of absorbed photons increases with concentration but not linearly. It is observed that 25 mol% Er^{3+} has higher absorptance than that calculated for 30% and 35 mol% Er^{3+}. This appears to be counter intuitive as a greater concentration would lead to a higher number of absorbed photons with an increase in active ions. Furthermore, when the spectra are

normalised, as in Figure 6.7(b), the 25 mol% Er^{3+} concentration is also seen to absorb a broader range of photons; breaking the overall trend seen for increasing concentration.

The broadening of the absorption spectra is related to the microenvironment and crystal field structure of the doped ions which suggests that the density of ions [150], impurities [151] and defects [152] could be a cause for this behaviour. It is well known that impurity doping can be used to change the crystal field structure of lanthanides or co-doping of stronger absorbing ions to increase efficiency [153]. With an increase in Er^{3+} doping there is an associated reduction in that of the Y^{3+} of the host lattice due to substitution. Therefore, the crystal field of the active ions will be altered due to the increasing probability that the nearest neighbour will be a substituted Er^{3+} ion. This variation in line shape and broadening has been observed in BaY_2F_8: Er^{3+} where high resolution absorption spectra were recorded for a range of Er^{3+} concentrations (0.5% to 20 at%) and temperatures (9K to 300K). Inhomogeneous broadening was attributed to the increase in Er^{3+} concentration, which is randomly substituted for Y^{3+}, which leads to greater Er^{3+}-Er^{3+} interaction. Hence, this resulted in a reduction of the crystal field symmetry and an increase in the absorption [150]. Furthermore, this was observed for several transitions from the ground state which would indicate an increase in energy transfer mechanisms due to a greater overlap of interacting levels and would lead to an increase in *iPLQY*. Hence, this could be an explanation for a change of line shape in the absorbed photons measured under broadband excitation herein. Other studies have also observed homogeneous broadening of the EQE response, shown to be indicative of the excitation spectrum [141], when using a white light bias in conjunction with a tuneable laser. This would also support the effect observed here under broadband excitation but does not explain the anomalous increase in absorption. Another possible explanation of the broadening of the absorptance spectra could be contribution from ESA which can be speculated in regards to broadband excitation at high irradiances but again does not explain the anomalous behaviour of 25 mol% Er^{3+}. To analyse the contribution of GSA/ESA and GSA/ETU in regards to the UC emission, time dependant measurements would be required which would mean further adaption of the current experimental system, which is beyond the scope of this work. However, the fact that 25 mol% Er^{3+} shows an appreciable broader range of absorption in relation to its closest counterparts (20, 30 and 35 mol%) puts this material at a significant advantage under broadband excitation.

The emission spectrum with relation to the Er^{3+} concentration can also be used to analyse the effect of ion doping and energy transfer mechanisms. In Figure 6.8(a), the emission from the $^4I_{11/2}$ to $^4I_{15/2}$ is shown for all Er^{3+} concentrations under 1.97 ± 0.26 Wm^{-2} irradiance. From previous analysis of the *ePLQY*, it is expected that the 25% Er^{3+} doped sample is the most efficient emitter. Accordingly, it shows the strongest emission in Figure 6.8(a). It is also interesting to note here, that the peak emission at 979 nm is equally strong for the 20 and 25% Er^{3+} samples, but the integral of emission is stronger for 25% Er^{3+} due to increased contribution at longer wavelengths. When the spectra are normalised to the peak emission the effect of inhomogeneous broadening becomes more apparent for higher concentrations. As this effect is concentration dependant it can be ascribed to absorption and energy transfer mechanisms which increase with ion doping and the reduction in ion separation, respectively. As higher concentrations have higher rates of energy transfer the emission decreases due to saturation. The emission is also red shifted which can be ascribed to energy migration and non-radiative decay at defect sites. Moreover, what is more striking is that 25% Er^{3+} again shows anomalous broadening in regards to the expected trend. It can be seen in Figure 6.8 that 25%Er^{3+} is comparable with the concentrations of 30 and 35% Er^{3+}.

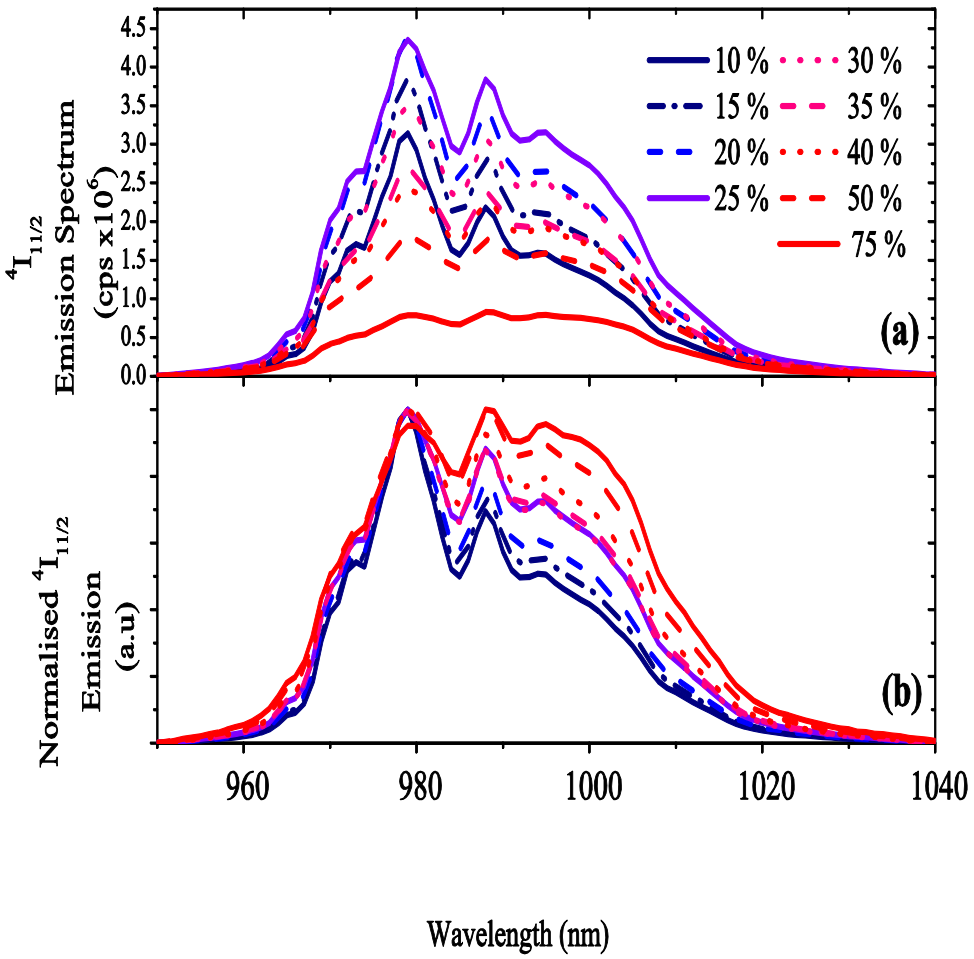

Figure 6.8 $^4I_{11/2} \rightarrow {}^4I_{15/2}$ emission spectra for various Er^{3+} concentrations at an irradiance of 1.97 ± 0.26 Wm^{-2}. The emission increases with Er^{3+} concentration up to a maximum at 25% and then decreases due to concentration quenching. (b) Emission spectra normalised to the peak at λ = 979 nm.

6.7 Conclusions

The main aim of this Chapter was to discern the optimum Er^{3+} concentration for broadband excitation UC in the low phonon energy host lattice β-$NaYF_4$ – with respect to an application in Si solar cells. The broadband excitation is a more realistic model for the solar spectrum than any other laser excitation. The measurements were conducted over a range of irradiances, or equivalently various solar concentrations, to determine the most efficient UC material for an application with a PV device for increased photon harvesting. It was shown that the optimum concentration was dependent on the interplay of absorption to populate the intermediate energy level and the rate of energy transfer; this was advantageous in the low pump regime for higher Er^{3+} concentrations (>25 mol%) however, a deleterious effect was observed at higher pump irradiances due to saturation and quenching. The sample with the highest *iPLQY*

of 10.7 ± 1.2% was doped with 20 mol% Er^{3+} with a normalised efficiency of (5.43 ± 0.90) $\times 10^{-4}$ cm^2W^{-1} at an irradiance of 1.97 ± 0.24 MWm^{-2} ((108 ± 13) $\times 10^3$ Suns) and was embedded in the PFCB matrix at a 55.6 w/w% ratio. A comparison with monochromatic [66] to that of broadband excitation showed a normalised efficiency two orders of magnitude lower which was ascribed to lower absorption of non-resonant photons. However, a good agreement was observed in regards to the optimum Er^{3+} concentration, determined by *ePLQY* values for solar applications. Thus either of the methods can be used to investigate the optimum material as long as a thorough sample range is used. The highest *ePLQY* for broadband excitation was 6.6 ± 0.7% for 25 mol% Er^{3+} with an irradiance of 1.97 ± 0.24 MWm^{-2} (normalised efficiency, (3.35 ± 0.56) $\times 10^{-4}$ cm^2W^{-1}). However, broadband excitation is necessary as only this method can both determine the actual efficiency and improvement, unlike monochromatic measurements, for an applied UC-PV device. The optimum Er^{3+} concentration of 25 mol% was shown to have an anomalous increase and homogenous broadening in absorptance with respect to its nearest counterparts which was advantageous to its improved performance.

Finally, the solar concentrations of (108 ± 13) $\times 10^3$ Suns estimated for the highest efficiencies are still beyond those achievable with a practical device. Although more reasonable values as low as (2.73 ± 0.53) $\times 10^3$ Suns were investigated, lower concentrations would be advantageous to the overall design requirements. The UC of sub-band-gap photons technology has the potential to increase the irradiance of the incident light for Si solar cells at a feasible level of solar concentration.

CHAPTER 7 - SUMMARY AND FUTURE WORK

7.1 Summary

The work contained within this thesis has focused on the characterisation of UC layers for application to c-Si PV devices. More specifically, a method for determining the *iPLQY* under broadband excitation, similar to that of the solar spectrum, has been developed to achieve this aim [154]. Firstly, the utilisation of this method was necessitated by previous research in the literature which has used only monochromatic methods for characterisation [53, 57, 70]. Thus, the broad spectral content of the illumination conditions, which would be evident in its application, are not effectively replicated. Secondly, as the efficiency of the UC process is non-linear with excitation power and dependent on the wavelength of excitation these factors are critical in the evaluation of *iPLQY*. Therefore, characterisation under broadband excitation is needed to determine more accurately the efficiency limits of the UC process and the possible enhancement of a coupled PV device. The first stage in this method required the adaption of a commercially available fluorospectrometer, used for measurement of the *iPLQY* under monochromatic excitation, to incorporate the broadband excitation from a SC laser. However, this method presented a challenge in determining the absorptance of the UC sample due to spectral overlap of the excitation spectrum, re-emission and absorption of the sample. An experimental procedure was developed to correct for this spectral artefact by removing the contribution from re-emitted photons [154]. The effect of re-emission on the determination of the absorptance and *iPLQY* will also be present for determination under monochromatic excitation. Thus, an overestimate in the *iPLQY* has led to the incorrect reporting of these results throughout the literature. Due to the dependence of the *iPLQY* on the irradiance and ion-ion separation this method was evaluated using a range of solar irradiances and ion doping concentrations. Although this was developed for the characterisation of UC layers due to their application under broad spectral illumination for solar energy harvesting, it can also be used for other spectral converters used in PV applications. This may also prove to be relevant for imaging techniques, such as UC bio labelling [155], where cheaper excitation sources, such as LEDs, could achieve the same resolution as more expensive lasers.

This method facilitated the quantitative characterisation and optimisation of an UC layer under a broad spectrum of illumination for the first time. The next step in the use of broadband excitation was to determine the effect of excitation bandwidth on the

enhancement of the UC emission. Initially, the UC emission of a TGC with embedded YF_3: 10% Er^{3+} NC's was investigated under 12 and 38 nm bandwidths and a range of irradiances [156]. It is prudent for the performance of an upconverting material to be reported with regards to the irradiance of excitation due to its non-linear nature. However, to clarify this form of analysis for the solar PV community the irradiance was normalised to the AM 1.5d spectrum for the first time. Furthermore, this was important for demonstrating that the enhancement of UC emission, with an increase in the bandwidth of excitation, does not require additional solar concentration. This was confirmed by the YF_3: 10% Er^{3+} NC sample which showed that the same UC emission could be achieved with a reduction in the solar concentration by a factor of 7.6, when the bandwidth was increased by a factor of 3.17 [156]. When the solar concentration is kept equal and the bandwidth is increased by a factor of 3.17 the UC emission revealed a 55 fold increase. This outlines the importance of broadband characterisation for UC-PV performance, especially when normalised to intuitive units of solar concentration, in comparison to monochromatic investigations from the literature. To understand the effect of bandwidth on the *iPLQY* of the UC process the most efficient phosphor β-$NaYF_4$: 10% Er^{3+} was investigated due to its improved measurability. Here, it was shown that the *iPLQY* saturated for bandwidths greater than 60 nm due to weak absorption of photons at the extremes of the β-$NaYF_4$: 10% Er^{3+} lineshape. Under broad spectral illumination, 61 ± 1 nm bandwidth centred at 1523 nm, with an irradiance of (155 ± 7) $\times 10^3$ Suns, the highest *iPLQY*, known to the author, of 16.2 ± 0.5% was achieved [89]. Although an enhancement in *iPLQY* by a factor of 1.9, with a reduction in solar concentration by a factor of 2.9 was observed, this required a solar concentration well beyond the diffraction limit achievable on Earth.

The final stage of this thesis was to determine the optimum Er^{3+} doping concentration within the efficient host lattice β-$NaYF_4$ under broadband excitation. This was also necessary to determine, if any, difference in optimum concentration existed between monochromatic investigations. The highest *iPLQY* of 10.7 ± 1.2% was measured for β-$NaYF_4$: 20% Er^{3+}, embedded within a PFCB matrix at a 55.6 w/w%, at an irradiance of 1.97 ± 0.24 MWm^{-2} ((108 ± 13) $\times 10^3$ Suns) [157]. However, at lower values of irradiance β-$NaYF_4$: 25% Er^{3+} was shown to be the optimum concentration. The most recent investigations using monochromatic characterisation have determined that β-$NaYF_4$:25% Er^{3+} was the optimum, which agrees with that measured here, except for the highest irradiance. This can be explained by the saturation in *iPLQY* and

photoluminescence, with respect to power, which indicates that at higher irradiances lower concentrations will have higher *iPLQY*. This has recently been supported by Fischer *et al.* [158] who also observed a change in the optimum concentration which decreased with increasing irradiance The most important parameter in determining the optimum UC layer for application within a PV device is the *ePLQY*. The *ePLQY* of β-$NaYF_4$:25% Er^{3+} was consistently the highest for all irradiances measured under broadband excitation within the range of irradiances measured.

7.2 Future Research

There are many challenges still to overcome before the realisation of a commercial UC-PV device is achieved. The maximum, or ideal, efficiency that can be achieved in any of the UC process is 50%, in regards to the quantum nature of the process. The work herein has achieved a record efficiency of 16.2% [89] which indicates more progress is needed to reach this potential.

The materials currently used for UC-PV devices, such as β-$NaYF_4$: Er^{3+} investigated in this work, are inherently limited by the narrow and weak absorption of sub-bang gap photons (approximately 6 cm^{-1} at 1523 nm over a bandwidth of 100 nm). Thus, spectral concentration is necessary to utilise the entire spectrum between the band edge of the PV device and the upconverter. Spectral concentration has already been discussed using semiconductor QD's however, the photophysical properties (such as *iPLQY* and a narrow emission spectrum) of these materials must also improve before this goal is achieved. One of the most important criteria is that the size distribution must be narrow to reduce the emission bandwidth to that of the upconverter absorption range. The work herein has shown that a requirement in the emission bandwidth of 60 nm would be necessary to achieve the best performance in this regard [89]. Furthermore, this could be achieved by embedding QD's within an optimised PhC to achieve a very narrow emission bandwidth at the peak resonant wavelength of the upconverter [159] [160]. This would have the further benefit of reducing reabsorption events and preservation of the QD *iPLQY*. Further improvements due to the combination of these advanced techniques has recently been tested with the inclusion of PbSe core QD's within an InP graphite PhC [161]. This resulted in: 1) a higher number of photons within the absorption range of the upconverter through spectral concentration, 2) red-shifting of the QD emission due to the PhC, thus, reducing parasitic re-absorption, and 3) the vertical emission is increased due to the guided modes of the PhC. Thus, with careful

consideration, various and significant improvements can be achieved with the combination of these technologies.

To determine if the performance of the upconverter measured here would be possible an estimate of the performance enhancement associated with an advanced system design can be made. First of all secondary optics can be used behind the cell for concentration. There has been few papers published on this [110-112] with improvements seen only for low concentration factors of 2 -3. This was due to poor coupling efficiencies and lack of optimisation. A factor of 9 enhancement would not be considered unrealistic if ray tracing was used to improve design. The proposal of QD's as spectral concentrators has also been suggested as means of achieving higher solar concentration. These spectral converters can also be incorporated in to a geometric concentrator to further enhance the UC response. Work conducted by Goldschmidt *et al.* [113] predicted a factor of ~ 70 enhancement in concentration using QD's of an efficiency of 90%. This would be an achievable target as QD's are already achieving efficiencies of 80%. As stated by Goldschmidt *et al.* [113] these QD's can be embedded within a tertiary geometric concentrator after the UC layer achieving an additional concentration of 10. Through the combination of these techniques a concentration factor of 6,400 suns would be possible using current technologies. Lastly, using the high efficiency Amonix c-Si solar cell at its operating concentration of 92 suns would bring this total to 588 x 10^3 suns which is significantly higher than the solar concentration measured for the highest UC material measured here (16.2% at 155 x 10^3 suns). This means that these efficiencies measured herein have the potential, through combination of advanced systems, to be realised within the near future.

In regards to characterisation techniques that have been developed it would be of significant interest to the field to determine the UC mechanisms under broadband excitation. Although it is expected that ETU would be dominant, as it is also the most efficient process, time resolved measurements would determine if there is any contribution to this process through ESA. Furthermore, the work contained herein focused on broadband excitation in the range of 1480 – 1560 nm however, ESA would be possible via dual excitation experiments with additional pumping between 1600 – 1700 nm. This should be investigated to determine if any synergistic effects may improve the UC process and the charge generation within a coupled PV device. Although the focus here has been on single doped Er^{3+} there is also potential research in

dual excitation of Er^{3+}/Yb^{3+} which can benefit from both absorption ranges of the respective ions. The use of multiple absorption bands would increase the range of photons that could be harvested from the solar spectrum further reducing transmission losses. This has further implications in regards to the PV device used which is discussed further below.

The focus of this investigation has been in the enhancement of c-Si devices however, solar cells with a larger band gap such as GaAs and organic solar cells suffer from greater losses due to transmission of sub-band gap photons. These devices would thus be a preferred option for enhancement through UC. This is especially true for DSC and organic devices which are limited by poor current generation. In addition, the use of Er^{3+}/Yb^{3+} co-doped phosphors, which are more efficient due to the higher absorption cross section of the Yb^{3+}, would be possible. This ion combination can currently take advantage of increased absorption through the use of antenna ligands and therefore would be more likely to achieve commercialisation of this technology. A further advantage of working with DSC and organic devices is that they are less mature than GaAs and c-Si. This would allow the incorporation and development of these technologies in a symbiotic fashion.

REFERENCES

1. R. Lee, The Outlook for Population Growth, Science, 333 (2011) 569-573.
2. International Energy Agency, Key World Energy Statistics 2013, in: SOREGRAPH (Ed.), International Energy Agency (IEA), 9 rue de la Federation, 75739 Paris Cedex 15, France, 2013.
3. G.L. Foster, E.J. Rohling, Relationship between sea level and climate forcing by CO2 on geological timescales, Proceedings of the National Academy of Sciences, 110 (2013) 1209-1214.
4. European Union, L140, Official Journal of the European Union, 52 (2009).
5. N.S. Lewis, D.G. Nocera, Powering the planet: Chemical challenges in solar energy utilization, Proceedings of the National Academy of Sciences, 103 (2006) 15729-15735.
6. M.A. Green, Solar Cells: Operating principals, Technology and System Applications, The University of New South Wales, Kensington, NSW 2033, 1998.
7. A.B. Arons, M.B. Peppard, Einstein's Proposal of the Photon Concept—a Translation of the Annalen der Physik Paper of 1905, American Journal of Physics, 33 (1965) 367-374.
8. M. Planck, On the Law of Distribution of Energy in the Normal Spectrum, Annalen der Physik, 4 (1901) 6.
9. D.M. Chapin, C.S. Fuller, G.L. Pearson, A New Silicon p- n Junction Photocell for Converting Solar Radiation into Electrical Power, Journal of Applied Physics, 25 (1954) 676-677.
10. M.A. Green, Third Generation Photovoltaics Advanced Solar Energy Conversion, Springer, 2006.
11. C.H. Henry, Limiting efficiencies of ideal single and multiple energy gap terrestrial solar cells, Journal of Applied Physics., 51 (1980) 4494-4500.
12. W. Shockley, H.J. Queisser, Detailed Balance Limit of Efficiency of p‐n Junction Solar Cells, Journal of Applied Physics., 32 (1961) 510-519.
13. A. Richter, M. Hermle, S.W. Glunz, Reassessment of the Limiting Efficiency for Crystalline Silicon Solar Cells, Photovoltaics, IEEE Journal of, 3 (2013) 1184-1191.
14. C. Honsberg, and S. Bowden, PV Education, http://www.pveducation.org/pvcdrom/manufacturing/first-photovoltaic-devices#ref10., Accessed 15th December 2014

15. M.A. Green, Recent developments in photovoltaics, SoEn, 76 (2004) 3-8.
16. University of New South Wales (2008, October 24). Highest Silicon Solar Cell Efficiency Ever Reached. ScienceDaily. Retrieved May 31st, 2011, from http://www.sciencedaily.com /releases/2008/10/081023100536.htm.
17. M.A. Green, Third generation photovoltaics: Ultra-high conversion efficiency at low cost, Progress in Photovoltaics: Research and Applications, 9 (2001) 123-135.
18. R.M. Swanson, A vision for crystalline silicon photovoltaics, Progress in Photovoltaics: Research and Applications, 14 (2006) 443-453.
19. A. Shah, P. Torres, R. Tscharner, N. Wyrsch, H. Keppner, Photovoltaic Technology: The Case for Thin-Film Solar Cells, Science, 285 (1999) 692-698.
20. K.L. Chopra, P.D. Paulson, V. Dutta, Thin-film solar cells: an overview, Progress in Photovoltaics: Research and Applications, 12 (2004) 69-92.
21. M. Green, Thin-film solar cells: review of materials, technologies and commercial status, J Mater Sci: Mater Electron, 18 (2007) 15-19.
22. G.V. Slade A, 27.6% efficient silicon concentrator cell for mass production, Technical Digest, 15th International Photovoltaic Science and Engineering Conference, Shanghai, 701., (October 2005).
23. N.R.E. Laboratory, Best Research-Cell Efficiency, in: E. Chart (Ed.) JPEG, National Centre for Photovoltaics, Online, 2014.
24. G. Conibeer, Third-generation photovoltaics, Materials Today, 10 (2007) 42-50.
25. M. Yamaguchi, T. Takamoto, K. Araki, N. Ekins-Daukes, Multi-junction III–V solar cells: current status and future potential, SoEn, 79 (2005) 78-85.
26. P.V. Kamat, Quantum Dot Solar Cells. Semiconductor Nanocrystals as Light Harvesters†, The Journal of Physical Chemistry C, 112 (2008) 18737-18753.
27. R.L. Tuan M. Trinh, Wieteke D.A.M. de Boer, Juleon M. Siebbeles, Tom Gregorkiewics, Direct generation of multiple excitons in adjacent silicon nanocrystals revealed by induced absorption, Nature Photonics, 6 (2012) 6.
28. A.M. Antonio Luque, Colin Stanley, Understanding intermediate-band solar cells, Narture Photonics, 6 (2012) 7.
29. Y. Takeda, T. Ito, T. Motohiro, D. König, S. Shrestha, G. Conibeer, Hot carrier solar cells operating under practical conditions, Journal of Applied Physics., 105 (2009) -.
30. E. Klampaftis, M. Congiu, N. Robertson, B.S. Richards, Luminescent Ethylene Vinyl Acetate Encapsulation Layers for Enhancing the Short Wavelength

Spectral Response and Efficiency of Silicon Photovoltaic Modules, IEEE Journal of Photovoltaics, , 1 (2011) 29-36.

31. E. Klampaftis, D. Ross, S. Seyrling, A.N. Tiwari, B.S. Richards, Increase in short-wavelength response of encapsulated CIGS devices by doping the encapsulation layer with luminescent material, Solar Energy Materials and Solar Cells, 101 (2012) 62-67.
32. D. Ross, E. Klampaftis, J. Fritsche, M. Bauer, B.S. Richards, Increased short-circuit current density of production line CdTe mini-module through luminescent down-shifting, Solar Energy Materials and Solar Cells, 103 (2012) 11-16.
33. E. Klampaftis, D. Ross, K.R. McIntosh, B.S. Richards, Enhancing the performance of solar cells via luminescent down-shifting of the incident spectrum: A review, Solar Energy Materials and Solar Cells, 93 (2009) 1182-1194.
34. R.T. Wegh, H. Donker, K.D. Oskam, A. Meijerink, Visible Quantum Cutting in LiGdF4:Eu3+ Through Downconversion, Science, 283 (1999) 663-666.
35. D.L. Dexter, Possibility of Luminescent Quantum Yields Greater than Unity, Physics Review, 108 (1957) 630-633.
36. B.S. Richards, Luminescent layers for enhanced silicon solar cell performance: Down-conversion, Solar Energy Materials and Solar Cells, 90 (2006) 1189-1207.
37. F. Auzel, Upconversion and Anti-Stokes Processes with f and d Ions in Solids, Chemical Reviews, 104 (2003) 139-174.
38. N. Bloembergen, Solid State Infrared Quantum Counters, Physics Review Letters, 2 (1959) 84-85.
39. F. Wang, Y. Han, C.S. Lim, Y. Lu, J. Wang, J. Xu, H. Chen, C. Zhang, M. Hong, X. Liu, Simultaneous phase and size control of upconversion nanocrystals through lanthanide doping, Nature, 463 (2010) 1061-1065.
40. X. Chen, T. Nguyen, Q. Luu, B. DiBartolo, Green and red luminescence of YSGG: Er under up-conversion and regular excitation at different Er concentrations, Journal of Luminescence, 83–84 (1999) 471-475.
41. Z. Li, Y. Zhang, S. Jiang, Multicolor Core/Shell-Structured Upconversion Fluorescent Nanoparticles, Advanced Materials, 20 (2008) 4765-4769.
42. S. Baluschev, V. Yakutkin, G. Wegner, B. Minch, T. Miteva, G. Nelles, A. Yasuda, Two pathways for photon upconversion in model organic compound systems, Journal of Applied Physics., 101 (2007) 023101-023104.

43. K. Kawano, B.C. Hong, K. Sakamoto, T. Tsuboi, H.J. Seo, Improvement of the conversion efficiency of solar cell by rare earth ion, Optical Materials, 31 (2009) 1353-1356.

44. A. Boccolini, J. Marques-Hueso, D. Chen, Y. Wang, B.S. Richards, Physical performance limitations of luminescent down-conversion layers for photovoltaic applications, Solar Energy Materials and Solar Cells, 122 (2014) 8-14.

45. A. Boccolini, R. Faoro, E. Favilla, S. Veronesi, M. Tonelli, BaY2F8 doped with Er3+: An upconverter material for photovoltaic application, Journal of Applied Physics., 114 (2013) -.

46. J.A. Vallés, M.A. Rebolledo, J. Used, Energy-transfer efficiency in Er/Yb-codoped phosphate waveguides in dynamic regime, Optical Materials, 31 (2009) 1346-1348.

47. V.P. Gapontsev, S.M. Matitsin, A.A. Isineev, V.B. Kravchenko, Erbium glass lasers and their applications, Optics & Laser Technology, 14 (1982) 189-196.

48. N.D. Afify, R. Grisenti, G. Dalba, C. Armellini, M. Ferrari, S. Larcheri, F. Rocca, A. Kuzmin, Short-range order around Er3+ in silica waveguides containing aluminium, titanium and hafnium, Optical Materials, 28 (2006) 864-867.

49. G. Dantelle, M. Mortier, D. Vivien, G. Patriarche, Influence of Ce3+ doping on the structure and luminescence of Er3+-doped transparent glass-ceramics, Optical Materials, 28 (2006) 638-642.

50. A.J. Kenyon, C.E. Chryssou, T.M. Smeeton, C.J. Humphreys, D.E. Hole, Sensitisation of erbium luminescence in erbium-implanted alumina, Optical Materials, 28 (2006) 655-659.

51. O. Péron, C. Duverger-Arfuso, Y. Jestin, B. Boulard, M. Ferrari, Enhanced spectroscopic properties in Er3+/Yb3+-activated fluoride glass-ceramics planar waveguides, Optical Materials, 31 (2009) 1288-1291.

52. Y.W. Lee, B. Lee, High resolution cryogenic optical fiber sensor system using erbium-doped fiber, Sensors and Actuators A: Physical, 96 (2002) 25-27.

53. A. Shalav, B.S. Richards, T. Trupke, K.W. Krämer, H.U. Güdel, Application of NaYF4:Er3+ up-converting phosphors for enhanced near-infrared silicon solar cell response, Applied Physics Letters, 86 (2005) 013505-013503.

54. A. Shalav, B.S. Richards, K. Krämer, H. Güdel, Improvements of an Up-Conversion NaYF4:Er3+ Phosphor/Silicon Solar Cell System for an Enhanced Response in the Near-Infrared, IEEE Conference paper, (2005).

55. A. Shalav, B.S. Richards, M.A. Green, Luminescent layers for enhanced silicon solar cell performance: Up-conversion, Solar Energy Materials and Solar Cells, 91 (2007) 829-842.

56. B.S. Richards, Enhancing the performance of silicon solar cells via the application of passive luminescence conversion layers, Solar Energy Materials and Solar Cells, 90 (2006) 2329-2337.

57. S. Fischer, J.C. Goldschmidt, P. Löper, G.H. Bauer, R. Bruggemann, K. Krämer, D. Biner, M. Hermle, S.W. Glunz, Enhancement of silicon solar cell efficiency by upconversion: Optical and electrical characterization, Journal of Applied Physics., 108 (2010) 044912-044911.

58. J. de Wild, J.K. Rath, A. Meijerink, W.G.J.H.M. van Sark, R.E.I. Schropp, Enhanced near-infrared response of a-Si:H solar cells with β-NaYF4:Yb3+ (18%), Er3+ (2%) upconversion phosphors, Solar Energy Materials and Solar Cells, 94 (2010) 2395-2398.

59. J. de Wild, A. Meijerink, J.K. Rath, W.G.J.H.M. van Sark, R.E.I. Schropp, Towards upconversion for amorphous silicon solar cells, Solar Energy Materials and Solar Cells, 94 1919-1922.

60. G.H. Dieke, Spectran and Energy Levels of Rare Earth Ions in Crystals, Wilely-Interscience, New York, 1968.

61. S. Fischer, H. Steinkemper, P. Löper, M. Hermle, J.C. Goldschmidt, Modeling upconversion of erbium doped microcrystals based on experimentally determined Einstein coefficients, Journal of Applied Physics., 111 (2012) -.

62. A. Aebischer, M. Hostettler, J. Hauser, K. Krämer, T. Weber, H.U. Güdel, H.-B. Bürgi, Strukturelle und spektroskopische Charakterisierung von lichtemittierenden Natriumlanthanoidtetrafluoriden, Angewandte Chemie, 118 (2006) 2869-2873.

63. S.R. Lüthi, M. Pollnau, H.U. Güdel, M.P. Hehlen, Near-infrared to visible upconversion in Er3+-doped Cs3Lu2Cl9, Cs3Lu2Br9, and Cs3Y2I9 excited at 1.54 μm, Physics ReviewB, 60 (1999) 162-178.

64. J.F. Suyver, A. Aebischer, D. Biner, P. Gerner, J. Grimm, S. Heer, K.W. Krämer, C. Reinhard, H.U. Güdel, Novel materials doped with trivalent lanthanides and transition metal ions showing near-infrared to visible photon upconversion, Optical Materials, 27 (2005) 1111-1130.

65. J.F. Suyver, J. Grimm, M.K. van Veen, D. Biner, K.W. Krämer, H.U. Güdel, Upconversion spectroscopy and properties of NaYF4 doped with , and/or, Journal of Luminescence, 117 (2006) 1-12.

66. A. Ivaturi, S.K.W. MacDougall, R. Martin-Rodriguez, M. Quintanilla, J. Marques-Hueso, K.W. Kramer, A. Meijerink, B.S. Richards, Optimizing infrared to near infrared upconversion quantum yield of β-NaYF4:Er3+ in fluoropolymer matrix for photovoltaic devices, Journal of Applied Physics., 114 (2013) 013505-013509.

67. D.L. Dexter, J.H. Schulman, Theory of Concentration Quenching in Inorganic Phosphors, The Journal of Chemical Physics, 22 (1954) 1063-1070.

68. T. Trupke, M.A. Green, P. Wurfel, Improving solar cell efficiencies by up-conversion of sub-band-gap light, Journal of Applied Physics., 92 (2002) 4117-4122.

69. M. Wolf, Limitations and Possibilities for Improvement of Photovoltaic Solar Energy Converters: Part I: Considerations for Earth's Surface Operation, PIRE, 48 (1960) 1246-1263.

70. P. Gibart, F. Auzel, J.-C. Guillaume, K. Zahraman,
Below Band-Gap IR Response of Substrate-Free GaAs Solar Cells Using Two-Photon Up-Conversion, Japanese Journal of Applied Physics, 35 (1996) 2.

71. V. Badescu, A.M. Badescu, Improved model for solar cells with up-conversion of low-energy photons, Renewable Energy, 34 (2009) 1538-1544.

72. A.C. Atre, J.A. Dionne, Realistic upconverter-enhanced solar cells with non-ideal absorption and recombination efficiencies, Journal of Applied Physics., 110 (2011) 034505-034509.

73. C.M. Johnson, G.J. Conibeer, Limiting efficiency of generalized realistic c-Si solar cells coupled to ideal up-converters, Journal of Applied Physics., 112 (2012) 103108-103109.

74. C.M. Johnson, P.J. Reece, G.J. Conibeer, Slow-light-enhanced upconversion for photovoltaic applications in one-dimensional photonic crystals, Optical Letters, 36 (2011) 3990-3992.

75. C.M. Johnson, P.J. Reece, G.J. Conibeer, Theoretical and experimental evaluation of silicon photonic structures for enhanced erbium up-conversion luminescence, Solar Energy Materials and Solar Cells, 112 (2013) 168-181.

76. T. Trupke, A. Shalav, B.S. Richards, P. Würfel, M.A. Green, Efficiency enhancement of solar cells by luminescent up-conversion of sunlight, Solar Energy Materials and Solar Cells, 90 (2006) 3327-3338.

77. B.S. Richards, A. Shalav, Enhancing the Near-Infrared Spectral Response of Silicon Optoelectronic Devices via Up-Conversion, IEEE Transactions on Electron Devices, 54 (2007).

78. S. Ivanova, F. Pellé, Strong 1.53 ?m to NIR-VIS-UV upconversion in Er-doped fluoride glass for high-efficiency solar cells, Journal of the Optical Society of America B, 26 (2009) 1930-1938.

79. S. Ivanova, F. Pellé, A. Tkachuk, M.F. Joubert, Y. Guyot, V.P. Gapontzev, Upconversion luminescence dynamics of Er-doped fluoride crystals for optical converters, Journal of Luminescence, 128 (2007) 914-917.

80. M. Liao, Evaluating upconversion materials developed to improve the efficiency of solar cells: comment, Optical Society of America B., 27 (2010) 1352-1355.

81. J.C. Goldschmidt, S. Fischer, P. Löper, K.W. Krämer, D. Biner, M. Hermle, S.W. Glunz, Experimental analysis of upconversion with both coherent monochromatic irradiation and broad spectrum illumination, Solar Energy Materials and Solar Cells, 95 (2011) 1960-1963.

82. B. Fröhlich, S. Fischer, H. Steinkemper, J.C. Goldschmidt, K. Krämer, Absolute Upconversion Quantum Yield of β-NaYF4:Er3+ under Broadband Excitation in Dependence on the Erbium Concentration - Measurements and Simulations, in, Optical Society of America, 2012, pp. PW2B.4.

83. Y.Y. Cheng, B. Fuckel, R.W. MacQueen, T. Khoury, R.G.C.R. Clady, T.F. Schulze, N.J. Ekins-Daukes, M.J. Crossley, B. Stannowski, K. Lips, T.W. Schmidt, Improving the light-harvesting of amorphous silicon solar cells with photochemical upconversion, Energy & Environmental Science, 5 (2012) 6953-6959.

84. N.C. Greenham, I.D.W. Samuel, G.R. Hayes, R.T. Phillips, Y.A.R.R. Kessener, S.C. Moratti, A.B. Holmes, R.H. Friend, Measurement of absolute photoluminescence quantum efficiencies in conjugated polymers, Chemical Physics Letters, 241 (1995) 89-96.

85. E.G.J. Staring, R.C.J.E. Demandt, D. Braun, G.L.J. Rikken, Y.A.R.R. Kessener, A.H.J. Venhuizen, M.M.F. van Knippenberg, M. Bouwmans, Electroluminescence and photoluminescence efficiency of poly(p-phenylenevinylene) derivatives, Synthetic Metals., 71 (1995) 2179-2180.

86. M. Grabolle, M. Spieles, V. Lesnyak, N. Gaponik, A. Eychmu□ller, U. Resch-Genger, Determination of the Fluorescence Quantum Yield of Quantum Dots: Suitable Procedures and Achievable Uncertainties, Analytical Chemistry, 81 (2009) 6285-6294.

87. S.A. Pollack, D.B. Chang, N.L. Moise, Upconversion- pumped infrared erbium laser, Journal of Applied Physics., 60 (1986) 4077-4086.

88. L.R. Wilson, B.S. Richards, Measurement method for photoluminescent quantum yields of fluorescent organic dyes in polymethyl methacrylate for luminescent solar concentrators, Applied Optics, 48 (2009) 212-220.

89. S.K.W. MacDougall, A. Ivaturi, J. Marques-Hueso, K.W. Krämer, B.S. Richards, Ultra-high photoluminescent quantum yield of β-NaYF4: 10% Er3+ via broadband excitation of upconversion for photovoltaic devices, Optics Express, 20 (2012) A879-A887.

90. J.C. Goldschmidt, M. Peters, A. Bösch, H. Helmers, F. Dimroth, S.W. Glunz, G. Willeke, Increasing the efficiency of fluorescent concentrator systems, Solar Energy Materials and Solar Cells, 93 (2009) 176-182.

91. S. Fischer, F. Hallermann, T. Eichelkraut, G. von Plessen, K.W. Krämer, D. Biner, H. Steinkemper, M. Hermle, J.C. Goldschmidt, Plasmon enhanced upconversion luminescence near gold nanoparticles: simulation and analysis of the interactions, Optics Express, 20 (2012) 271-282.

92. G.A. Crosby, J.N. Demas, Measurement of photoluminescence quantum yields. Review, The Journal of Physical Chemistry, 75 (1971) 991-1024.

93. J.B. Birks, Fluorescence Quantum Yield Measurements, Journal of Research of NBS, Section A: Physics and Chemistry, 80A (1976) 11.

94. J.C. de Mello, H.F. Wittmann, R.H. Friend, An improved experimental determination of external photoluminescence quantum efficiency, Advanced Materials, 9 (1997) 230-232.

95. C. Würth, J. Pauli, C. Lochmann, M. Spieles, U. Resch-Genger, Integrating Sphere Setup for the Traceable Measurement of Absolute Photoluminescence Quantum Yields in the Near Infrared, Analytical Chemistry, 84 (2011) 1345-1352.

96. C.L. Mulder, P.D. Reusswig, A.M. Velázquez, H. Kim, C. Rotschild, M.A. Baldo, Dye alignment in luminescent solar concentrators: I. Vertical alignment for improved waveguide coupling, Optics Express, 18 (2010) A79-A90.

97. Labsphere, Spectralon® Diffuse Reflectance Standards, in, Labsphere Inc., 231 Shaker St. North Sutton, NH 03260, USA, 2013.

98. L. Porrès, A. Holland, L.-O. Pålsson, A. Monkman, C. Kemp, A. Beeby, Absolute Measurements of Photoluminescence Quantum Yields of Solutions Using an Integrating Sphere, Journal of Fluorescence, 16 (2006) 267-273.

99. D.O. Faulkner, J.J. McDowell, A.J. Price, D.D. Perovic, N.P. Kherani, G.A. Ozin, Measurement of absolute photoluminescence quantum yields using integrating spheres – Which way to go?, Laser & Photonics Reviews, 6 (2012) 802-806.

100. T.-S. Ahn, R.O. Al-Kaysi, A.M. Muller, K.M. Wentz, C.J. Bardeen, Self-absorption correction for solid-state photoluminescence quantum yields obtained from integrating sphere measurements, Review Scientific Instruments, 78 (2007) 086105-086103.

101. J.-C. Boyer, F.C.J.M. van Veggel, Absolute quantum yield measurements of colloidal NaYF4: Er3+, Yb3+ upconverting nanoparticles, Nanoscale, 2 (2010) 1417-1419.

102. R.H. Page, K.I. Schaffers, P.A. Waide, J.B. Tassano, S.A. Payne, W.F. Krupke, W.K. Bischel, Upconversion-pumped luminescence efficiency of rare-earth-doped hosts sensitized with trivalent ytterbium, Journal of the Optical Society of America B, 15 (1998) 996-1008.

103. J. de Wild, A. Meijerink, J.K. Rath, W.G.J.H.M. van Sark, R.E.I. Schropp, Upconverter solar cells: materials and applications, Energy & Environmental Science, 4 (2011) 4835-4848.

104. S. Baluschev, T. Miteva, V. Yakutkin, G. Nelles, A. Yasuda, G. Wegner, Up-Conversion Fluorescence: Noncoherent Excitation by Sunlight, Physics Review Letters, 97 (2006) 143903.

105. S. Baluschev, F. Yu, T. Miteva, S. Ahl, A. Yasuda, G. Nelles, W. Knoll, G. Wegner, Metal-Enhanced Up-Conversion Fluorescence: Effective Triplet−Triplet Annihilation near Silver Surface, Nano Letters, 5 (2005) 2482-2484.

106. S. Baluschev, V. Yakutkin, T. Miteva, G. Wegner, T. Roberts, G. Nelles, A. Yasuda, S. Chernov, S. Aleshchenkov, A. Cheprakov, A general approach for non-coherently excited annihilation up-conversion: transforming the solar-spectrum New Jounal of Physics, 10 (2008).

107. W. Zou, C. Visser, J.A. Maduro, M.S. Pshenichnikov, J.C. Hummelen, Broadband dye-sensitized upconversion of near-infrared light, Nature Photonics, advance online publication (2012).

108. J. de Wild, T.F. Duindam, J.K. Rath, A. Meijerink, W.G.J.H.M. van Sark, R.E.I. Schropp, Increased Upconversion Response in a-Si:H Solar Cells With Broad-Band Light, IEEE Journal of Photovoltaics, , PP (2012) 1-5.

109. S. Fischer, A. Ivaturi, B. Frohlich, M. Rudiger, A. Richter, K.W. Kramer, B.S. Richards, J.C. Goldschmidt, Upconverter Silicon Solar Cell Devices for Efficient Utilization of Sub-Band-Gap Photons Under Concentrated Solar Radiation, IEEE Journal of Photovoltaics, , PP (2013) 1-7.

110. C. Strumpel, Application of Erbium Doped Up-converters to Silicon Solar Cells, in, Universitat Konstanze, 2007, pp. 139.

111. T.F. Schulze, Y.Y. Cheng, T. Khoury, M.J. Crossley, B. Stannowski, K. Lips, T.W. Schmidt, Micro-optical design of photochemical upconverters for thin-film solar cells, Journal of Photonics for Energy, 3 (2013) 034598-034598.

112. G.E. Arnaoutakis, J. Marques-Hueso, A. Ivaturi, K.W. Krämer, S. Fischer, J.C. Goldschmidt, B.S. Richards, Enhanced up-conversion for photovoltaics via concentrating integrated optics, Optics Express, 22 (2014) A452-A464.

113. J.C. Goldschmidt, P. Löper, S. Fischer, S. Janz, M. Peters, S.W. Glunz, G. Willeke, E. Lifshitz, K. Krämer, D. Biner, Advanced upconverter systems with spectral and geometric concentration for high upconversion efficiencies, Proc. of IEEE Conference on Optoelectronic and Microelectronic Materials and Devices (COMMAD 2008), Sydney, Australia (2008) 307-311.

114. A.C. Pan, C. del Cañizo, E. Cánovas, N.M. Santos, J.P. Leitão, A. Luque, Enhancement of up-conversion efficiency by combining rare earth-doped phosphors with PbS quantum dots, Solar Energy Materials and Solar Cells, 94 (2010) 1923-1926.

115. A.C. Pan, C. del Cañizo, A. Luque, Characterization of up-converter layers on bifacial silicon solar cells, Materials Science and Engineering: B, 159-160 (2009) 212-215.

116. J.C. Goldschmidt, nanospec, in, Fraunhofer ISE, 2011.

117. J.F. Suyver, J. Grimm, K.W. Krämer, H.U. Güdel, Highly efficient near-infrared to visible up-conversion process in NaYF4:Er3+,Yb3+, Journal of Luminescence, 114 (2005) 53-59.

118. F. Auzel, Compteur quantique par transfert d´energie entre deux ions de terres rares, Comptes Rendus Chimie, 262B (1966).

119. J.Z. Zhi Yuan Wang, Xianguo Wu, Maria Birau, Guomin Yu, Hongan Yu, Yinghua Qi, Pierre Desjardins, Xiansheng Meng, Jian Ping Gao, Erin Todd, Naiheng Song, Yaowen Bai, Andrew M. R. Beaudin, and Gaetan LeClair, Near-infrared absorbing organic materials, Pure and Applied Chemistry, 76 (2004) 9.

120. Y.H. Qi, P. Desjardins, X.S. Meng, Z.Y. Wang, Electrochromic ruthenium complex materials for optical attenuation, Optical Materials, 21 (2003) 255-263.

121. B. Ahrens, P. Löper, J.C. Goldschmidt, S. Glunz, B. Henke, P.-T. Miclea, S. Schweizer, Neodymium-doped fluorochlorozirconate glasses as an upconversion model system for high efficiency solar cells, Physica Status Solidi (a), 205 (2008) 2822-2830.

122. S.A. Maier, H.A. Atwater, Plasmonics: Localization and guiding of electromagnetic energy in metal/dielectric structures, Journal of Applied Physics., 98 (2005) -.

123. W. Zhang, F. Ding, S.Y. Chou, Large Enhancement of Upconversion Luminescence of NaYF4:Yb3+/Er3+ Nanocrystal by 3D Plasmonic Nano-Antennas, Advanced Materials, 24 (2012) OP236-OP241.

124. M. Florescu, H. Lee, I. Puscasu, M. Pralle, L. Florescu, D. Z. Ting, J.P. Dowling, Improving solar cell efficiency using photonic band-gap materials, Solar Energy Materials and Solar Cells, 91 (2007) 1599-1610.

125. A. Bielawny, C. Rockstuhl, F. Lederer, R.B. Wehrspohn, Intermediate reflectors for enhanced topcell performance in photovoltaicthin-film tandem cells, Optics Express, 17 (2009) 8439-8446.

126. P. Bermel, C. Luo, L. Zeng, L.C. Kimerling, J.D. Joannopoulos, Improving thin-film crystalline silicon solar cell efficiencies with photonic crystals, Optics Express, 15 (2007) 16986-17000.

127. S. John, Strong localization of photons in certain disordered dielectric superlattices, Physics Review Letters, 58 (1987) 2486.

128. J.D. Joannopoulos, Photonic Crystals: Molding the Flow of Light, Princeton University Press, Princeton, NJ, 1995.

129. E. Yablonovitch, Photonic band-gap structures, Journal of the Optical Society of America B, 10 (1993) 283-295.

130. E. Yablonovitch, Inhibited Spontaneous Emission in Solid-State Physics and Electronics, Physics Review Letters, 58 (1987) 2059.

131. A. Chutinan, S. John, Light trapping and absorption optimization in certain thin-film photonic crystal architectures, Physics ReviewA, 78 (2008) 023825.

132. Z. Yang, K. Zhu, Z. Song, D. Zhou, Z. Yin, J. Qiu, Effect of photonic bandgap on upconversion emission in YbPO4:Er inverse opal photonic crystals, Applied Optics, 50 (2011) 287-290.

133. Z.-X. Li, L.-L. Li, H.-P. Zhou, Q. Yuan, C. Chen, L.-D. Sun, C.-H. Yan, Colour modification action of an upconversion photonic crystal, Chemical Communications, (2009) 6616-6618.

134. M. Rüdiger, S. Fischer, J. Frank, A. Ivaturi, B.S. Richards, K.W. Krämer, M. Hermle, J.C. Goldschmidt, Bifacial n-type silicon solar cells for upconversion applications, Solar Energy Materials and Solar Cells, 128 (2014) 57-68.

135. K.W. Krämer, D. Biner, G. Frei, H.U. Güdel, M.P. Hehlen, S.R. Lüthi, Hexagonal Sodium Yttrium Fluoride Based Green and Blue Emitting Upconversion Phosphors, Chemistry of Materials, 16 (2004) 1244-1251.

136. J. Ballato, S.H. Foulger, J.D.W. Smith, Optical properties of perfluorocyclobutyl polymers. II. Theoretical and experimental attenuation, Journal of the Optical Society of America B, 21 (2004) 958-967.

137. M.A. Schreuder, J.D. Gosnell, N.J. Smith, M.R. Warnement, S.M. Weiss, S.J. Rosenthal, Encapsulated white-light CdSe nanocrystals as nanophosphors for solid-state lighting, Journal of Material Chemistry, 18 (2008) 970-975.

138. J. Marques-Hueso, D. Chen, S.K.W. MacDougall, Y. Wang, B.S. Richards, Advances in spectral conversion for photovoltaics: up-converting Er3 doped YF3 nano-crystals in transparent glass ceramic, in: L. Tsakalakos (Ed.) SPIE, SPIE, San Diego, California, USA, 2011, pp. 811102-811109.

139. S.E. Braslavsky, Glossary of Terms Used in Photochemistry,3rd Edition (IUPAC Recommendations 2006), Pure Applied Chemistry, 79 (2007) 173.

140. N. Stu□rzl, S. Lebedkin, M.M. Kappes, Revisiting the Laser Dye Styryl-13 As a Reference Near-Infrared Fluorophore: Implications for the Photoluminescence Quantum Yields of Semiconducting Single-Walled Carbon Nanotubes, The Journal of Physical Chemistry A, 113 (2009) 10238-10240.

141. A. Shalav, Rare-Earth Up-converting Phosphors for an Enhanced Silicon Solar Cell Response, in: Centre of Excellence for Advanced Silicon Photovoltaics and Photonics, University of New South Wales, Sydney, 2006, pp. 166.

142. A. Pires, S. Heer, H. Güdel, O. Serra, Er, Yb Doped Yttrium Based Nanosized Phosphors: Particle Size, "Host Lattice" and Doping Ion Concentration Effects on Upconversion Efficiency, Journal of Fluorescence, 16 (2006) 461-468.

143. F. Wang, J. Wang, X. Liu, Direct Evidence of a Surface Quenching Effect on Size-Dependent Luminescence of Upconversion Nanoparticles, Angewandte Chemie International Edition, 49 (2010) 7456-7460.

144. E. Klampaftis, B.S. Richards, Improvement in multi-crystalline silicon solar cell efficiency via addition of luminescent material to EVA encapsulation layer, Progress in Photovoltaics: Research and Applications, 19 (2011) 345-351.

145. S.B. D.A. Hardy, A. Kerrouche, S.C. Roaf, B.S. Richards, Creative Use of BIPV Materials: Barriers and Solutions, 27th European Photovoltaic Solar Energy Conference and Exhibition, PV Systems, PV and Architecture (2012) 6.

146. Y.Y. Cheng, T. Khoury, R.G.C.R. Clady, M.J.Y. Tayebjee, N.J. Ekins-Daukes, M.J. Crossley, T.W. Schmidt, On the efficiency limit of triplet-triplet annihilation for photochemical upconversion, Physical Chemistry Chemical Physics., 12 (2010).

147. M.A. Green, Solar Cells: Operating Principles. Technology and System Applications, in, The University of New South Wales, Kensington, NSW 2033, 1982.

148. E. Verhagen, L. Kuipers, A. Polman, Field enhancement in metallic subwavelength aperture arrays probedby erbium upconversion luminescence, Optics Express, 17 (2009) 14586-14598.

149. M. Pollnau, D.R. Gamelin, S.R. Lüthi, H.U. Güdel, M.P. Hehlen, Power dependence of upconversion luminescence in lanthanide and transition-metal-ion systems, Physics Review B, 61 (2000) 3337-3346.

150. A. Baraldi, R. Capelletti, M. Mazzera, A. Ponzoni, G. Amoretti, N. Magnani, A. Toncelli, M. Tonelli, Role of Er3+ concentration in high-resolution spectra of BaY2F8 single crystals, Physics Review B, 72 (2005) 075132.

151. T. Böttger, C.W. Thiel, R.L. Cone, Y. Sun, Controlled compositional disorder in Er3+:Y2SiO5 provides a wide-bandwidth spectral hole burning material at 1.5μm, Physics Review B, 77 (2008) 155125.

152. A.M. Stoneham, Shapes of Inhomogeneously Broadened Resonance Lines in Solids, Reviews of Modern Physics, 41 (1969) 82-108.

153. D. Chen, Y. Wang, Impurity doping: a novel strategy for controllable synthesis of functional lanthanide nanomaterials, Nanoscale, 5 (2013) 4621-4637.

154. S. K. W. MacDougall, A. Ivaturi, J. Marques-Hueso, K. W. Krämer, B. S. Richards, Measurement Procedure for Absolute Broadband Up-Conversion Photoluminescent Quantum Yields: Correcting for Absorption/Re-Emission, Review of Scientific Instruments, 85, 063109 (2014)

155. C.G. Liu S, Ohulchanskyy TY, Swihart MT, Prasad PN, Facile Synthesis and Potential Bioimaging Applications of Hybrid Upconverting and Plasmonic NaGdF4: Yb3+, Er3+/Silica/Gold Nanoparticles. , Theranostics 3(2013) 7.

156. S.K.W. MacDougall, A. Ivaturi, J. Marques-Hueso, D. Chen, Y. Wang, B.S. Richards, Broadband excitation of upconversion in lanthanide doped fluorides for enhancement of Si solar cells, in: R. Wehrspohn, A. Gombert (Eds.), SPIE, Brussels, Belgium, 2012, pp. 84380Y-84389.

157. S.K.W. MacDougall, A. Ivaturi, J. Marques-Hueso, K.W. Krämer, B.S. Richards, Broadband photoluminescent quantum yield optimisation of Er3+-doped β-NaYF4 for upconversion in silicon solar cells, Solar Energy Materials and Solar Cells, 128 (2014) 18-26.

158. S. Fischer, B. Fröhlich, K.W. Krämer, J.C. Goldschmidt, Relation between Excitation Power Density and Er3+ Doping Yielding the Highest Absolute Upconversion Quantum Yield, The Journal of Physical Chemistry C, 118 (2014) 30106-30114.

159. R.K. Lee, O. Painter, B. Kitzke, A. Scherer, A. Yariv, Emission properties of a defect cavity in a two-dimensional photonic bandgap crystal slab, Journal of the Optical Society of America B, 17 (2000) 629-633.

160. A. Kress, F. Hofbauer, N. Reinelt, M. Kaniber, H.J. Krenner, R. Meyer, G. Böhm, J.J. Finley, Manipulation of the spontaneous emission dynamics of quantum dots in two-dimensional photonic crystals, Physics Review B, 71 (2005) 241304.

161. J. Marques-Hueso, R. Peretti, R. Abargues, B.S. Richards, C. Seassal, J.P. Martínez-Pastor, Photonic Crystal-Driven Spectral Concentration for Upconversion Photovoltaics, Advanced Optical Materials, (2014).